

This PDF was created from the British Library's microfilm copy of the original thesis. As such the images are greyscale and no colour was captured.

Due to the scanning process, an area greater than the page area is recorded and extraneous details can be captured.

This is the best available copy

D76202

THE BRITISH LIBRARY DOCUMENT SUPPLY CENTRE

ON THE PUNCTURE STRENGTH OF RUBBER.

TITLE

.....

.....

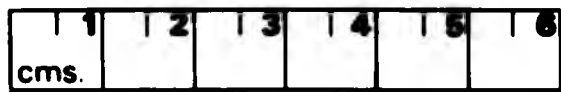
K. AB-MALEK. PH.D.

AUTHOR

.....

Attention is drawn to the fact that the copyright of this thesis rests with its author.

This copy of the thesis has been supplied on condition that anyone who consults it is understood to recognise that its copyright rests with its author and that no information derived from it may be published without the author's prior written consent.



THE BRITISH LIBRARY
DOCUMENT SUPPLY CENTRE
Boston Spa, Wetherby
West Yorkshire
United Kingdom

REDUCTION X **12**

ON THE PUNCTURE STRENGTH OF RUBBER

A thesis presented to the
COUNCIL OF NATIONAL ACADEMIC AWARDS
for the degree of
DOCTOR OF PHILOSOPHY

by

KAMARUDIN AB-MALEK

Malaysian Rubber Producers' Research Association
Brickendonbury
Hertford, SG13 8NL
and
London School of Polymer Technology,
Polytechnic of North London,
Holloway Road,
London, N7 8DB.

OCTOBER 1987

DECLARATION BY THE CANDIDATE

I declare that while registered as a candiadte for the degree of Doctor of Philosophy I have not been a registered candidate for another award of the CNAAB, or of a University.

ABSTRACT

A fracture mechanics study has been carried out on the fracture of rubber by cylindrical indentors. Several phenomena have been identified which affect the puncture process.

It has been observed that a ring crack forms on the rubber surface before puncture occurs. By treating this crack as a starter crack, an equation has been derived for the puncture energy. The values of puncture energy so obtained were found to agree well with the catastrophic tearing energy obtained from the trouser tear test.

The energy stored in the rubber influenced the value of the puncture energy calculated. The energy beneath the indenter was determined using a model experiment based on the biaxial stretching of rubber by inflation. The energy stored in the rubber surrounding the indenter was calculated. The contribution of these energies was shown to be small.

The puncture test was used to study the strength of thick rubber blocks which had been exposed to long-term ageing and to high temperatures. These rubber blocks were taken from rubber bearings of 20 and 96 years of age respectively. A study was also carried out on a natural rubber tyre after forty two years immersion in sea water.

ACKNOWLEDGMENTS

The author is indebted to the Malaysian Rubber Research and Development Board for the Postgraduate Training Award and to the Malaysian Rubber Research Producers' Research Association for the provision of the experimental facilities described in this thesis.

The author is also grateful to Dr. A. Stevenson* who is his Director of Studies at the Malaysian Rubber Producers' Research Association, and Dr. D. Blackley and Dr. E. Southern, his supervisors at the London School of Polymer Technology, for their guidance and encouragement. The author's thanks are due to Mr. M.J.R. Loadman for the TGA and TLC analyses, Mr. A. Cobbold for the the electron microscopy work, Mr. J.E. Davey for the oxygen content analyses, and the staff of the MRPRA physical testing laboratory for carrying out routine physical testing.

* Now at Materials Engineering Research Laboratory,
Tamworth Road, Hertford.

To my beloved wife, Araf and Comel

CONTENTS

	Page
TITLE PAGE	(i)
ABSTRACT	(ii)
ACKNOWLEDGMENTS	(iv)
CONTENTS	(vi)
CHAPTER 1	1
INTRODUCTION	
CHAPTER 2	3
FAILURE OF RUBBER	
2.1 Introduction	3
2.2 The Griffith theory of failure	4
2.3 Tearing of rubber	7
2.4 Crack growth characteristics	11
2.5 Applications of the fracture mechanics to practical problems	13
CHAPTER 3	18
INDENTATION FRACTURE OF SOLIDS	
3.1 Introduction	18
3.2 Indentation on brittle materials by rigid indenter	19
3.2.1 Hertzian fracture	19
3.2.2 Point-indentation failure	21
3.3 Indentations of rubber by a rigid indenter	27

3.4	Puncture of rubber	32
3.5	Cutting of rubber	39
CHAPTER 4		42
EXPERIMENTAL METHOD		
4.1	Experimental apparatus	42
4.2	Test-pieces	50
4.3	Experimental procedure	50
4.4	Experimental precautions	54
4.5	Measurement of tearing energy using trouser tear test	55
CHAPTER 5		62
SOME FACTORS AFFECTING THE RESULTS OF THE PUNCTURE TEST		
5.1	Interfacial conditions	62
5.2	Effect of rubber thickness and hardness of backing blocks	66
5.3	Effect of proximity between successive indentations and of distance of indentation from free edge of test block.	71
5.4	Surface condition of test-pieces	73
5.5	Effect of corner radius of indenter	78
CHAPTER 6		86
THE MECHANICS OF PUNCTURE		
6.1	Introduction	86
6.2	Phenomenology of puncture	87
6.2.1	Ring crack characteristics	90
6.2.2	Characteristics of puncture	98

6.3	Fracture mechanics	109
6.4	A direct determination of catastrophic tearing energy	117
6.5	Discussion	119
CHAPTER SEVEN		126
EVALUATION OF THE TERMS WHICH CONTRIBUTE TO PUNCTURE ENERGY		
7.1	Introduction	126
7.2	Energy stored in rubber beneath indenter	126
7.2.1	Theory	126
7.2.2	Model experiment for equibiaxial tearing	133
7.2.3	Bursting of the rubber sheet	145
7.3	Energy stored in the rubber surrounding the column	148
7.3.1	Theory	148
7.3.2	Determination of C_1 and C_2 : results	156
7.4	Effect of corner radius on puncture energy	157
7.5	Conclusions concerning relative importance of terms in puncture energy equation	167
CHAPTER EIGHT		171
APPLICATION OF PUNCTURE TEST TO A STUDY OF AGEING		
8.1	Introduction	171
8.2	Conditions of natural rubber pad after 96 years service	174
8.3	Experimental method	177
8.4	Variation of puncture energy with time of ageing	179

8.5	Uptake of oxygen	190
8.6	Discussion	195
CHAPTER NINE		202
STUDY OF USED RUBBER COMPONENTS		
9.1	Introduction	202
9.2	Twenty-year-old rubber bearing	203
9.2.1	Introduction	203
9.2.2	Experimental method	203
9.2.3	Contour strength	207
9.2.4	Physical properties based on conventional tests	209
9.2.5	Summary and conclusions	213
9.3	Condition of a tyre after 42 years immersion in sea-water	214
9.3.1	Introduction	214
9.3.2	Experimental method	214
9.3.3	Contour strength	216
9.3.4	Scanning electron microscopy	219
9.3.5	Physical properties of rubber samples	224
9.3.6	Conclusions	224
CHAPTER TEN		226
CONCLUSIONS AND SUGGESTIONS FOR FURTHER WORK		
REFERENCES		229

CHAPTER ONE
INTRODUCTION

Rubber engineering components such as tyres, bridge bearings, and antivibration mounts for buildings and engines usually incorporate relatively thick layers of rubber whose physical properties (stiffness, strength etc) determine the performance of the components. Standard tests for the mechanical properties of rubber rely however on small test-pieces - usually thin strips cut from moulded rubber sheets. It is known that the moulding and curing processes can cause that nominally identical rubber vulcanizates to show different properties in thick blocks compared with those of thin sheets. Also, ageing affects thick blocks differently from thin sheets. It is therefore of interest to develop a test for the physical condition of rubber in thick blocks - without the need for any elaborate process of cutting out standard (i.e. thin) strip test-pieces.

Indentation tests are widely used to determine the hardness of rubbers, plastics and metals. In the

case of rubber, the tests are simple, rapid, can often be made directly on finished products, and are non-destructive. For rubber, hardness tests, measure essentially the modulus or stress-strain behaviour in the Hookean region when the indenter is pressed against the test-piece surface. The indentation process can be continued until the rubber surface is punctured, thus giving a material strength parameter ('puncture strength' or 'puncture load'). The indentation test can be conveniently carried out on the surface of a rubber product without the need to prepare a special test-piece.

It would facilitate comparison with other tear tests to provide a fracture mechanics interpretation of puncture load for example in terms of the more fundamental parameter tearing energy. Thus this thesis will analyse the mechanisms and mechanics of the puncture process in these terms.

The test can be used to study the strength properties of rubber blocks exposed to high-temperature ageing. The results will be used to model and interpret the condition of rubber in large rubber engineering components such as bridge bearings after long periods of service.

CHAPTER TWO
FAILURE OF RUBBER

2.1 Introduction

All solid materials will fracture when stressed beyond some critical level. Fracture usually involves the rupture of molecular bonds which intersect the fracture plane. A theoretical strength can be defined which is the sum of the strengths of all the individual ruptured bonds. In practice, most materials fail at a stress two or three orders of magnitude below the theoretical strength(1,2). The discrepancy between the theoretical and observed strength was first explained by Griffith(3) in his classic work on the brittle fracture of glass. He postulated that solids usually contains imperfections such as inhomogeneities or flaws which act as stress raisers creating localised stresses much greater than those in the bulk. It is at such a site of high stress concentration that failure usually initiates to form a crack which may ultimately propagate through the material under the action of the applied forces and boundary conditions.

2.2 The Griffith theory of failure

The principles laid down in the Griffith(3) theory of brittle fracture effectively foreshadowed the entire field of present day fracture mechanics. Griffith evaluated the conditions under which a crack in a strained elastic solid should propagate, by considering the balance of energy within the body. A crack will increase in length if, in so doing, the energy released from changes in the stored strain energy exceeds the surface free energy of the freshly cleaved interface. Thus the condition for propagation is

$$-\left(\frac{\partial U}{\partial A}\right)_1 \geq 2s \quad 2.1$$

where U is the total strain energy stored in the specimen, A is the area of one of the fracture surfaces formed, s is the surface energy of a unit area of new surface and $|$ indicates that the partial differentiation is carried out under conditions where the external forces on the specimen do no work.

Griffith calculated the strain energy release rate, $\left(\frac{\partial U}{\partial A}\right)_1$,

for the case of an elliptical crack in a plate subject to a uniform tensile stress, t_0 , in a direction perpendicular to the major axis of the

ellipse. In doing so he made use of Inglis's(4) solution for the stress at the end of the major axis of such an elliptical crack.

The solution showed that the maximum tensile stress, t_m , occurs at the ends of the major axis, and that this could be several times that of the applied stress. The relationship between t_m and t_o is

$$t_m = t_o \left(1 + 2 \frac{c}{b} \right) \quad 2.2$$

where c is the major and b the minor semi axis of the ellipse. For an elliptical crack, $c \gg b$ and equation 2.2 reduces to

$$t_m = 2t_o \sqrt{\frac{c}{r}} \quad 2.3$$

where r is equal to b^2/c and is the radius of curvature of the ellipse at the extremity of the major axis.

Griffith arrived at the solution

$$-\left(\frac{\partial U}{\partial A} \right)_1 = \frac{2t_o^2 \pi c}{E} \quad 2.4$$

where E is Young's modulus of the material undergoing fracture. As two increments of surface area are created at each end of the elliptical crack of length $2c$, the rupture criterion 2.1 therefore becomes

$$\frac{2t^2 \pi c}{E} \geq 4S$$

or, in terms of the tensile breaking stress

$$t_0 = \sqrt{\frac{2ES}{\pi c}}$$

2.5

On the basis of this equation, Griffith could predict the size of the crack or flaws in the glass that he was working with. He also produced impressive proof that the strength of glass could be increased on removing the most dangerous cracks by etching.

In its original form, Griffith's theory is only valid in a very limited number of cases. In addition to the surface energy already taken into account in the energy balance, energy is often absorbed in other ways - for example in local plastic deformation at the tip prior to fracture.

Furthermore, the theory is strictly inapplicable to most materials because it assumes Hookean behaviour, perfect elasticity and infinitesimal strain. This, of course, is a consequence of using Inglis' results for the stress at the crack tip derived using classical elasticity theory. These are inapplicable in the case of rubber, which displays non-linear elastic behaviour as well as the strain being non-infinitesimal.

2.3 Tearing of Rubber

An important application of the Griffith theory was proposed by Rivlin and Thomas(5) in 1953. Like Griffith, they consider the energy balance, and thus avoid any detailed stress-strain analysis. They postulated that tearing would occur in a stretched rubber test-piece containing a crack when the tearing energy, T , defined as the rate of release of strain energy, exceeded a critical tearing energy, T_c , that is when

$$-\left(\frac{\partial U}{\partial A}\right) \geq T_c \quad 2.6$$

T_c includes viscous and all other forms of irreversible energy dissipated during fracture. Its magnitude far exceeds that of the true surface energy. For T_c to be a material property, all the energy has to be dissipated at the crack, and T_c has to be independent of the shape of the test piece and the way forces are applied to it.

In order to verify the criterion 2.6, Rivlin and Thomas carried out tear tests using test-pieces of different shapes which could be cut from a thin uniform sheet of rubber. These were called the pure shear, trouser and tensile strip test-pieces and are illustrated in Figure 2.1. The tearing energies, T , for these test-pieces were derived and could be calculated from readily measured forces or strains.

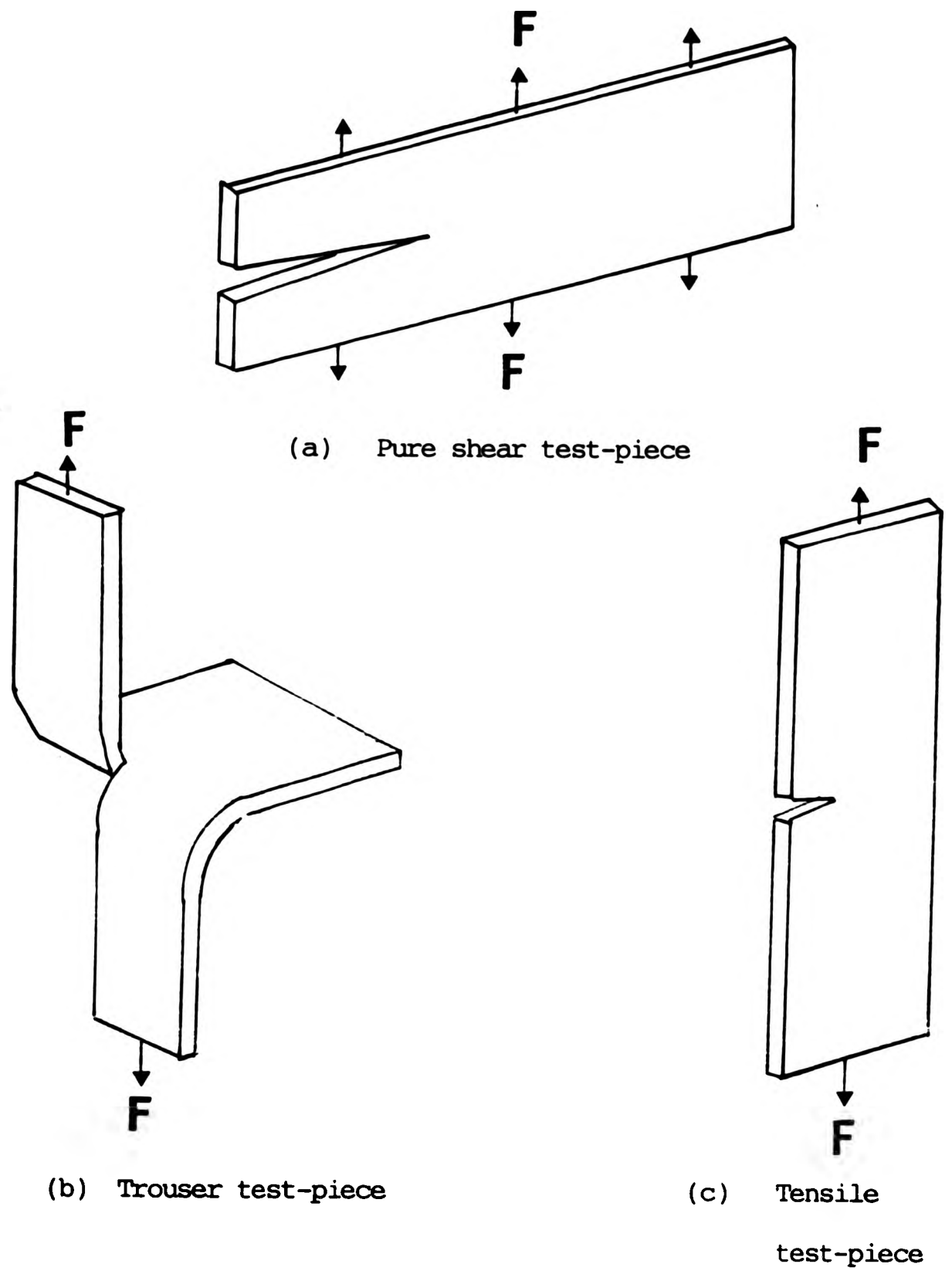


Figure 2.1 Tear test-pieces.

For the pure shear testpiece(5), for a long crack

$$T = Wl_0 \quad 2.7$$

where W is the strain energy density in pure shear and l_0 the undeformed length between the clamps. For the trouser testpiece(5),

$$T = \frac{2F\lambda}{h} - wW \quad 2.8$$

where F is the applied force, λ the extension ratio, h is the width of tear path, w is the width of one of the legs, and W is the strain energy density in the legs which are in simple extension. For the tensile strip with an edge crack of length c ,

$$T = 2kWc \quad 2.9$$

where W is the strain energy density in the bulk of the test-piece, and k is a non-dimensional function of strain. The variation of k with strain, e , was determined experimentally by Greensmith(6) and later numerically by Lindley(7) for a range of natural rubber vulcanizates.

Having obtained expressions for the tearing energy for the three different types of test-piece, Rivlin and Thomas proceeded to verify the validity of their criterion on a range of natural rubber

vulcanizates. The results showed that there was a 'catastrophic' tearing, in which the crack propagates suddenly for several millimetres or more, and this occurred at a critical tearing energy, T_c , which is characteristic of that particular rubber and is independent of the type of test-piece. This verified the Rivlin and Thomas criterion for tearing in rubber. The magnitude found for T_c is of the order of $1-10\text{kJ/m}^2$ which is at least a thousand times greater than free surface energies of solids(8). Thus the irreversible energy-dissipation processes referred to earlier dominate the tear behaviour of rubber.

Equations (2.7)-(2.9) for tearing energy are in terms of the forces or overall strains applied to the test-pieces. Thomas(9) has also related the tearing energy to the deformation of the localised region around a crack tip. He found experimentally that, to a fair approximation,

$$T = Wd \qquad 2.10$$

where W is the strain energy density at the tip and d the unstrained tip diameter. The validity of equation 2.10 was verified in rupture tests on trousers tear test-pieces with semi-circular crack tips of different diameters, d . At rupture, the value of W is the strain energy density at break

obtained experimentally from an extension stress-strain test to break. A good agreement was found between the tearing energies determined from equation 2.10 and 2.8.

2.4 Crack growth characteristics

Small scale crack growth can occur in rubbers, as in other materials, at energies below those required for tearing or catastrophic failure. In the case of a strain-crystallizing rubber such as natural rubber, if the testpiece is subjected to repeated stressing, the load being alternately removed and re-applied, crack growth takes place during the load-increasing part of each cycle; there is no crack growth when the load is held constant. This is in contrast to the crack growth behaviour of a non-crystallizing rubber such as styrene-butadiene rubber(SBR), for which crack growth is a time-dependent process, i.e., the crack will continue to propagate even at constant deformation. Thus, for natural rubber, the amount of growth depends primarily on the number of cycles rather than the period of cycling.

If the amount of crack growth per cycle is plotted against the maximum tearing energy attained during the cycle(Fig.2.2), the results are independent of the form of testpiece used(10,11). This further illustrates the validity of the tearing energy concept.

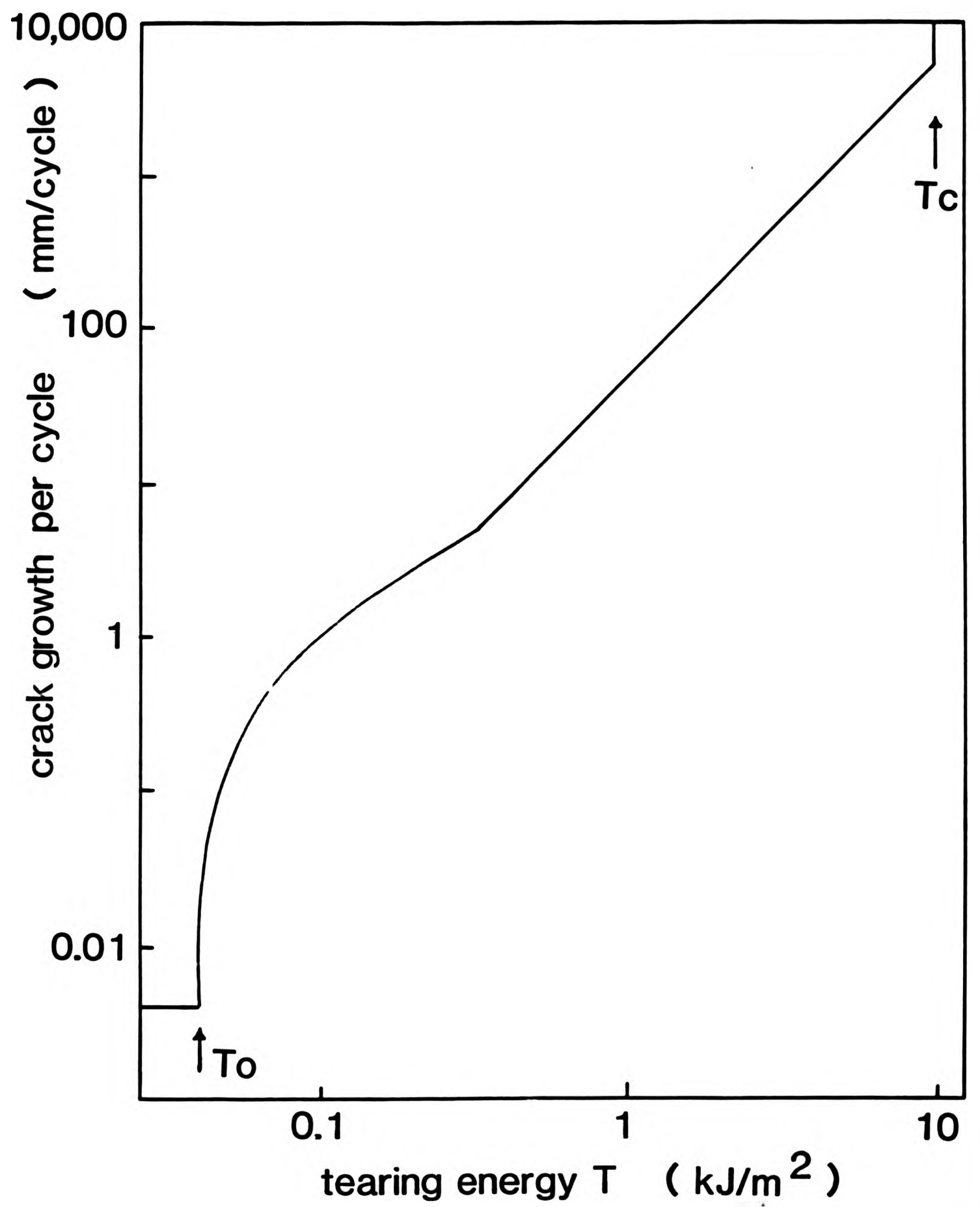


Figure 2.2 Crack growth characteristics for an unfilled natural rubber(11).

The relation between crack growth rate and tearing energy is therefore an intrinsic property of the material.

It is evident from Fig.2.2 that T_0 is an important parameter. It is the lowest tearing energy for crack growth to occur due to mechanical rupture. However, it is surprising, that once T_0 is reached, a crack does not propagate indefinitely and catastrophic failure of a test-piece will occur. Lake and Thomas(12) suggested an explanation for this behaviour based on the fact that rubbers are not perfectly elastic. For an ideally elastic rubber having no hysteresis, catastrophic rupture would occur at T_0 and the crack growth characteristic would be a vertical line. In practice, all rubbers are to some extent hysteretical. As the hysteresis increases, T_0 is unaffected but the slope of the crack growth characteristic is reduced, and the onset of catastrophic rupture delayed.

2.5 Applications of the fracture mechanics to practical problems

Rubber-cord laminated structures are often used in practise - for example, in tyres, conveyor belting and hose. In common with other laminates, failure can occur in these structures and can be complex in nature; possible causes include loss of adhesion between the cords and the rubber and various forms of

cracking. Two forms of cracking in rubber-cord laminates have been treated by the fracture mechanics approach(13,14): (i) growth of cracks between the ply layers and (ii) growth of roughly cylindrical cracks around individual cords - "socketing".

In inter-ply cracking, the growth of a crack in a plane parallel to the major surfaces of the laminated sample relaxes the elastic strain energy stored in the material. Consideration of this energy release allows the calculation of the tearing energy in terms of the thickness of the laminate and the strain energy density(13). A somewhat similar calculation may be made for the case of socketing failure. In this case the cord spacing and the cord diameter are important. The theory predicts that there will be a change from inter-ply to socketing failure when the number of cords per unit length is reduced to a value of $1/(\pi \times \text{cord diameter})$ (14).

Experimental measurements were made on a model laminate for both the failure processes described above, and comparison was made with predictions based on the independently measured crack growth behaviour of the rubber. Satisfactory agreement was found, and the observed transition between the two failure processes was correctly predicted(13,14). This type of failure is known to occur in tyres, and may lead to distortion of a tyre or in extreme cases to detachment of the tread or blow-out. The approach

described above appears to identify correctly the general mechanisms of failure which at first sight seem intractable.

The adhesion of the cord to the rubber is very important in tyre applications, and various tests have been used to evaluate its quality. Recently a test designed to evaluate it in terms of an adhesion energy has been developed(15), using an approach essentially similar to that employed in the analysis of the socketing failure described above. It appears that this method has the advantage that, like the tearing energy derived from tear measurements, the adhesion energy is a characteristic of the cord-rubber-bonding system rather than a function of the detailed geometry of the test specimen.

Another tyre problem is the development of cracks in the base of the tread grooves. The cause of the cracking is the cyclic strains undergone by the groove region as the tyre rotates in contact with the road. The main problem in applying the energetics approach is in determining the energy release rate for a crack in the appropriate region. A method that was found to be of use was the measurement of the amount by which an intentionally inserted crack opened under the applied deformation, in conjunction with a knowledge of the modulus of the rubber and the groove dimensions(16). By consideration of the work required to close the crack

up the energy release rate could be estimated, the validity of the method being confirmed by model experiments. The groove cracking observed under service condition or rig tests could then be compared with that predicted from the results of measurements described above in combination with the independently measured crack growth characteristics of the rubber which shows a satisfactory agreement(16).

Fatigue failure due to crack growth can be a limiting factor in determining the maximum permissible strains under operating conditions. The failure of bonded rubber/metal springs under large compression cycles has been studied using the fracture mechanics approach. In this case the tearing energies were determined by an approximate theoretical approach, utilizing experimental observations on the crack locus from the edge of the rubber/metal bond(17,18). The relationship between tearing energy and crack growth rate was the same as that obtained from fatigue crack growth testing with tensile strips of the same rubber. This is a conclusive evidence that the relationship is a fundamental material property independent of the geometry and mode of deformation, and extended the range of tearing energy solutions to a genuine plane strain configuration. This shows that for rubber there is a lack of plane strain/plane stress

complications which are observed in glassy
polymers(19,20).

CHAPTER THREE
INDENTATION FRACTURE OF SOLIDS

3.1 Introduction

Small cracks which develop during the indentation of brittle solids are features which are basic to a wide range of phenomena. For example the abrasion, grinding, drilling and wear of surfaces are all associated with the manner in which small-scale fractures initiate and propagate within highly localised stress fields. Indentation is also important in the context of the hardness test, widely used for the quality control of the mechanical properties of a material. Most of the fundamental work on indentation fracture has been on brittle materials, with very little, if any, on rubber. This chapter will first review the literature on brittle materials and then subsequently on rubber.

3.2 Indentation on brittle materials by rigid indenter

3.2.1 Hertzian fracture

Historically, the problem of indentation between two solid bodies has developed from a background of well-founded principles. As early as 1881(21), Hertz analysed the elastic contact between two curved bodies using classical elasticity theory. Hertz described qualitatively the cone-shaped crack that runs around the contact circle and spreads downward into one of the bodies at critical loading. Today, the Hertzian test used to determine material properties consists of a hard spherical indenter loaded on to a flat specimen. This system provides a well-defined elastic stress field up to the point of fracture. Therefore an analysis in terms fracture mechanics is feasible as has been shown by Lawn and co-workers(22,23,24).

According to the Hertzian analysis, the radius, a , of the circle of contact between spherical indenter and flat specimen, and the depth of penetration, d , are given by the following equations:

$$a^3 = \frac{4kFr}{3E} \quad 3.1$$

$$d^3 = \left(\frac{4k}{3E}\right)^2 \frac{F^2}{r} \quad 3.2$$

where F is the applied load on the indenter, r is the

radius of the indenter, E is the Young's modulus of the specimen and k is the dimensionless constant,

$$k = \frac{9}{16} (1 - \mu^2) + (1 - \mu'^2) \frac{E}{E'} \quad 3.3$$

where E' is the Young's modulus of the indenter, and μ and μ' are the Poisson's ratio of the specimen and indenter respectively. These three equations are sufficient to specify the loading conditions for any commonly-used ball indentation arrangement(25).

The mechanics of crack growth are determined by the distribution of stresses beneath the indenter. In 1904, Huber(26) extended the Hertz analysis and produced a solution for the stress field. The nature of Hertzian stress field has been discussed in a great detail in reference 22,23 and 25.

The main features are summarised below:

(1) Within the drop-shaped area underneath the indenter, all the principal stresses are compressive.

(2) The tensile stress reaches its maximum at the contact circle, and falls off slowly with increasing radial distance from the contact centre along the specimen surface.

(3) The tensile stresses decrease rapidly with depth below the specimen surface.

(4) The trajectories of the minimum principal stresses start orthogonal to the specimen surface and rapidly deviate outward from the contact circle to

form a family of near-parallel curves resembling the shape of the cone cracks.

According to Lawn and Frank(22), fracture initiates from a pre-existing flaw in the surface just outside the contact circle where the principal tensile stress is a maximum. Fracture grows initially by running around the contact circle and it then follows closely the circular trajectories and forms a ring crack(22,23,27). Further increasing the load causes the surface ring cracks to propagate downward to form a fully developed Hertzian cone. The most systematic experimental work on the Hertzian fracture has been carried out on silicate glass(21,22,25,28), quartz(29-31), and diamond(23,32,33,34,35).

Lawn and Frank(22) derived the fracture energy, T as

$$T = \frac{F}{kr} \left[\Phi\left(\frac{c}{a}\right) \right] \quad 3.4$$

where ϕ is a dimensionless function and a and c are parameters of the Hertzian cone-configuration (Figure 3.1).

3.2.2 Point-indentation failure

The problem of a point-indentation was first analysed by Boussinesq in 1885(36).

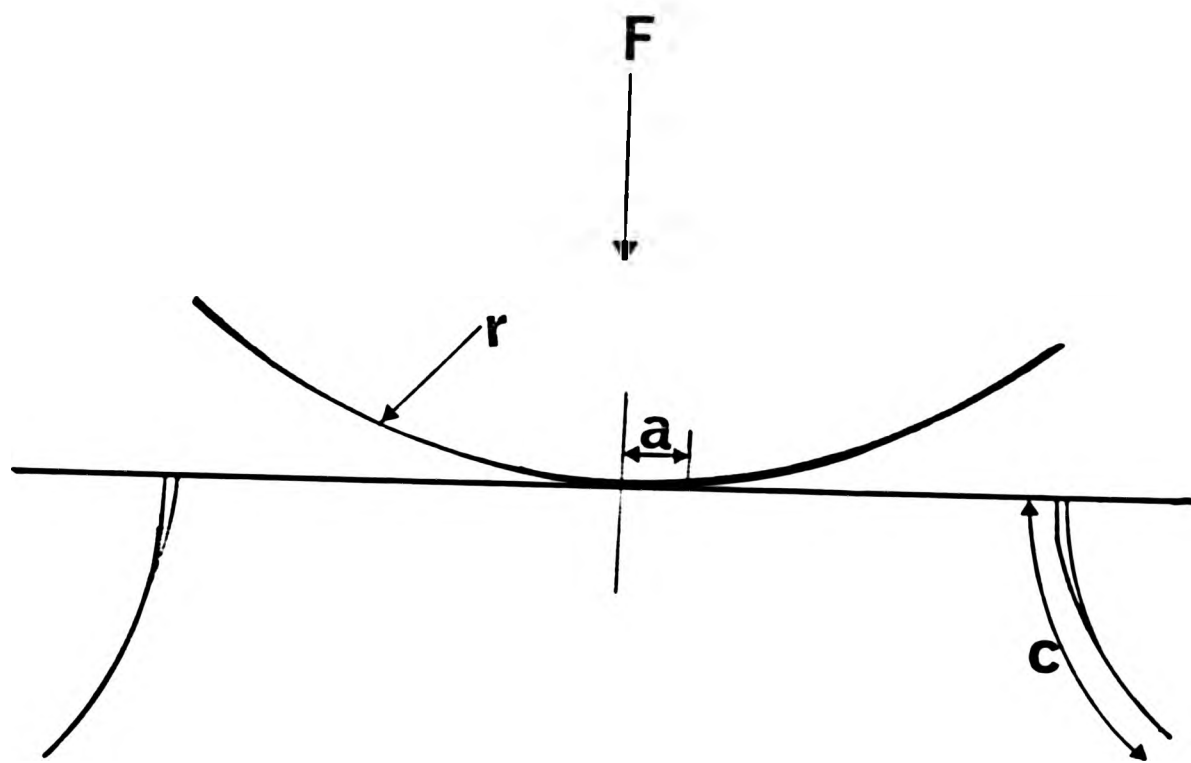


Figure 3.1 Parameters of Hertzian cone-crack configuration

Point-indentation techniques have been used for a long time for routine hardness testing(e.g., the Vickers pyramid test). These tests are now frequently used in the study of the mechanical properties of brittle solids.

Boussinesq provided the solution for the stress field in a material subjected to a point loading. Lawn and Swain(37) investigated in detail the distributions and directions of the principal stresses. Unlike the Hertzian stress field, the principal stresses beneath the indenter are not all compressive. The maximum tensile stress occurs at the specimen surface, and cracks usually initiate at one of these favoured locations.

The indentation fracture produced by sharp indentors have been studied by many workers(37,38,39,40). The general features of this type of fracture are shown in Figure 3.2. At (a) is shown the sharp-point indenter being loaded on to the surface of the specimen at force F , and producing an inelastic deformation zone. At (b), is shown the load increasing to a threshold value, with deformation-induced flaws suddenly developing into a small crack called a "median vent". At (c), is shown the load is increasing, and the median vent growing further. At(d), is shown the load being removed, and the median vent beginning to close. At (e) is shown sideways-extending cracks called "lateral vents"

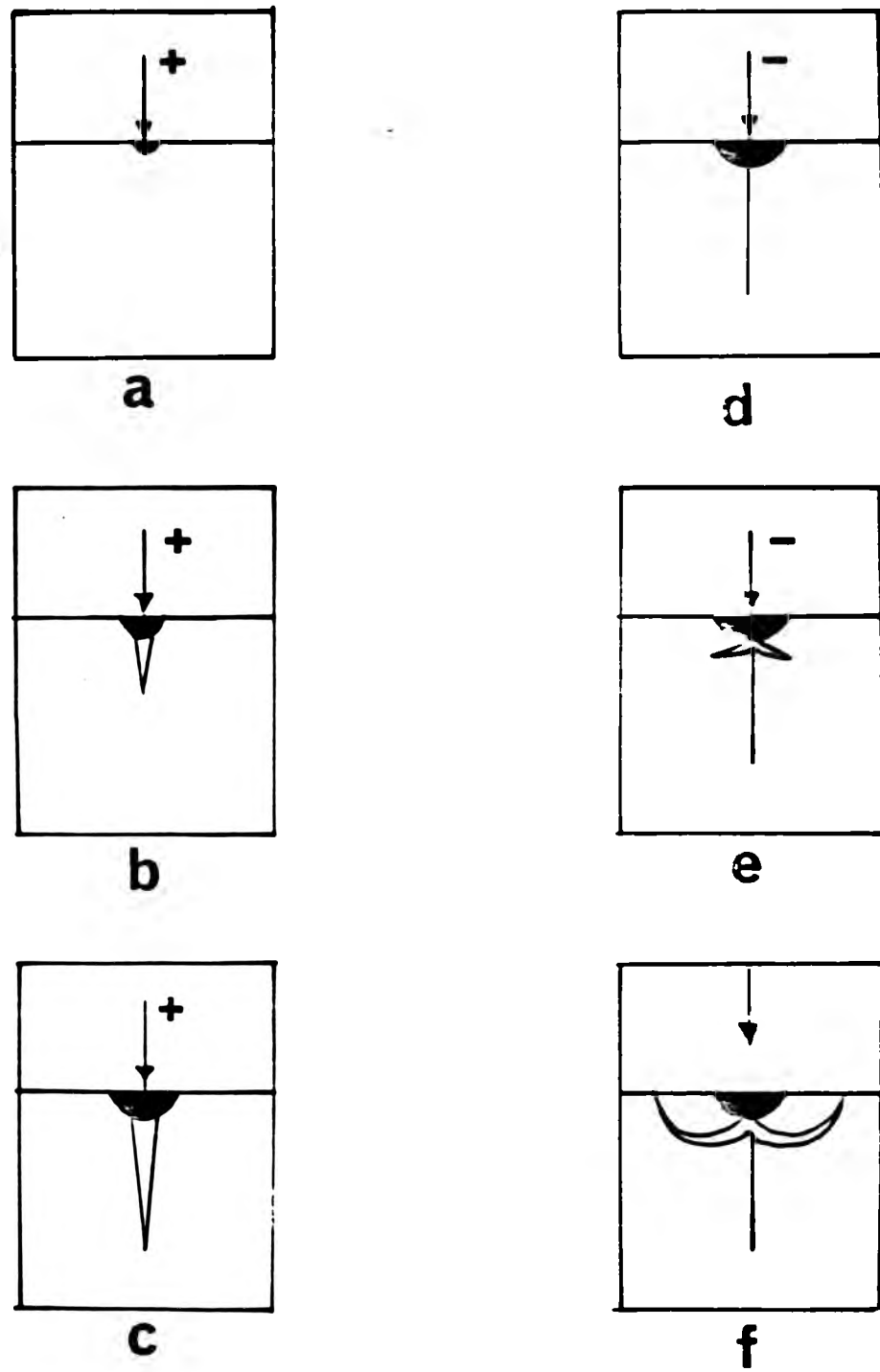


Figure 3.2 Formation of vent crack from point loading in brittle solids.

beginning to appear as the indenter is removed. At (f), is shown the lateral vents continuing to extend towards the specimen surface, and possibly leading to chipping, when the indenter is completely removed from the specimen.

Fracture mechanics analysis on lateral vents is complicated, because a detailed knowledge of the residual stress field imposed on the plastic zone after unloading is lacking. However, the geometry of the median vents is more amenable to analysis. This is because the crack propagation depends on the stress distribution over a distance large compared with the scale of the plastic zone (Figure 3.3). A fracture mechanics calculation then gives for the case $c \gg z$ (Figure 3.3) (37)

$$T = \psi(\mu) \left(\frac{\alpha}{\beta^2} \right) \left(\frac{H}{E} \right) \left(\frac{F}{C} \right) \quad 3.5$$

where $\psi(\mu)$ a dimensionless function of Poisson's ratio, μ , H is the hardness number, E is the Young's modulus, α and β are dimensionless geometrical factors.

One important practical implication of point-indentation is in glass-cutting, where smooth, damage-free edges are required. In this case, it is important that only a single well-formed median vent is formed and that no lateral vents are formed. On the other hand, in fragmentation processes it is the

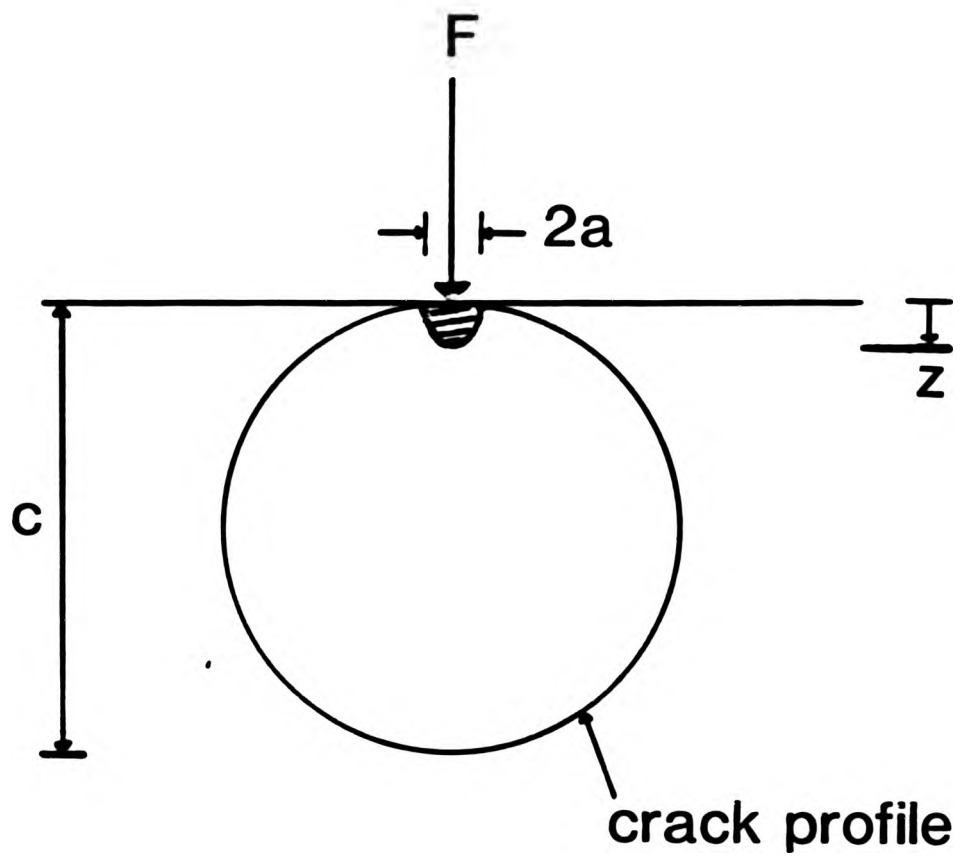


Figure 3.3 Parameters of the median vent configuration.

lateral vent configuration which is required to develop.

3.3 Indentations of rubber by a rigid indenter

The studies of the indentation of rubber have developed from work on rubber hardness test. This consists of measuring the increase in penetration depth of a rigid spherical indenter into a flat pad of rubber between the application of defined initial and final loads. International Rubber Hardness Degrees (IRHD) are not quoted directly as the increase in indentation but as numerical values denoted 'IRHD'. The scale of degrees is chosen so that 0 represents the hardness of a material having modulus of zero and 100 represents the hardness of a material of infinite modulus. The basis of the IRHD scale is a probit (integrated normal error) curve relating $\log(\text{modulus})$ to hardness (Figure 3.4.) and this curve is defined by the value of \log Young's modulus at the mid point and the maximum slope of the curve. These values are 0.364 Mpa and 57 IRHD per unit increase in \log Young's modulus respectively. The Young' modulus is calculated from an empirical relation obtained by Scott(41) from a study of the indentation behaviour of various vulcanizates, using two indentors of different radii.

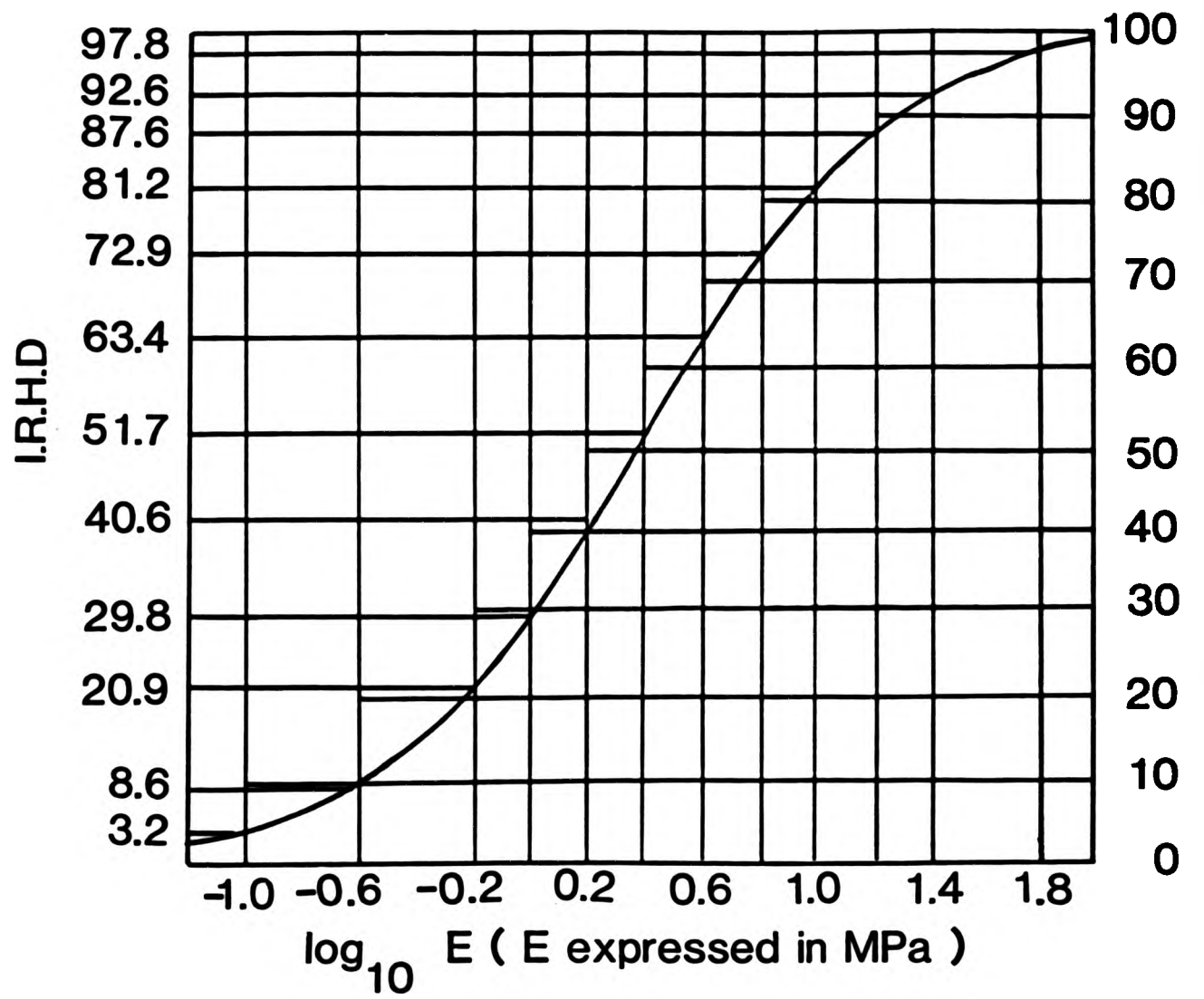


Figure 3.4 Relation of logarithm of Young's modulus, E , to hardness in International Rubber Hardness Degrees.

This relationship is

$$F = 1.91 E_r^{0.65} d^{1.35} \quad 3.6$$

for penetration to a depth not exceeding 80% of the indenter diameter.

For greater penetration, Scott(42) finds that equation 3.6 no longer holds but the theoretical relation of

$$F = 2.67 E_r d \quad 3.7$$

originally derived(43) for a flat-ended indenter applies.

At a very small deformations, the loading condition in the hardness test can also be specified using the Hertzian equation 3.2. Since the Poisson's ratio of rubber is approximately 0.5, and the Young's modulus of the rigid indenter is very high in comparison to that of rubber, then k is approximately $27/64$, i.e., 0.42. Substituting this value of k into equation 3.2, we get,

$$F = 1.78 E_r^{0.5} d^{1.5} \quad 3.8$$

Gent(44) used equation 3.8 and the relationship between the difference in penetration and IRHD to obtain an alternative relation between Young's

modulus and hardness. This relation is represented graphically by the full curve in Figure 3.5(44). The broken curve represents the results obtained using the empirical equation 3.6. The open circles result from experimental measurements. It can be seen from Figure 3.5 that the empirically-obtained relationship of equation 3.6(broken line) is in fairly close accord with that obtained theoretically from equation 3.8(full curve). However, the theoretical curve predicts greater values for Young's modulus than does the empirical relationship at hardnesses exceeding about 60° , and smaller values at hardnesses of less than about 30° . On balance, the experimental points seem to be better represented by the theoretical curve than by the empirical curve.

Equation 3.6 differs from equation 3.8, due to Hertz, in two respects: (a) the constant is 1.91 instead of 1.78, (b) the exponents are 1.35 and 0.65 instead of 1.5 and 0.5 respectively. Rewriting equations 3.6, 3.7 and 3.8 in a form:

$$F = jEr^2(d/r)^n \quad 3.9$$

where j and n are constants, Stiehler et al (45) found that the constants j and n depended on the radius of the spherical indenter: n approaches 1.5 for indentors of large radius and n becomes 1.0 as $r \rightarrow 0$. These are the values of n in

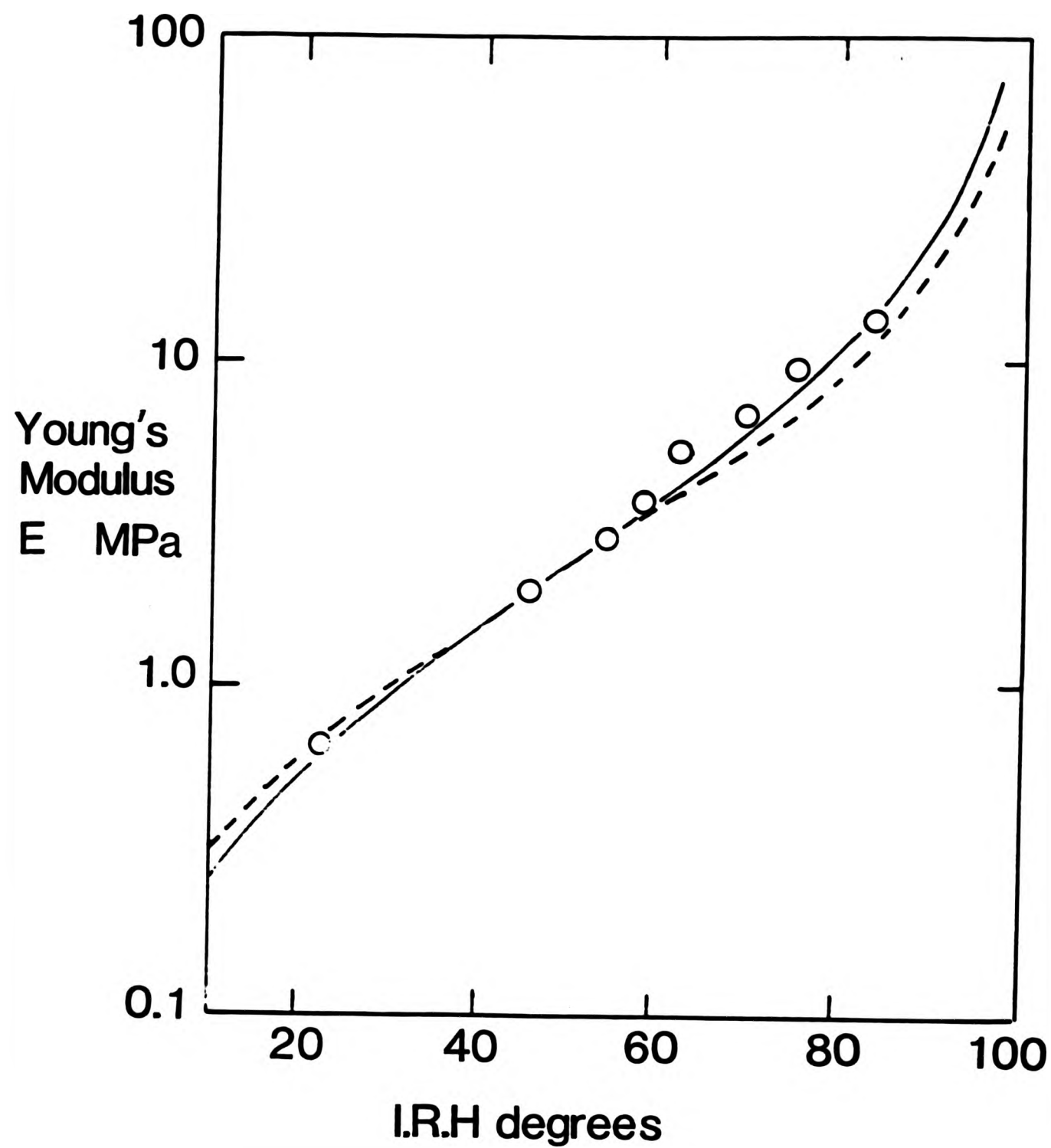


Figure 3.5 Relation of logarithm of Young's modulus, E , to hardness in International Rubber Hardness degrees. Full curve: theoretical relation (equation 3.8). Broken curve: empirical relation (equation 3.6). Open circles: experimental measurements.

equation 3.6 and 3.7, respectively. Correspondingly, the value of j must change from 1.78 to 2.67 as the spherical tip radius changes from infinity to zero.

3.4 Puncture of rubber

The puncturing of rubber was suggested by Vickers and Robinson(46) in 1959 as a means for studying the surface strength or penetration resistance of rubber using a flat-ended cylindrical indenter. They showed that, the higher the resistance to puncture exhibited by a material, the greater tended to be the abrasion resistance of the material. In a recent study(47) by Livingstone et al, using a flat-ended cylindrical indenter, the force required for puncture(i.e., the puncture load) of a number of rubber materials was shown to vary over a wide range of temperature and rate of loading. Upon examining the relation between the puncture load and the indentation depth, two regions of linearity were observed on a plot of logarithm of load versus logarithm of depth of indentation (Figure 3.6). The load-deflection relationship up to puncture was observed to be characteristic of all rubber materials studied, both unfilled and filled vulcanized rubbers. In a detailed study of the relationship between puncture load and indentation depth up to puncture, Yeh and Livingstone(48), using

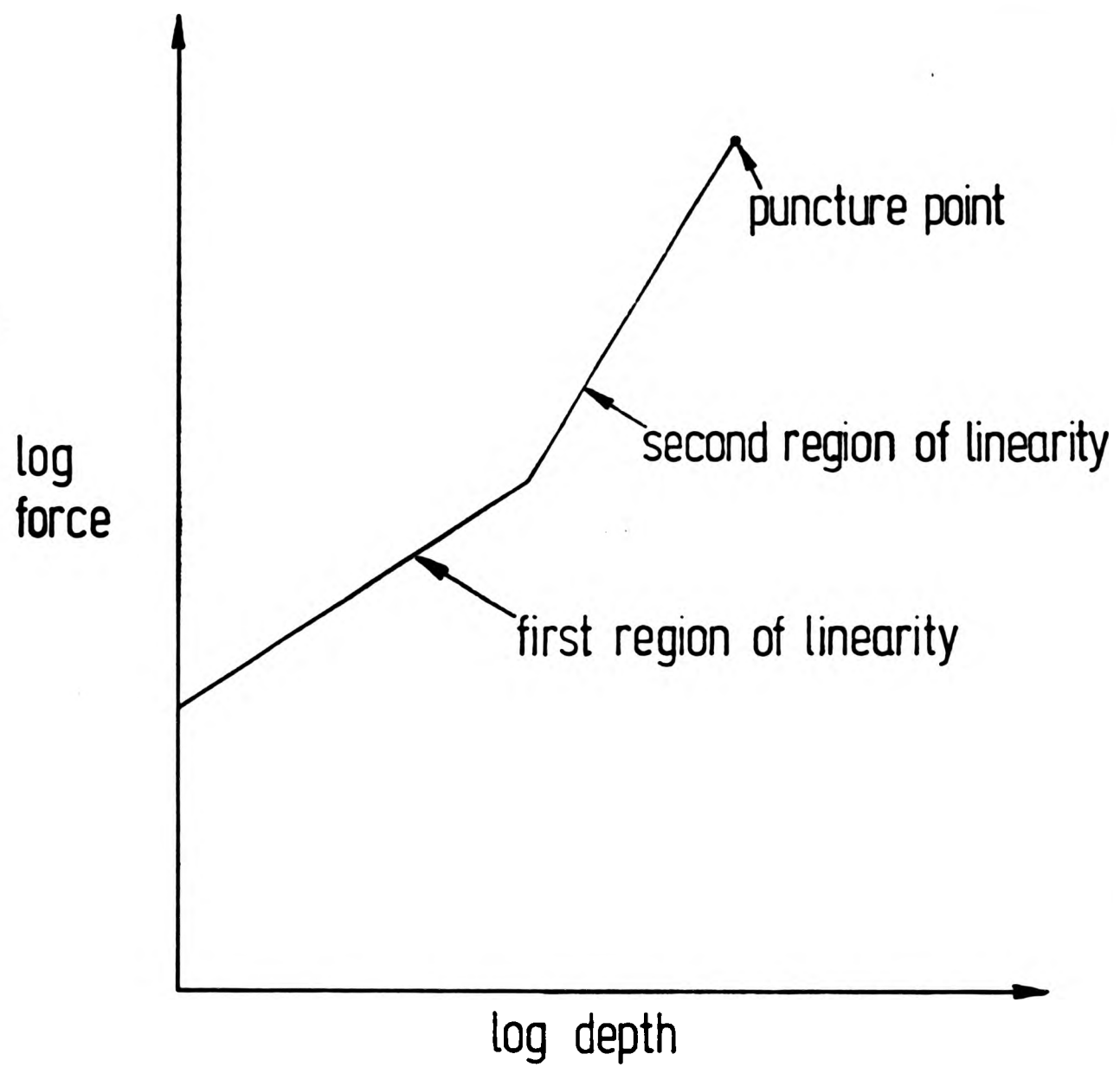


Figure 3.6 Plot of logarithm of force versus logarithm of depth of indentation(48).

flat-ended cylindrical indentors, found that, up to an indentation, d , of approximately four times the radius, r , of the indenter, the 'classical' relation (equation 3.8) holds. For $d > 4r$, the empirical relationship

$$F = 1.34Er^{0.5}d^{1.5} \qquad 3.10$$

was found to describe the behaviour up to puncture. This relationship is similar to equation 3.6, except that the constant is 1.34 instead of 1.78. For a given rubber compound, Young's modulus calculated from equation 3.10 was found to be in satisfactory agreement with the modulus obtained from equation 3.8. In this study, it was also found that the puncture load and depth of indentation were both dependent on compounding variations, and were found to provide useful information concerning matters such as the stiffness and the state of cure of vulcanizates.

It is well known that laboratory abrasion measurements on vulcanizates do not correlate well with roadwear ratings(49). Yeh and Livingstone(48) carried out puncture tests on a series of rubber compounds, and found that the product of puncture load and puncture depth (rather than simply puncture load as suggested by Vickers and Robinson(46)) correlated reasonably well with roadwear ratings.

Livingstone and Hildenbrand(50) compared puncture load and depth of indentation with conventional tensile test results of fourteen different black-filled vulcanizates at two different cure levels. They showed that puncture load and depth of penetration both correlated well with the tensile properties of these vulcanizates.

Dozortsev and Nechiptencho(51) developed a device for evaluating the mechanical properties of rubber by a puncture method. Their device consisted of a 0.4 mm diameter cylindrical indenter which had a hemispherical end. Using the device, Lukomskyer and Dozrotsev(52) showed that there was a direct correlation between the puncture load and the tear strength of the vulcanizates, but not between puncture load and tensile strength.

Using a portable puncture-testing device, Mihalov et al (53) found that puncture loads on tyres under laboratory conditions correlated to a certain extent with the mileage run by tyres in iron-ore quarries. These results led them to suggest that a puncture-test method could be used for checking the quality of large tyres, and also for assessing their remaining service life.

Kusano et al. (54) in 1980 reported the use of a sharp needle in an indentation test method designed to improve the measurement of the plasticity of unfilled unvulcanized rubbers. They defined an

'index of plasticity'(IP) in terms of the work done to penetrate the rubber to a fixed depth. It was found that the IP varied linearly with the logarithm of the indentation rate of the needle, and that the constant of proportionality seemed to depend on the Young's modulus of the sample. It was also observed that the IP correlated well with the Mooney viscosity of the unvulcanized rubber. The reproducibility and accuracy of the measurements were good.

Lindley and Teo(55), investigated the effects of high-temperature ageing on thick rubber blocks using a puncture test. The test was used to obtain the Young's modulus(from the low deformation part of the force-deformation curve and equation 3.8) and the puncture load of small blocks of a natural rubber gum vulcanizate aged for various periods of time at several elevated temperatures(70, 100, 125 and 150°C). Measurements were made, at the various temperatures, of (a) the time, t , at which a hard, brittle skin formed on the blocks(indicated by the rapid increase in Young's modulus), (b) the depth to which the surface layer became discoloured after ageing for one day, and (c) the time for a one-percent weight uptake of oxygen in a special apparatus.

The change in nature of the surface layer was said to be caused by a chemical reaction for which $1/t$ is proportional to its reactionrate coefficient,

q, the temperature dependence of which can be expressed by the Arrhenius equation

$$\ln q = - E_a / RT + \text{constant} \quad 3.11$$

where E_a is the activation energy of the reaction, R is the gas constant and T is the absolute temperature. From this, it follows that the temperature-dependence of t is given by

$$\log_{10} t = \frac{E_a}{2.303RT} + \text{constant} \quad 3.12$$

Arrhenius' plots of $\log_{10} t$ versus $1/T$, in accordance with equation 3.12, produced linear relationships. When the plots were extrapolated to lower temperatures, the following times at which the brittle skin should form were predicted:

temperature, °C	20	30	40	50	60
time, years	434	131	45	16	6

Lindley and Teo showed that the activation energy was the same whether it was obtained from measurements of the time at which a hard, brittle skin formed on the surface, or of the depth after one day of a discoloured oxidized surface layer, or of the time for a 1% uptake of oxygen. These findings

are based on an unfilled vulcanizate under unstrained condition.

However, none of this work on indentation and puncture of rubber dealt with factors which affect the puncture process itself. Recently, the most important features affecting the reproducibility of the puncture test have been studied in some detail(56). The main conclusion from this work is that the interfacial conditions at the indenter/rubber interface exert an important influence in the puncture process and on the reproducibility of the result of the test. There was a small reduction in initial puncture load observed during successive indentations using initially dry and clean indentors and rubber. This was thought to be due to the formation of a thin layer of a material originating from the rubber and acting as a partial lubricant. The geometry of indentors and test-pieces is also an important factor affecting the reproducibility of the puncture test. In particular, the sharpness of the tip of the indenter was found to be a dominant factor affecting the puncture process.

Work published so far has shown the indentation puncture test to be an effective tool for investigating the mechanical properties of the rubber. However, so far as the present author is aware, the puncture of rubber has not been studied in terms of fracture obtained by workers on puncture

using different geometry indentors and with other results on the strength of rubber, due to the dependence of the results on unknown geometrical factors, such as sharpness and diameter.

In the present work, an attempt has been made to analyse the mechanisms and mechanics of the puncture process in terms of fracture mechanics. This requires the derivation of a relationship relating tearing energy to readily-measurable quantities such as puncture load and penetration depth at puncture, which can be obtained from a force-deformation curve.

3.5 Cutting of rubber

Rubber articles, including tyres and belting, are known to fail in service due to cutting by sharp objects. Dobie(57) analysed the reasons for returns of car tyres under the warranty programme of a major US tyre company. He concluded that cutting was a major cause of failure for all the tyres returned.

In addition to being a major cause of failure in its own right, cutting is also responsible for the initiation and aggravation of other failure processes. Cracking at the base of the tread grooves is a common cause of failure in car and truck tyres. According to a theory of groove cracking proposed by Clapson and Lake(16), a minimum crack length of about

1 mm has to be present initially before groove cracking can occur. Cutting by sharp stones is believed often to be responsible for the initiation of cracks of this size.

In view of the practical importance of cutting, it is not surprising to find that rubber companies have devised ad hoc tests in attempting to evaluate compounds for relative resistance to cutting. Dobie(57) described a test-track consisting of a concrete trough filled with pieces of broken glass, well-hosed down with water, over which tyres were run. A similar test-track containing metal hazards placed at intervals was also described. The use of such test-tracks is quite common in the tyre industry.

Werkenthin(58) described a wire cutting test said to be suitable for testing rubber gloves. This test uses a standard dumbbell specimen doubled over and held in the jaws of one of the clamps of a tensile testing machine. A piano wire is held in the other clamp so that it passes through the loop formed by the rubber dumbbell. The clamps are separated at a constant speed and the force necessary to sever the dumbbell specimen by the wire is recorded as the cutting resistance of the rubber.

Dunn et al.(59) used a guillotine with a blunt blade to evaluate the resistance to 'chipping' of tyre-tread compounds.

In spite of the importance of cutting as a practical failure process, and of attempts to evaluate cutting resistance by ad hoc methods, there appears to have been relatively little work carried out on fundamental aspects of the problem.

Lake and Yeoh(60,61) studied cutting, a fracture mechanics approach. They used a technique in which a razor blade was applied to the tip of a crack in a stretched test-piece, so that the friction between the rubber and the razor blade was minimal. Their analysis was simplified because the geometry of the test-piece used was amenable to simple fracture mechanics calculations. Two forms of cutting were identified by Lake and Yeoh: one is a slow, time-dependent process which occurs when the force applied to the blade is less than a critical values; the other is a rapid, catastrophic process which occurs when the applied force is greater than or equal to the critical value. 'Catastrophic' cutting was studied in some detail by these workers. They found it to be markedly dependent on the deformation of the test-piece. The deformation was assessed quantitatively in terms of a fracture mechanics analysis(60,61).

CHAPTER FOUR
EXPERIMENTAL METHOD

4.1 Experimental apparatus

A puncture test was carried out on a universally test machine, which was either a J.J. Lloyd T5k testing machine or an Instron 1122 testing machine as shown in Figure 4.1. The main feature of the test is the indentation and rupture of the surface of a rubber block by a cylindrical indenter clamped in a pin chuck mounted in the test machine crosshead. Successive indentations can be made on fresh portions of the rubber surface by moving the rubber.

Various test blocks of rubber can be used. They were supported on a 23 x 23 x 2.5 cm rubber 'backing block'. During an indentation, the presence of a backing block beneath a rubber test block is important, in order to avoid the indenter penetrating the underside of the test block, contacting the metal plate of the load cell and being damaged. A close-up view of the rubber test block, the backing block, the indenter and the load-cell is shown in Figure 4.2



Figure 4.1 Experimental arrangement for puncture test.

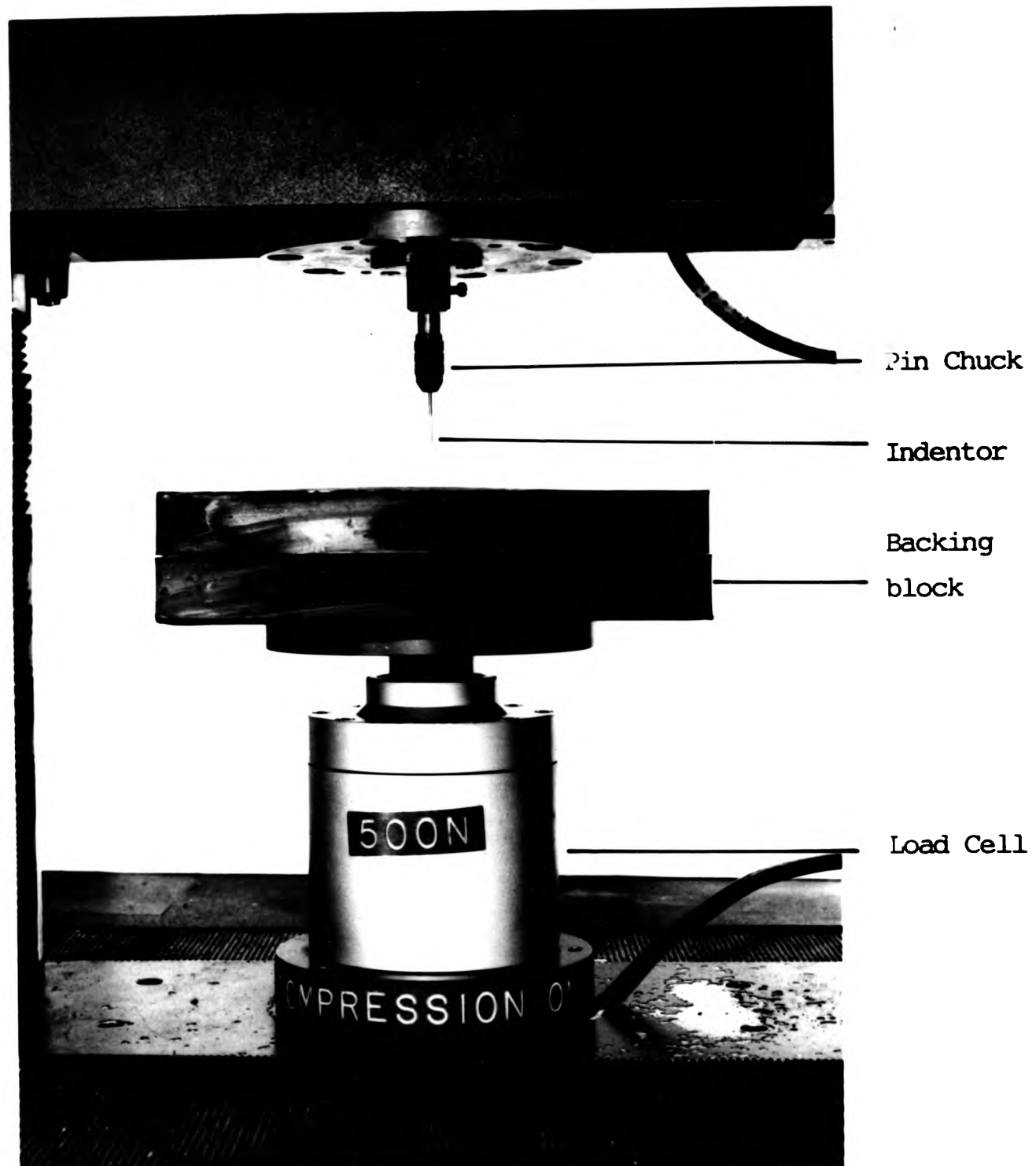
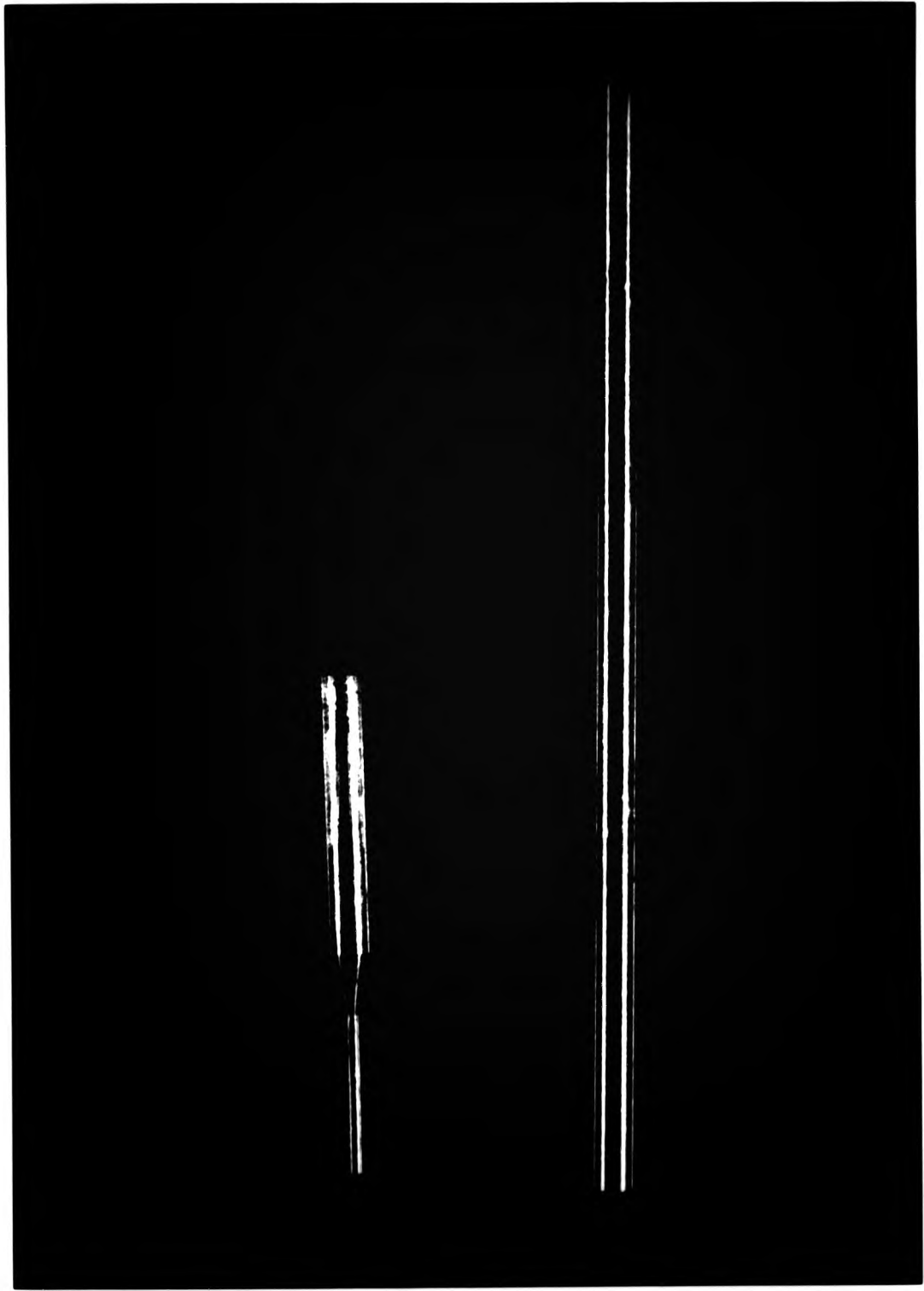


Figure 4.2 Close-up view of the rubber test block, the backing block, the indentor and the load-cell.

All the work described in this thesis was carried out using 1.5 and 0.5-mm diameter indentors made of Ti-64 (Titanium 89%, Aluminium 6%, Vanadium 4%). Typical titanium indentors of 1.5 and 0.5-mm diameter are shown in Figure 4.3.

The indenter ends were polished on a Kent Lapping Machine, first with 35 μm carborundum grinding paste for about ten minutes followed respectively by 14, 6 and 1 μm diamond paste, each for ten minutes. A typical scanning electron micrograph of the corner of an indenter (1.5-mm diameter) polished in this way is shown in Figure 4.4. The aim of this grinding was to produce corner angles of approximately 90° . The 'corner radius' (see Figure 4.5) of the indenter shown in Figure 4.4 was about 8 μm .

Indentors having larger corner radii were prepared by a diamond polishing company, Agate Products Limited, who had facilities to produce indentors with different corner radii to a tolerance of 5%. A typical micrograph of an indenter (1.5 mm Ti-64) of large corner radius (750 μm) is shown in Figure 4.6. Figure 4.7 shows another typical micrograph of an indenter of large corner radius (250 μm) for a 0.5 mm Ti-64 indenter.



(a)

(b)

Figure 4.3 Ti-64 indentors: (a) 0.5-mm diameter
(b) 1.5-mm diameter.



Figure 4.4 Typical electron micrograph of the corner of a polished indenter (1.5 mm diameter)

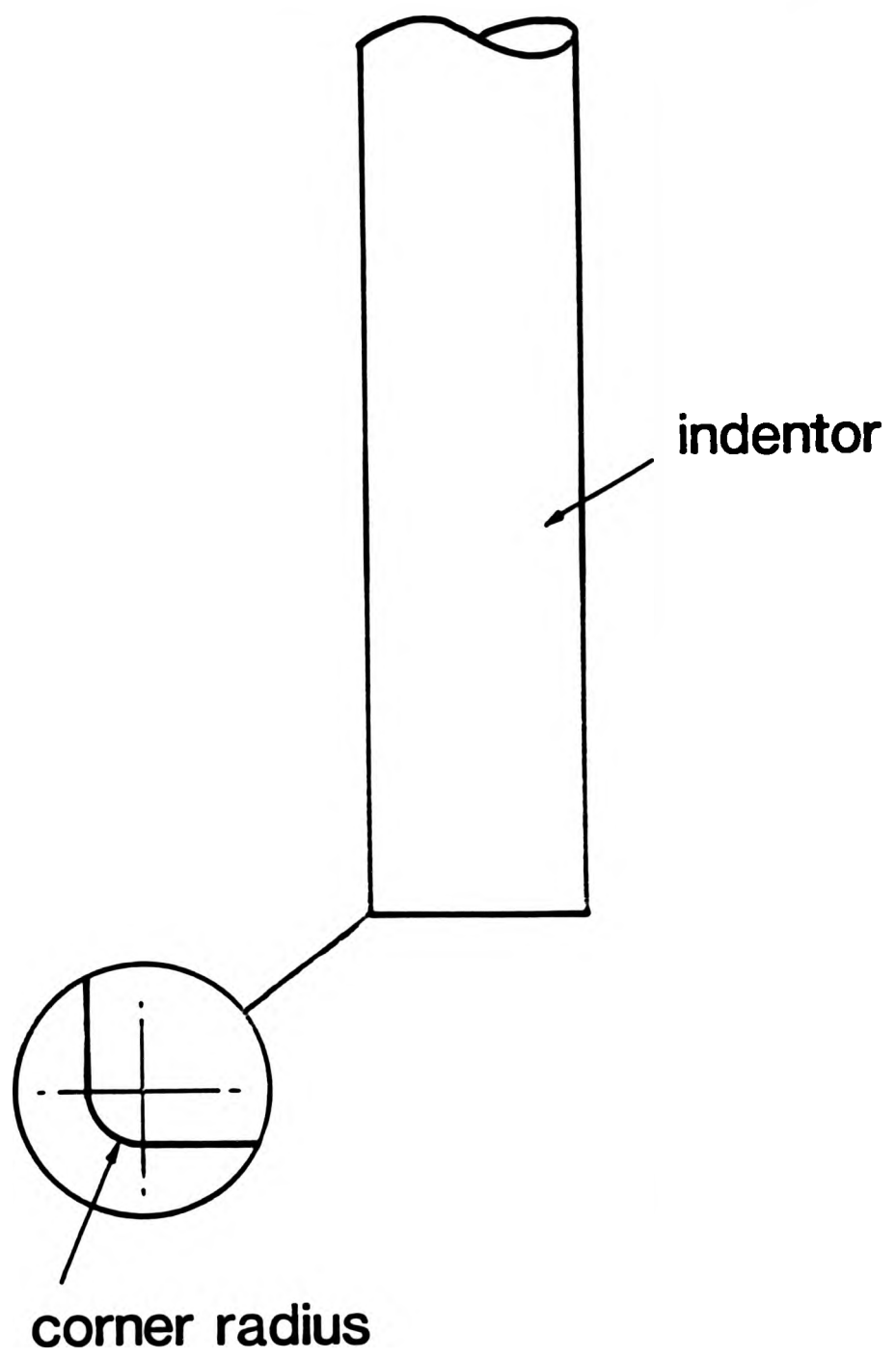


Figure 4.5 Corner radius of an indenter.



Figure 4.6 A typical micrograph of a 1.5-mm indenter of a large corner radius (750 μm).



Figure 4.7 A typical micrograph of a 0.5-mm Ti-64 indenter of large corner radius (250 μm).

4.2 Test pieces

Most of the rubber test blocks were of dimensions 2.5 x 2.5 x 2.5 cm and 23 x 23 x 2.5 cm. Details of formulations, and of the times and temperatures of vulcanization, for all the vulcanizates used in this work are shown in Table 4.1. However, some of the rubbers tested were used components. They were of different dimensions and formulations.

4.3 Experimental procedure

The puncture test consisted of indenting a rubber surface at a constant rate with an indenter until the rubber surface ruptured. The indentation force at rupture is referred as the 'puncture load'. All the puncture tests were carried out at an indentation rate of 5 mm per minute unless otherwise stated.

A typical indentation force-deflection curve is shown in Figure 4.8. This curve is for vulcanizate A using a 1.5 mm diameter indenter. The point of puncture (the point X in Figure 4.8) is characterised by a catastrophic drop in the indentation force. At this stage the indenter can be withdrawn if the cross-head movement is reversed. If indentation continues after puncture, a second

Table 4.1 Vulcanizate formulations (parts by weight)

	A	B	C	D	E	F	G	H	I	J	K
	100	100	100	100	100	100	100	100	100	100	100
Natural Rubber	3.5	3.5	3.5	-	5	-	-	-	-	3.5	3.5
SMRCV	-	2	2	-	1	-	-	-	-	-	-
Zinc oxide	2	-	-	-	-	-	-	-	-	-	-
Zinc-2-ethyl hexanoate	2	-	-	-	-	-	-	-	-	2.0	2.0
Stearic acid	-	1.7	1.7	-	1.7	-	-	-	-	-	-
MOR ¹	-	0.7	0.7	-	0.7	-	-	-	-	-	-
TBTD ²	20	-	50	-	85	-	-	-	-	-	25
Carbon black											
SRF (ASTM-N-762)											
Process oil ³	20	-	-	-	-	-	-	-	-	5	5
Antioxidant ⁴	-	2	2	-	2	-	-	-	-	-	-
HPPD ⁵	3	-	-	-	-	-	-	-	-	3	3
Wax ⁶	4	-	-	-	-	-	-	-	-	2	2
CBS ⁷	0.7	-	-	-	-	-	-	-	-	0.7	0.7
Sulphur	2.5	0.7	0.7	-	0.7	-	-	-	-	2.5	2.5
Dicumyl peroxide	-	-	-	1.0	-	3.0	4.0	2.0	5.0	-	-
Cure } Temperature °C	141	140	140	150	141	150	150	150	150	141	141
Schedule } Time hours	1	1	1	2	1	2	2	2	2	1	1

1 N-oxydiethylenebenzothiazole-2-sulphenamide

2 Tetrabutylthiuram disulphide

3 Fina Process Oil 2059 (Petrofina)

4 N-Isopropyl-N'-phenyl-p-phenylenediamine

5 N-(1,3-dimethylbutyl)-N'-phenyl-p-phenylenediamine

6 Sunproof Improved (Uniroyal)

7 N-cyclohexylbenzothiazole-2-sulphenamide

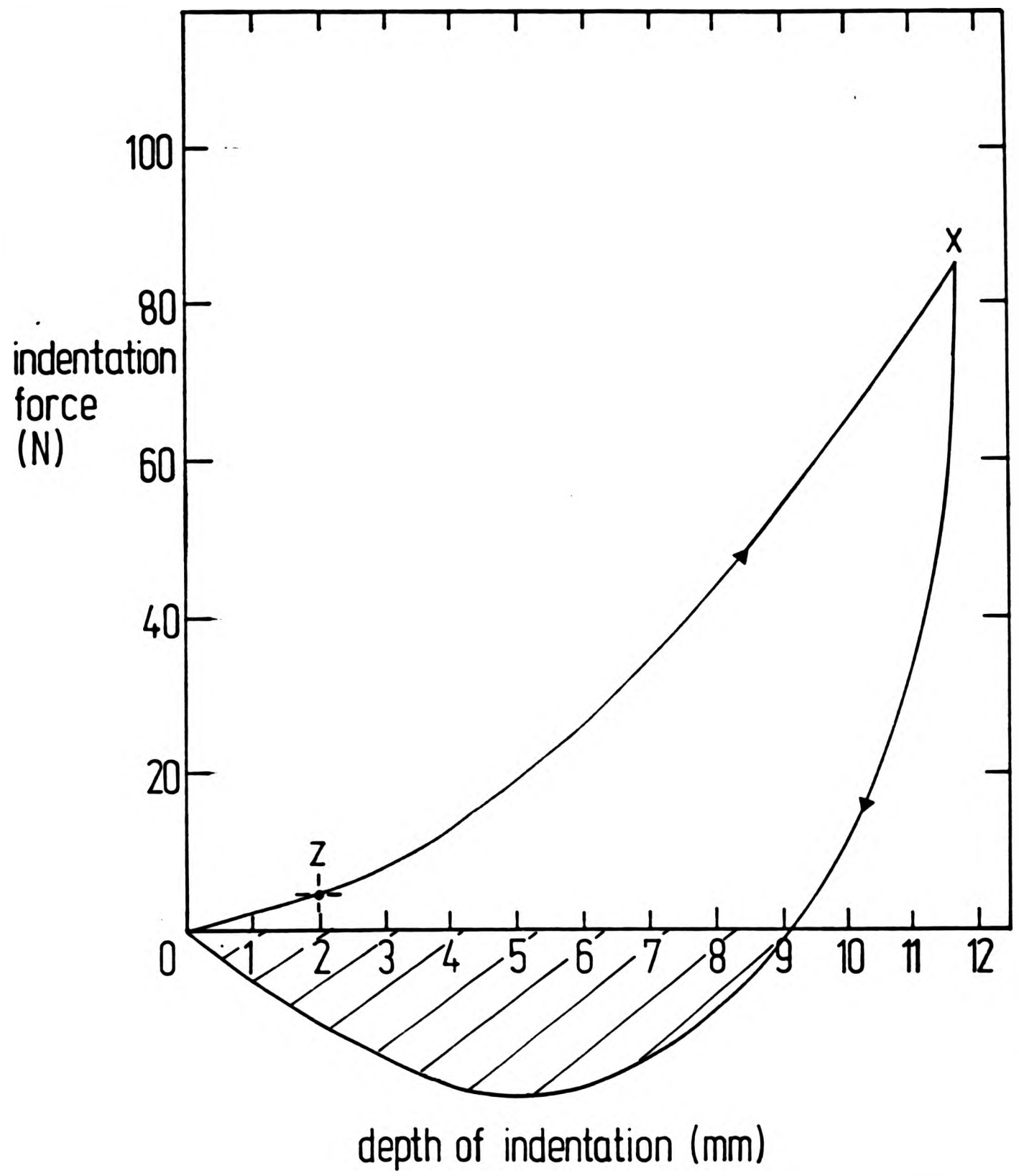


Figure 4.8 A curve showing the typical relationship between indentation force and the depth of indentation.

puncture is possible. This phenomenon will be discussed in detail in Chapter Six.

The negative loads shown in Figure 4.8 represent pull-out loads resulting from adhesion between the rubber and the indenter. The shaded area is the work done during the pull-out. The latter area is not very reproducible, as it is sensitive to the exact moment after puncture at which the indenter direction is reversed. This moment is difficult to control precisely. The deeper the indenter penetrates after puncture, the greater will be the work done because of the increased area of contact between the rubber and the indenter surface.

The initial section(0 - Z) of the curve shown in Figure 4.8 is linear. In this region, the classical relation(equation 3.7) can be used to determine the Young's modulus (when indentors of low corner radius are used).

On any given block of rubber, puncture load can be expressed either as a mean value of several puncture loads(P') or puncture load obtained from one measurement at one location. The mean value of puncture loads was obtained by carrying out a number of puncture tests spread across the rubber surface. The number of tests depended upon the size of the rubber block and the spacing between the indentations. The mean puncture loads can be expressed together with coefficient of variation

(C.V.). The latter is defined as the standard deviation (σ) of a group of puncture loads expressed as a percentage of the mean of the group, i.e.

$$\text{C.V.} = \frac{\sigma}{P'} \times 100\%$$

where

$$\sigma = \left[\frac{1}{n-1} \sum_{i=1}^n (P_i - P')^2 \right]^{\frac{1}{2}}$$

P_i and n are the puncture load and the number of puncture events respectively.

The reproducibility of the puncture test will be discussed in the next chapter.

4.4 Experimental precautions

To ensure that the puncture test was carried out consistently, each rubber surface was cleaned to free it from dirt, bloom etc. A standard cleaning procedure was therefore adopted. This consisted of cleaning the rubber surface with either analytical reagent (A.R.) acetone or A.R. propan-2-ol. The same procedure was also adopted to clean the indenter surface so that it was free from materials such as dirt and grease.

In addition, tests were carried out to determine the effect of small environmental changes

in temperatures and relative humidity on puncture load. A 0.5 mm diameter Ti-64 indenter was used on a vulcanizate A. The results over a period of about four years (see Figure 4.9) indicated that small changes in relative humidity and temperature had no significant effect on puncture load.

4.5 Measurement of tearing energy using trouser tear test

The dimensions of the trouser test-pieces used in this work are shown in Figure 4.10. The test-pieces were extended at the rate of 100mm/minute using the Instron machine. Figure 4.11 illustrates a typical tearing force and deflection characteristic showing the tear propagates in a series of jumps. The values of F_p and F_s correspond to tearing forces at which the tear propagates and stops respectively. The tearing force was then measured from the average value of F_p .

In Chapter Two it was shown that the tearing energy equation for the trouser tear test is

$$T = \frac{2F\lambda}{h} - wW$$

where F is the tearing force, λ the extension ratio, w is the width of one of the legs, W is the strain energy density in the legs, and h is the width

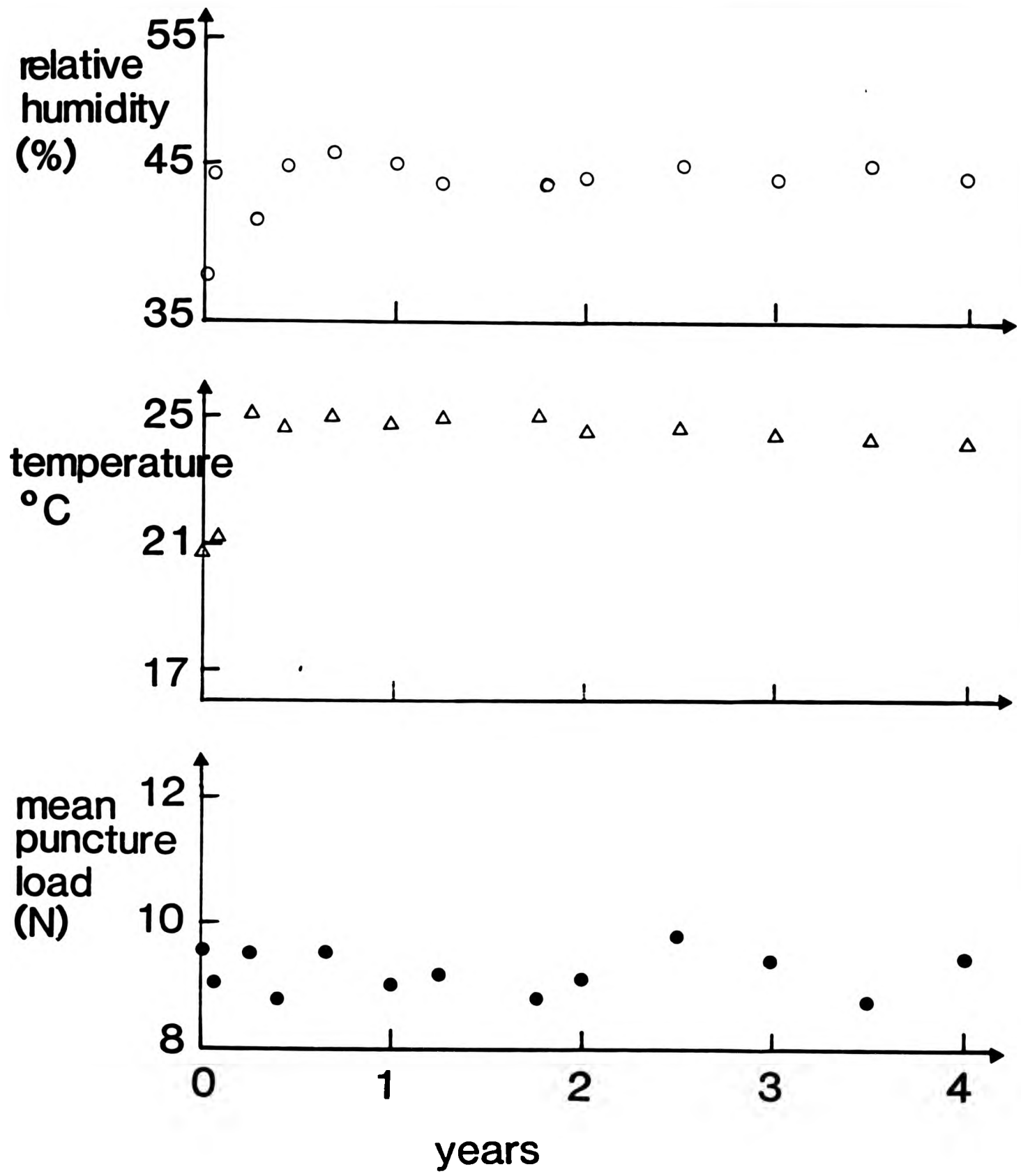


Figure 4.9 Effect of small environmental changes in relative humidity and temperature on puncture load over a period of about four years.

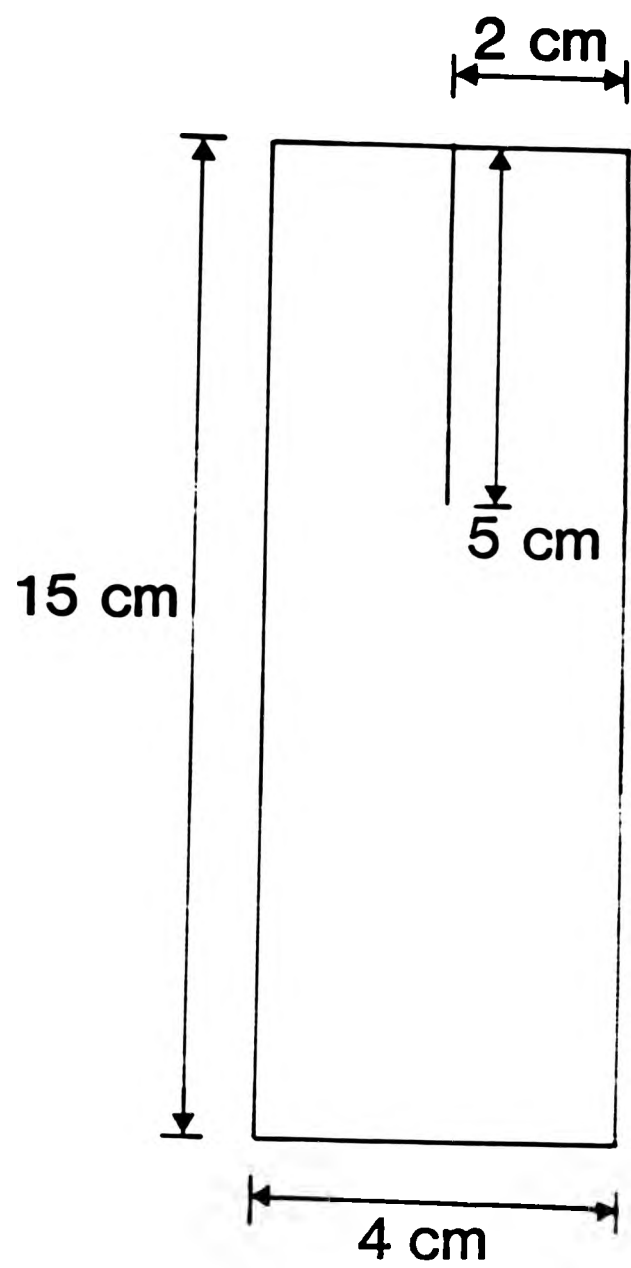
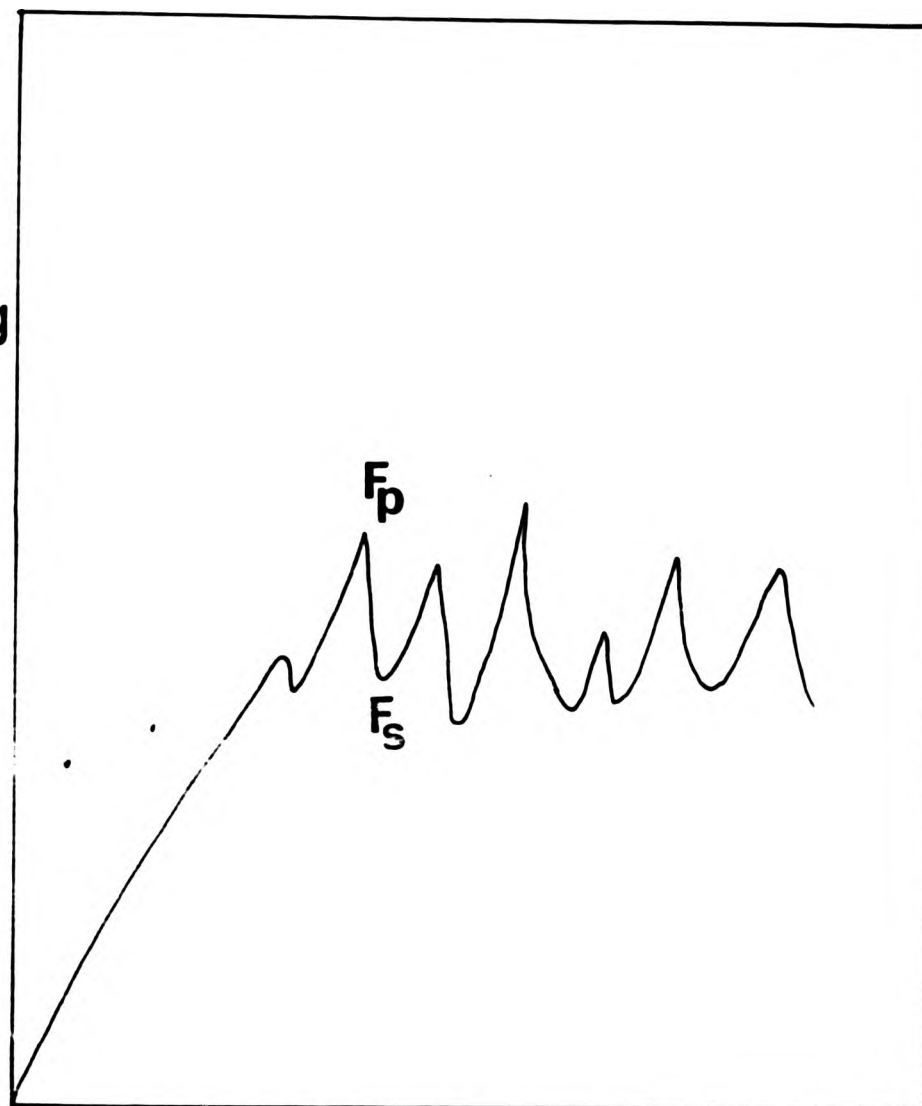


Figure 4.10 Dimensions of trouser tear test-piece in unstrained state.

tearing
force



extension

Figure 4.11 Tearing force versus extension.

of the tear path. The value of h was measured from the average test-piece thickness. When the test-piece tore at an angle as shown in Figure 4.12, h is equal to the thickness of the test-piece divide by $\sin\theta$.

In order to obtain the value W and λ , a test-piece whose dimensions were similar to the legs of the trouser tear test was subjected to a simple extension at the rate of 100mm/minute. From the force /deflection curve such as shown in Figure 4.13, W could be obtained by dividing the area under the curve by the volume of the test-piece. Knowing the tearing force, λ in each leg of the test-piece could also be determined from Figure 4.13.

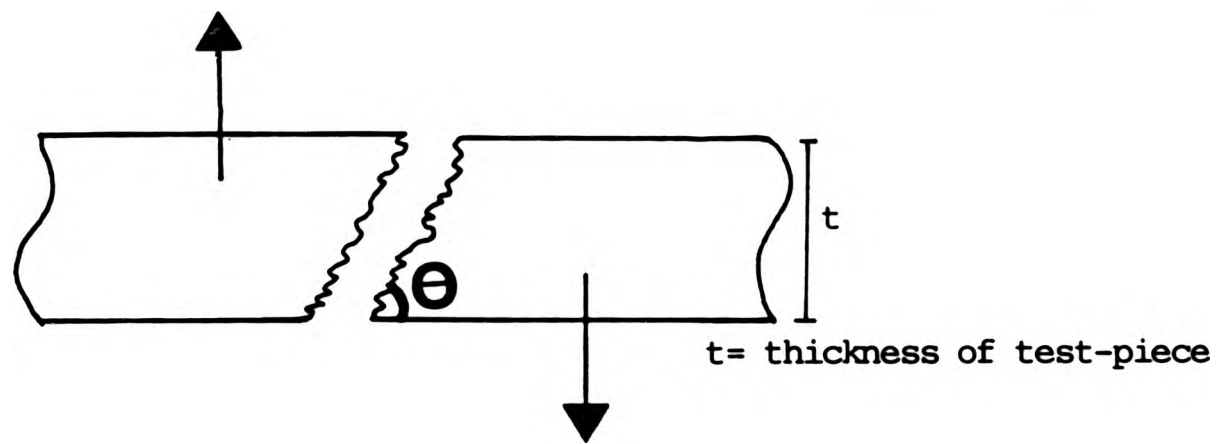


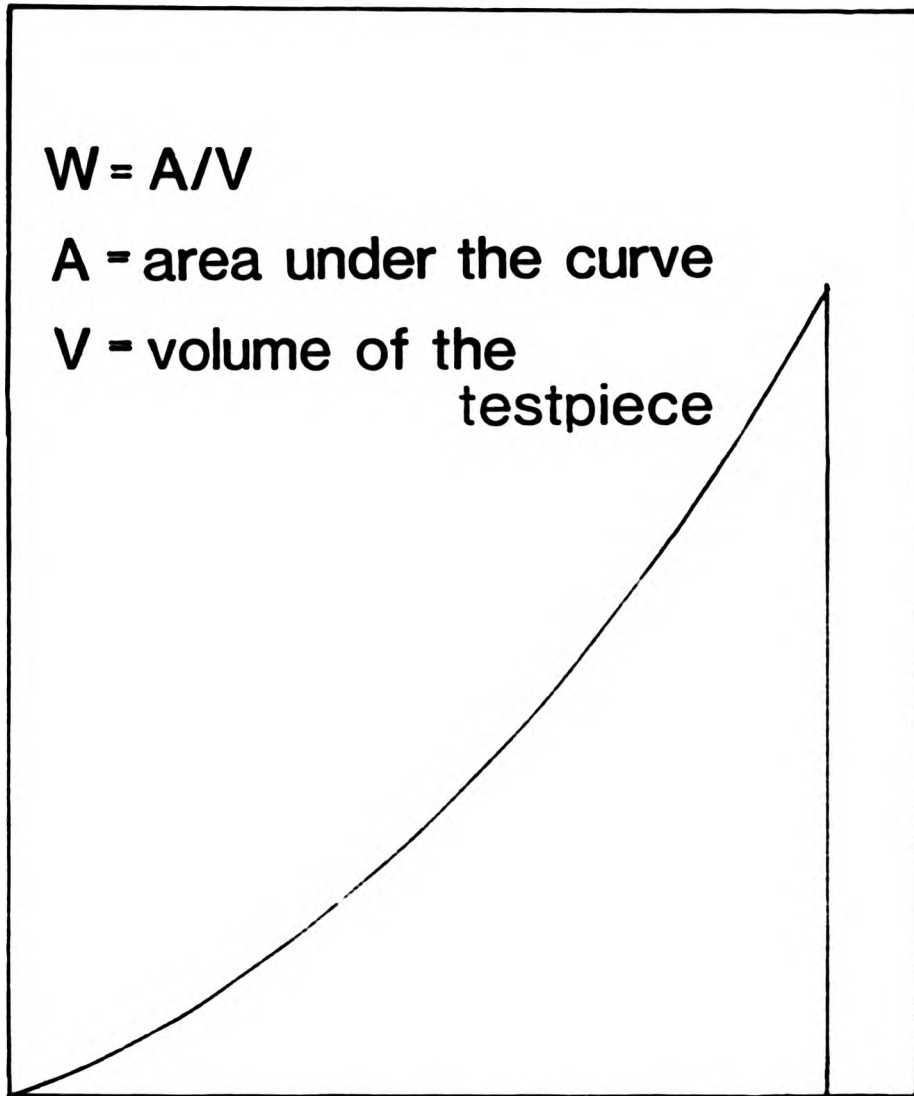
Figure 4.12 Trouser tear test showing tear angle.

force

$$W = A/V$$

A = area under the curve

V = volume of the
testpiece



deflection

Figure 4.13 Determination of strain energy density, W , of the trouser tear test.

CHAPTER FIVE
SOME FACTORS AFFECTING THE RESULTS OF
THE PUNCTURE TEST

5.1 Interfacial conditions

Each individual puncture event involves local contact between the metal of the indenter and the rubber surface followed by slippage between the indenter and the rubber. The interfacial conditions may therefore be expected to exert an important influence on the puncture process, and hence on the reproducibility of the test. For example, the degree of lubrication present at the interface may be expected to be influential. Recent work(62) has shown that a thin layer of rubbery material can form on indenter surface during puncture, and this will be expected to provide some form of lubrication. This formation of rubbery material occurs on titanium, tungsten carbide and steel indentors.

It has also been suggested that lubrication was responsible for the initial reduction of puncture load observed when successive indentations have been carried out using initially clean and dry indentors

and clean dry rubber(see Figure 5.1). This initial variation in puncture load can be avoided by cleaning the indenter between each indentation or by adding liquid lubricants to the rubber surface. A satisfactory lubricant was Tri-flon, a PTFE(polytetra fluoro ethylene)-based liquid lubricant consisting of PTFE particles dispersed in a low-viscosity liquid solvent which acts as a carrier film. However, there is a possibility of some interactions for example, swelling of the rubber by the solvent. Swelling may weaken the rubber surface, and so reduce the load required to puncture the rubber. This can be seen in Table 5.1, showing the mean puncture load values of vulcanizate B, before and after one day immersion in n-decane and in ASTM-3 oil. The indenter used was a 0.5 mm diameter Ti-64 indenter with corner radius of 10 μm .

To separate the effects of swelling and lubrication on puncture load, an investigation was carried out using vulcanizate B with Tri-flon and silicone oil(12,500 cst) as lubricants. The puncture tests were first carried out on lubricated surfaces. The tests were then repeated on the same surfaces, but after the lubricants had been cleaned away with a solvent. The test results on the cleaned surfaces should correspond to the results obtained on an unlubricated surfaces if the lubricants do not swell the rubber.

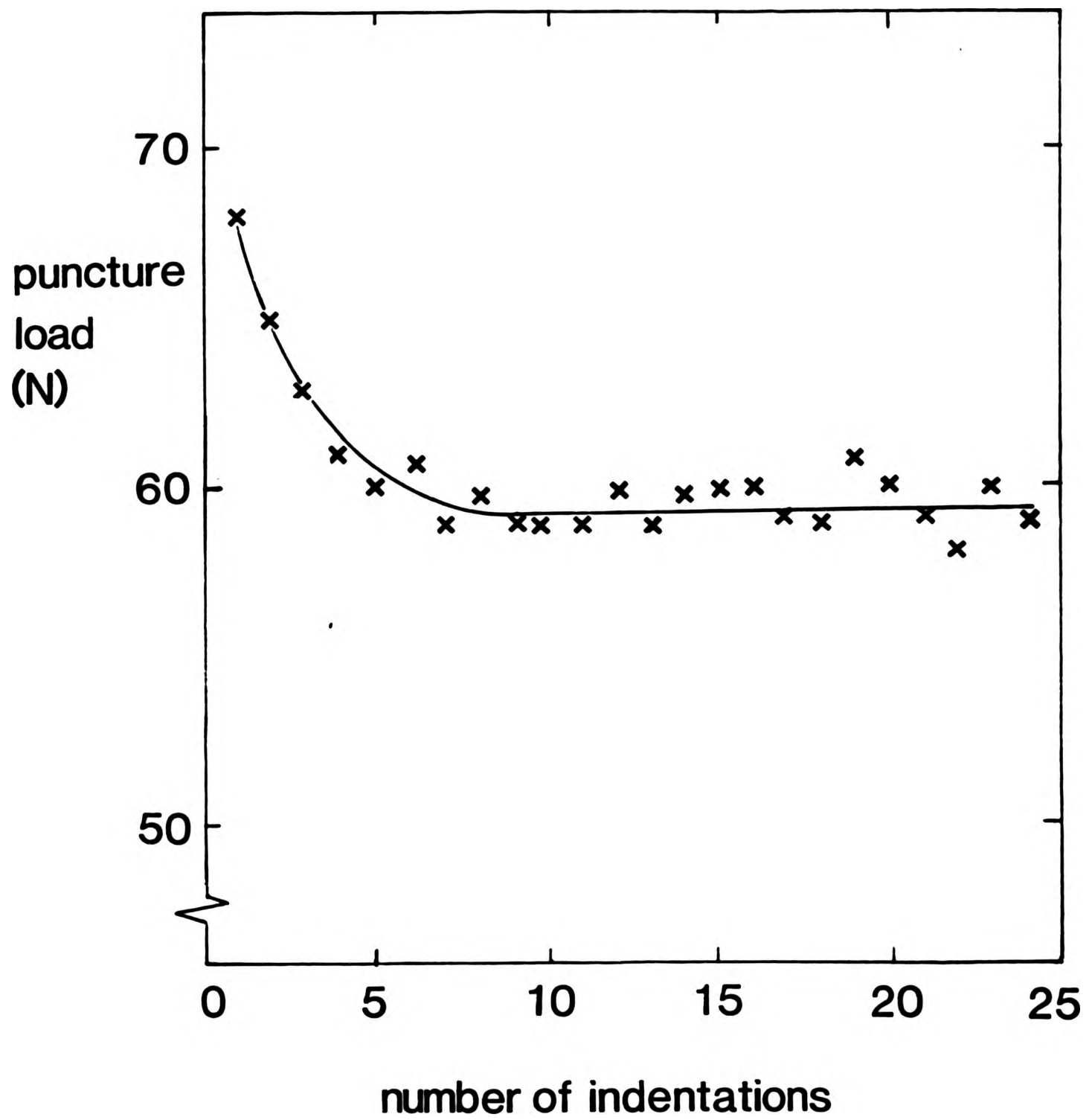


Figure 5.1 Variation of puncture load with number of indentations(62).

Table 5.1 Effect of one day immersion in n-decane
and in ASTM-3 oil

Vulcanizate B
0.5 mm indenter

	mean puncture load
	N
n-decane	8.5
ASTM-3 oil	6.0
dry control sample	12.5

Table 5.2 shows the puncture loads of vulcanizate B using the two lubricants. The indentors used were 1.5 and 0.5 mm diameter Ti-64 indentors with corner radii of 60 and 10 μm respectively. The results indicate that there is some interaction between the rubber and the Tri-flon during the initial contact, which led to the reduction in the puncture load. Cleaning the lubricant appears only to remove it from the rubber surface. On the other hand, it appears that there is no interaction between the silicone oil and the rubber; after cleaning with the solvent, the puncture load reverts to the value for an unlubricated surface.

On the basis of these results, all the puncture tests described in the subsequent chapters were carried out using the silicone-oil lubricant. For unlubricated tests, the indentors were cleaned before each successive indentation.

5.2 Effect of rubber thickness and hardness of backing blocks

Rubber components are made with rubber of different thicknesses. Therefore when testing these components it is essential to know how puncture load is affected by rubber thickness. In the present work, the vulcanizates B and C were used to

Table 5.2 Effect of lubricants on puncture load

Vulcanizate B

Lubricants	<u>mean puncture load in N</u>			
	<u>1.5 mm indenter</u>		<u>0.5 mm indenter</u>	
	lubricated	cleaned	lubricated	cleaned
Tri-flon	110	120	7	9
Silicone-oil	108	164	7	11.5
(12,500 cst)				
	unlubricated 165 N		unlubricated 12 N	

investigate the effect of the thickness of the rubber sample. The hardnesses of these vulcanizates were 32 and 56 IHRD respectively. The indentors used were 1.5 and 0.5 mm Ti-64 indentors whose corner radii were 30 and 10 μm respectively.

As described in Section 4.1, it was found to be essential to use backing blocks in the experimental arrangement for puncture testing. In this investigation of effect of rubber thickness, the backing blocks used were made from vulcanizates B and C (see Table 4.1).

Figure 5.2 shows the results of puncture tests on different thickness blocks of vulcanizate B using 25 mm thick backing blocks. The tests were carried out with a 1.5 mm diameter Ti-64 indenter lubricated and unlubricated. The results suggest that when the hardness of the backing block is dissimilar to that of the test-piece, then in both lubricated and unlubricated conditions the thickness of the test-piece should exceed about 20 mm in order to avoid thickness dependence.

Figure 5.3 shows the results of puncture tests on vulcanizate B lubricated and unlubricated using a 0.5 mm diameter indenter and 25 mm backing blocks. The results show that in both lubricated and unlubricated tests the puncture loads seem to be independent of test-piece thickness above about 5 mm.

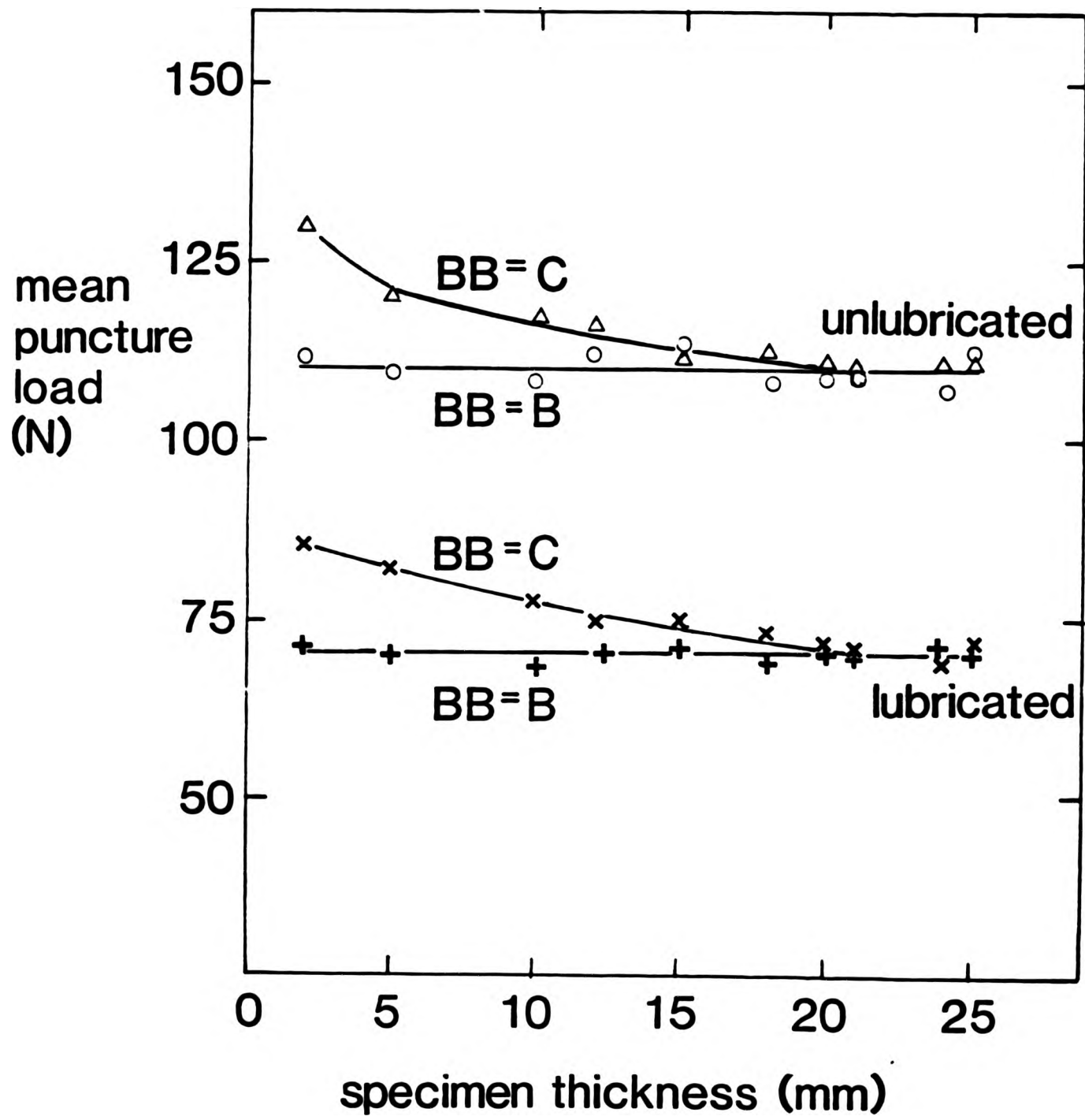


Figure 5.2 Variation of mean puncture load with different thicknesses of vulcanizate B. Backing blocks(BB) are B and C. Indentor: 1.5-mm Ti-64.

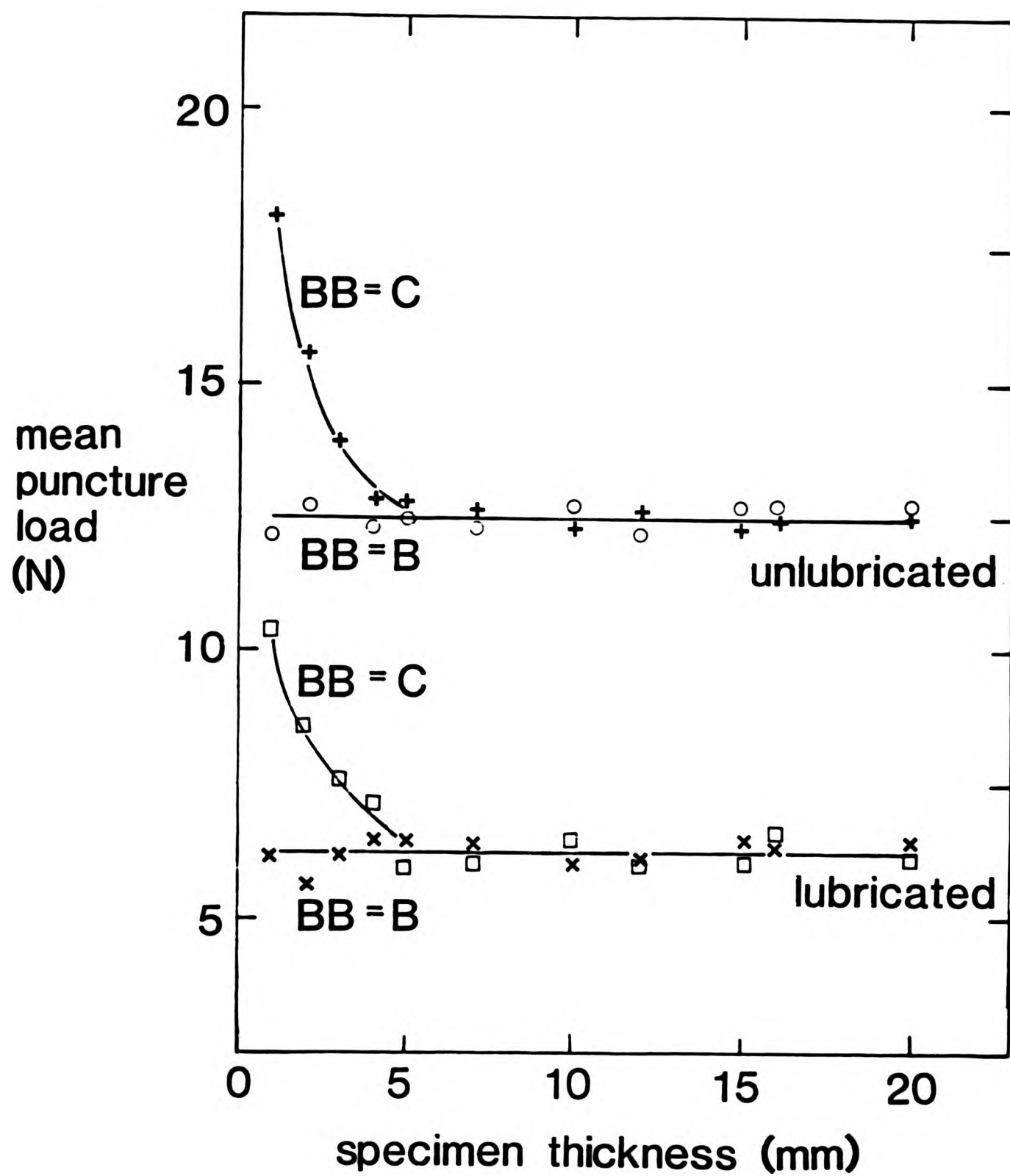


Figure 5.3 Variation of mean puncture load with different thicknesses of vulcanizate B. Backing blocks(BB) are B and C. Indentors: 0.5-mm Ti-64.

5.3 Effect of proximity between successive indentations and of distance of indentation from free edge of test block

In some cases the available test-piece area may be small. Successive punctures therefore have to be carried out as close together as possible. It is therefore essential to know the minimum distance between successive indentations which is necessary to ensure that the puncture load is not affected by the presence of neighbouring puncture holes.

A number of puncture tests were carried out to investigate the effect of distance between successive indentations. 1.5 and 0.5 mm diameter Ti-64 indentors were used. The results are shown in Figure 5.4. They indicate that, for a 1.5 mm indentor using the lubricant, a distance of about 1 mm or more, was required between each indentation before distance had no effect on puncture load. If the test was carried out without lubrication, the minimum distance increased to 4 mm. For a 0.5 mm diameter indentor, the minimum distance is about 1.0 mm regardless of whether or not the lubricant is used.

Puncture tests were also carried out to determine the minimum distance from the free edge of the test-piece which is necessary to ensure that proximity of the edge does not affect the puncture

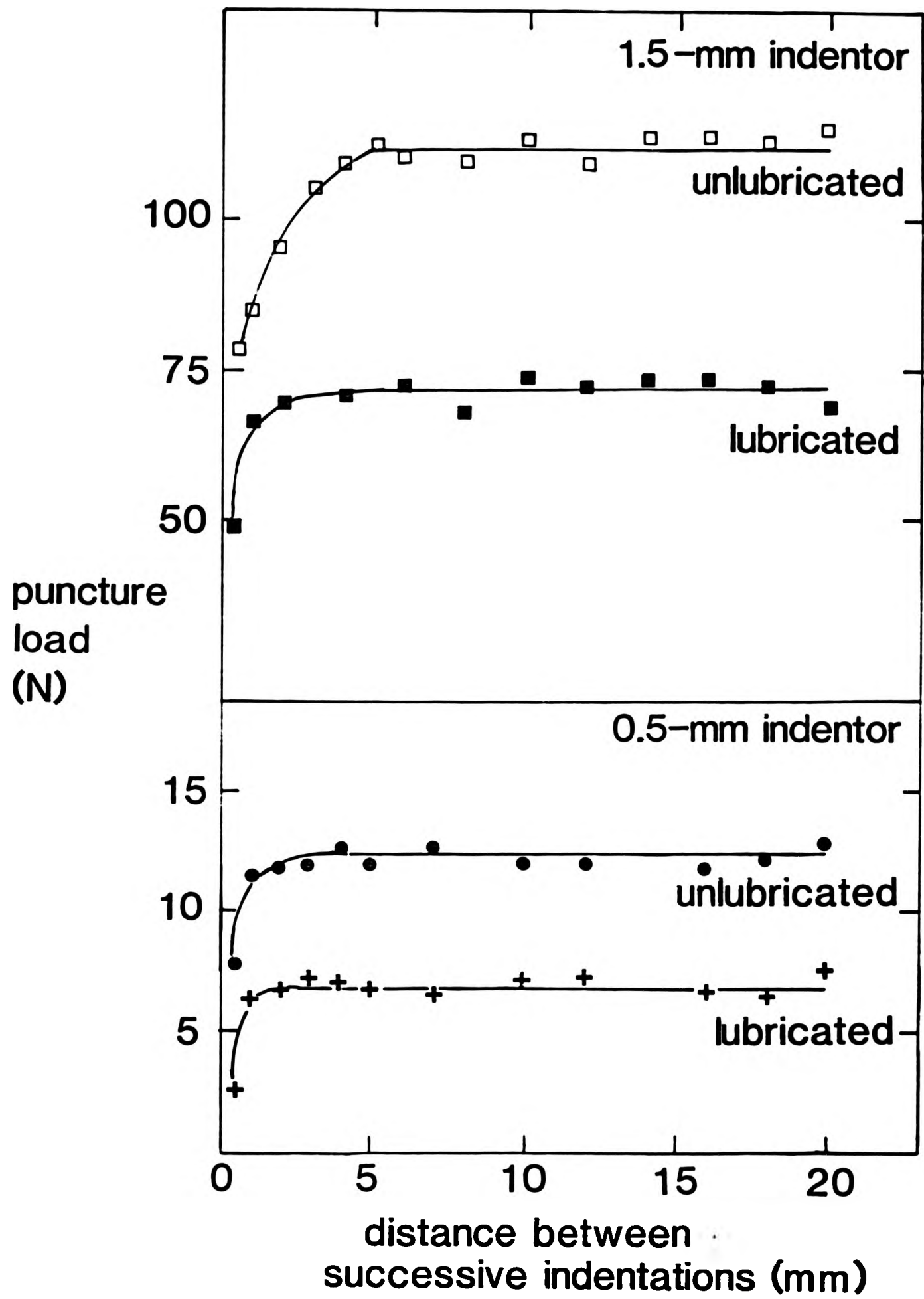


Figure 5.4 Variation of puncture load with distances between indentations. Vulcanizate B.

load. The tests were carried out using 25 mm thick blocks of vulcanizate B, and 0.5 and 1.5 mm diameter indentors with and without lubrication. It was found that the tests had to be performed at least a certain minimum distance from the free edge to prevent the indentors from bending. These distances were about 5 and 20 mm for the 0.5 and 1.5 mm diameter indentors respectively. When subsequent tests were performed at not less than these distances away from the free edge, there was no significant effect of distance on puncture load, as shown in Figure 5.5.

Tests were also carried out on thinner test-pieces with a backing block of similar hardness to that of the test-piece. In addition, the edge of the test-piece was positioned at least 5 and 20 mm away from the edge of the backing block for 0.5 and 1.5 mm diameter indentors respectively. The results of the tests for various test-piece thicknesses are given in Table 5.3. This table shows the minimum distances of the test from the free edge such that this distance does not affect the puncture load.

5.4 Surface condition of test-pieces

In testing thick rubber articles, it is necessary sometimes to obtain measurements on rubber below the surface. In addition, the rubber articles may not have a convenient geometry for puncture

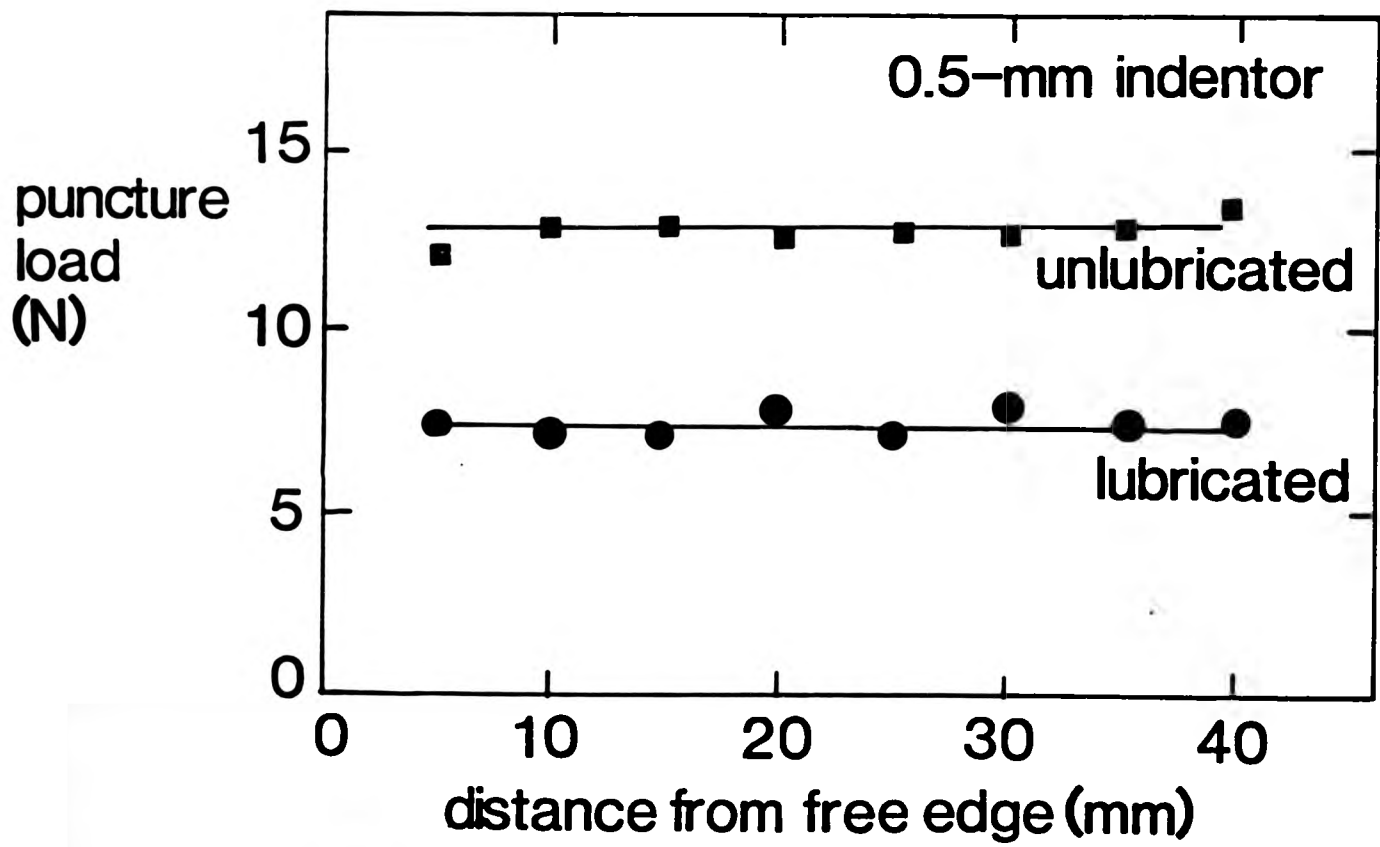
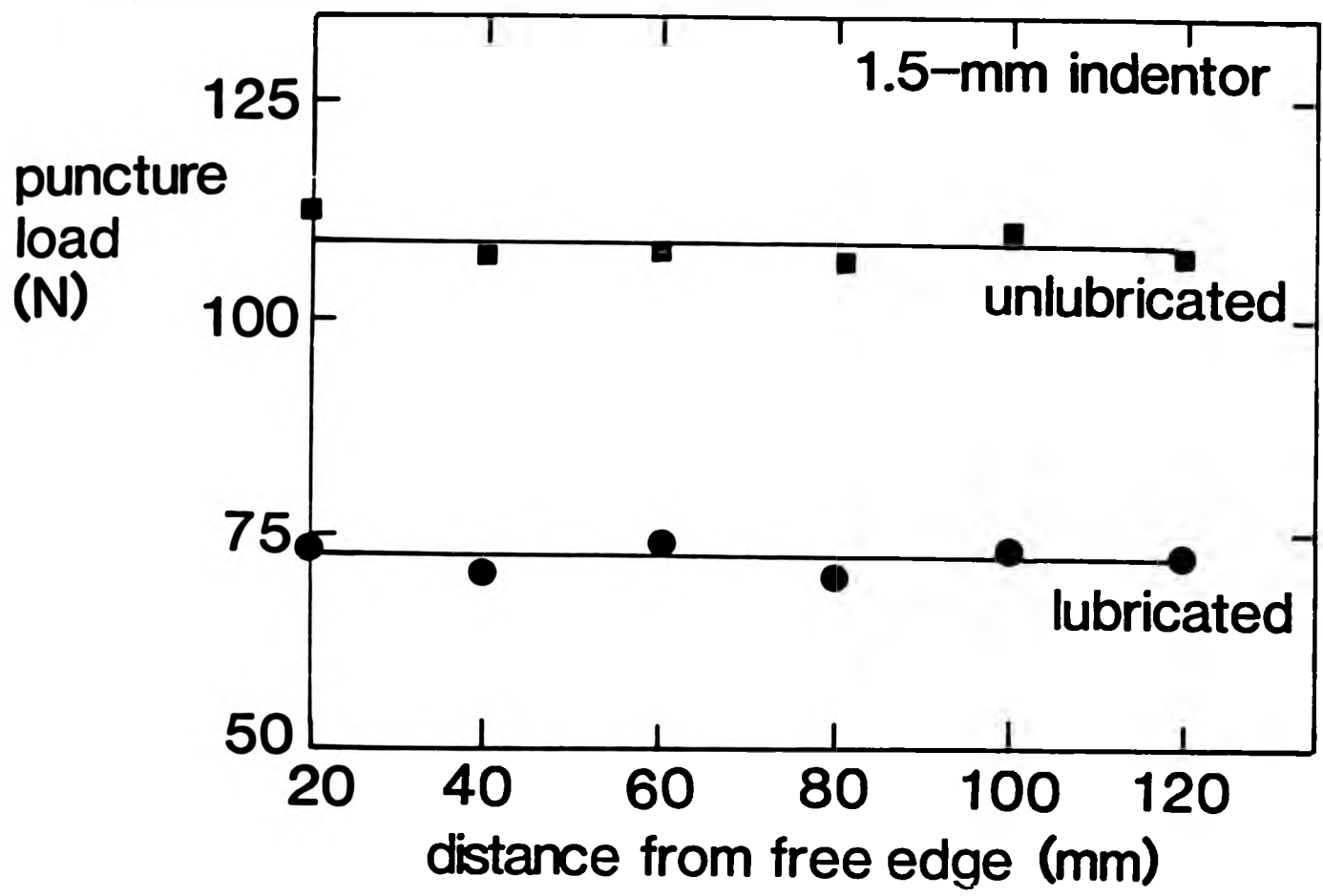


Figure 5.5 Variation of puncture load with distance from free edge. Vulcanizate B.

Table 5.3 Minimum distance from test-piece free edge

thickness of test-piece mm	<u>minimum distance of indentation from test-piece free edge(mm)</u>	
	1.5-mm indenter	0.5-mm indenter
2	4	3
8	6	3
10	7	3
15	10	4
25	20	5

testing. This inevitably will involve cutting of the rubber blocks. The test-pieces obtained in this way have different surface conditions from the surface of the moulded rubber. The surface conditions of the cut test-pieces will of course depend on the way the rubber is cut, and this may affect the puncture load.

Tests were carried out on surfaces of blocks of vulcanizate A using 0.5 and 1.5 mm diameter indentors and a lubricant. The surfaces of the blocks had been created by four different methods to yield surfaces of four different 'roughness'. The first method was to use the normal rubber block after it was vulcanized. The other two methods were basically using a razor blade and a band-saw respectively to cut the rubber. The last method was to use surface grinder to buff the moulded rubber surface and thus giving different roughness.

The results are shown in Table 5.4. For both sizes of indentor, the mean puncture loads for moulded, razor-cut, band-saw and buffed surfaces showed a good agreement. This result is of a major importance for the test, because it enables sections from the middle of a thick rubber block to be tested without too much concern for the effect of surface conditions upon the results.

Table 5.4 Effect of surface conditions on puncture load

surface conditions	<u>mean puncture load(N)</u>	
	0.5-mm indenter	1.5-mm indenter
moulded surface	22.0	102
razor-cut surface	21.0	106
band saw-cut surface	20.0	98
buffed surface	21.5	104

5.5 Effect of corner radius of indenter

Puncture tests on vulcanizate B showed that, as corner radius is increased, the mean puncture load first increases sharply to a maximum value and then drops gradually. This trend is shown for both lubricated and unlubricated puncture tests with indentors of diameter 0.5 mm (Figure 5.6) and 1.5 mm (Figure 5.7). These results indicate that the puncture load is dependent on the size of the corner radius.

The effect of corner radius on puncture load reproducibility was determined from a sequence of about 20 indentations by calculating the coefficient of variation. The results show that the coefficient of variation increases with increasing corner radius for both 0.5 and 1.5 mm diameter indentors (see Figure 5.8 and 5.9). Lubrication appeared to have little effect on the coefficient of variation.

The results shown in Figures 5.6-5.9 indicate that the value of puncture load and its reproducibility can depend strongly on the corner radius. Reproducible results therefore require the use of a corner radius chosen (at least for longer term-tests) in a region where puncture load is relatively insensitive to changes in corner radius - i.e., larger corner radii. But the reproducibility of test results at larger corner radii is poor, the coefficient of variation being more than 10%.

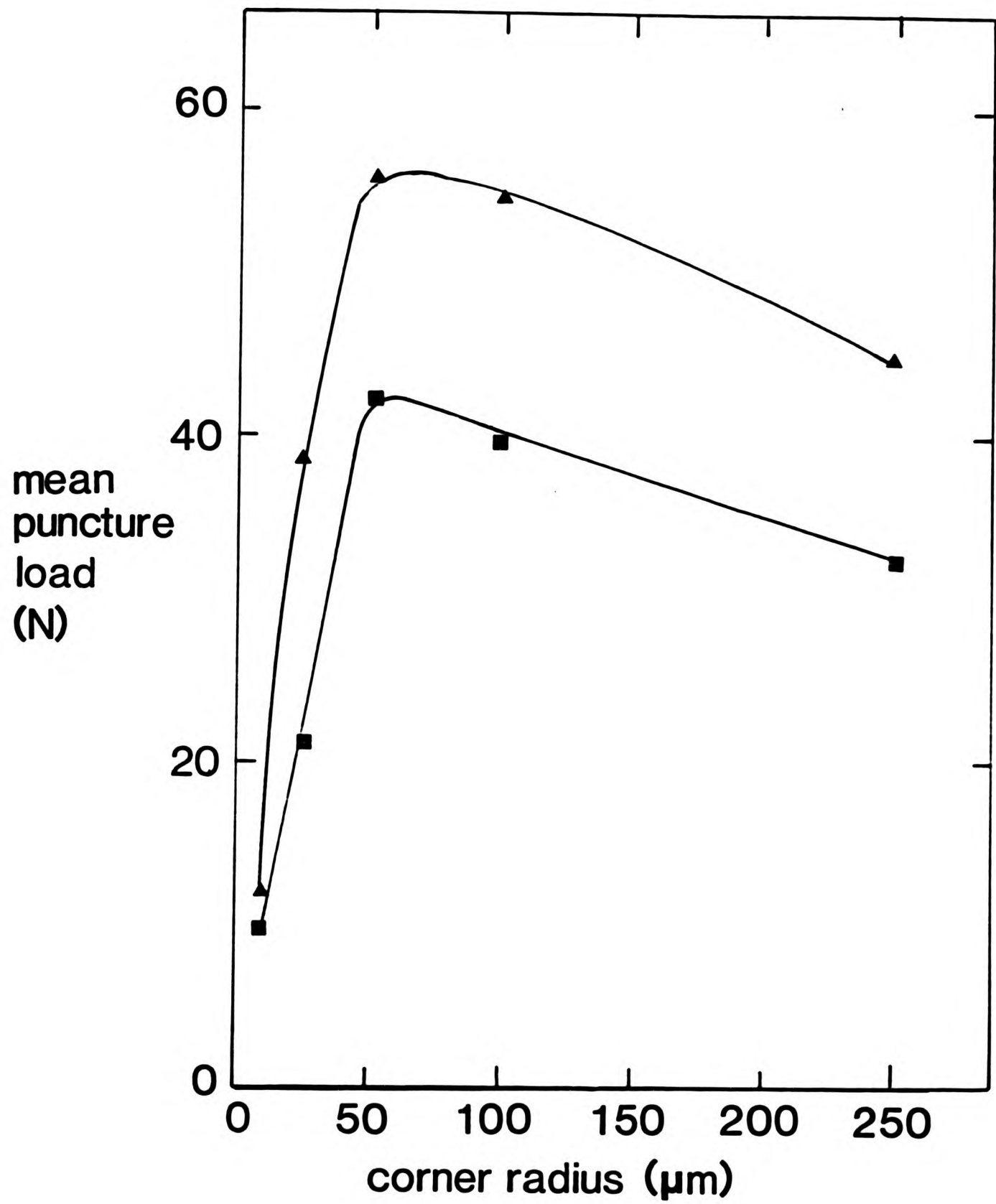


Figure 5.6 Variation of mean puncture load with corner radius of 0.5-mm Ti-64 indenter: un lubricated(▲), lubricated(■).
Vulcanizate B.

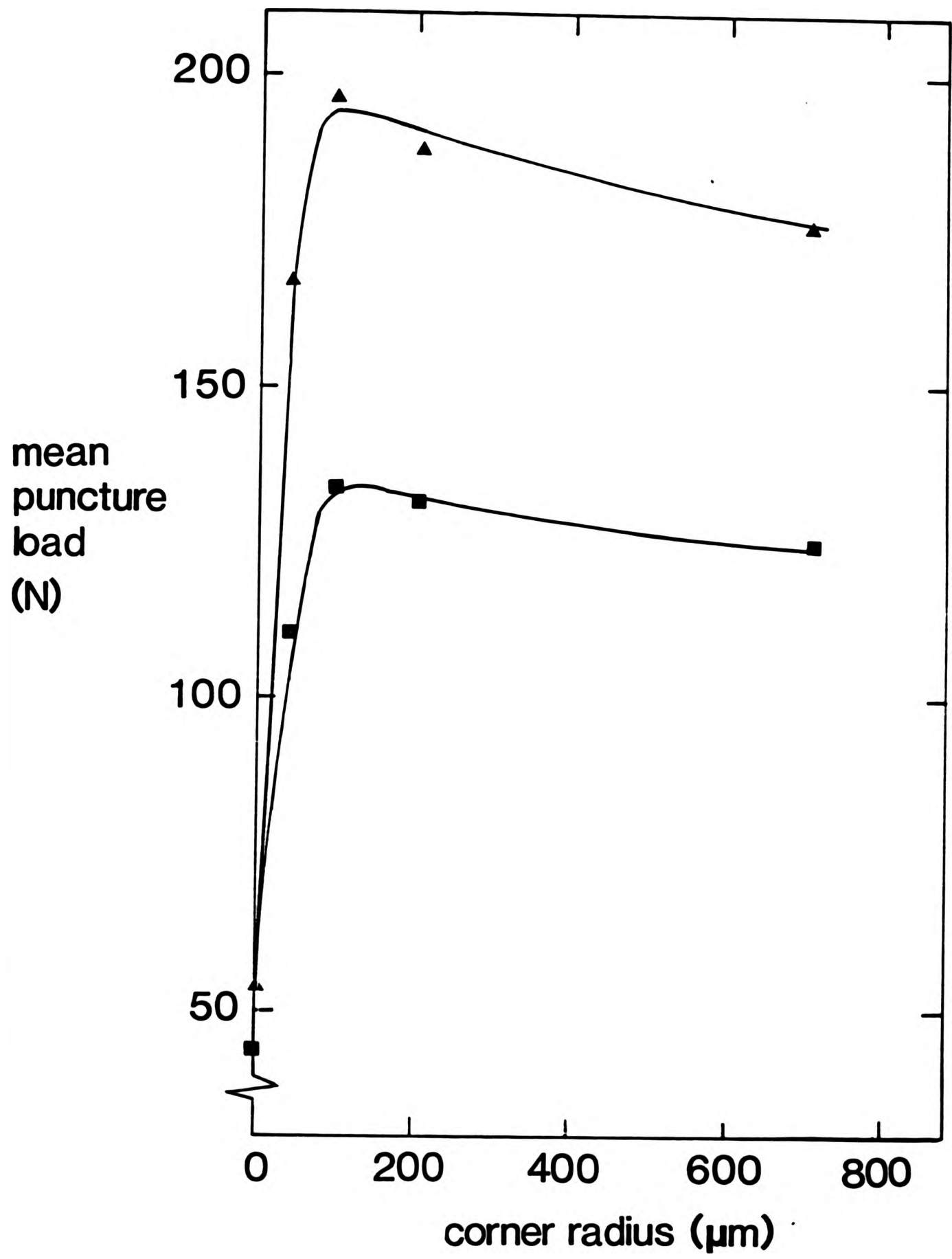


Figure 5.7 Variation of mean puncture load with corner radius for 1.5-mm Ti-64 indenter: un lubricated(▲), lubricated(■). Vulcanizate B.

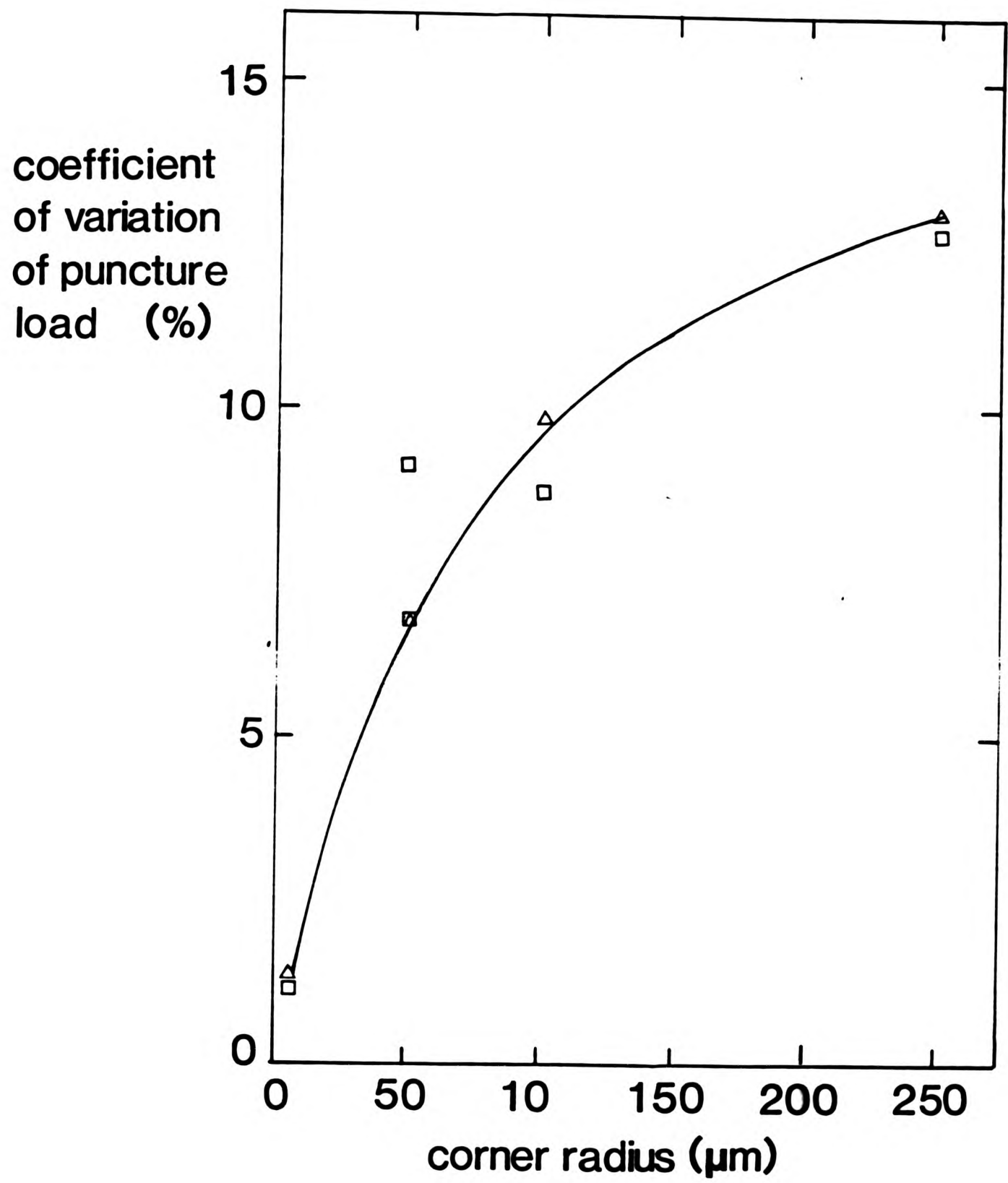


Figure 5.8 Plot of coefficient of variation of puncture load with corner radius for 0.5-mm Ti-64 indenter: lubricated(Δ), unlubricated(\square), Vulcanizate B.

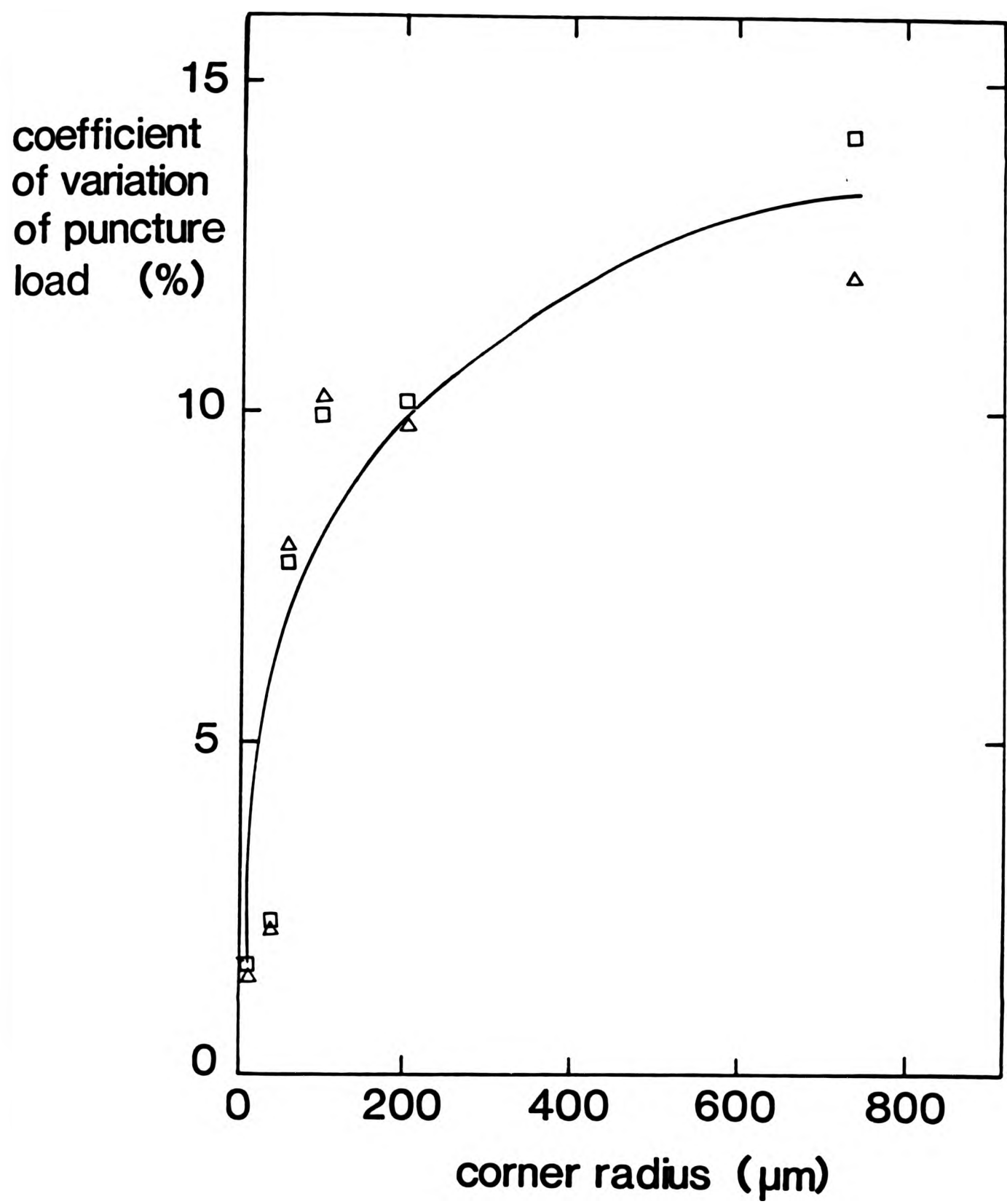


Figure 5.9 Plot of coefficient of variation of puncture load with corner radius for 1.5-mm Ti-64 indenter: lubricated(Δ), unlubricated(\square). Vulcanizate B.

The reproducibility of puncture load appears to improve with smaller corner radii. It is interesting by analogy that when a sharp cutter is used for preparing tensile strength test-pieces, it leads to improved reproducibility compared with a blunt cutter(63). But in the low corner radius regions the puncture loads are very sensitive to small change in corner radius as shown in Figure 5.6 and 5.7. In addition, it has been shown that the corner radius can also change significantly during successive puncture due to wear of metal at the indenter tip(62). Figure 5.10 illustrates the increase in corner radius observed for 0.5 and 1.5 mm diameter Ti-64 indentors when repeated puncture tests were carried out on vulcanizate B. For 1.5 mm diameter indenter, there appears to be an approach to an 'equilibrium radius' of about 60 μ m after about 10,000 repeated punctures. In the case of the 0.5 mm diameter indenter, the equilibrium radius is about 55 μ m after about 60,000 repeated punctures. In both cases the mean puncture loads also approach the equilibrium values at equilibrium radius.

It becomes clear now that the corner radius of the indenter is an important factor affecting both the absolute value of the puncture load and its reproducibility. The reproducibility improves with decreasing corner radius. The puncture load itself increases to a maximum value at an optimum corner

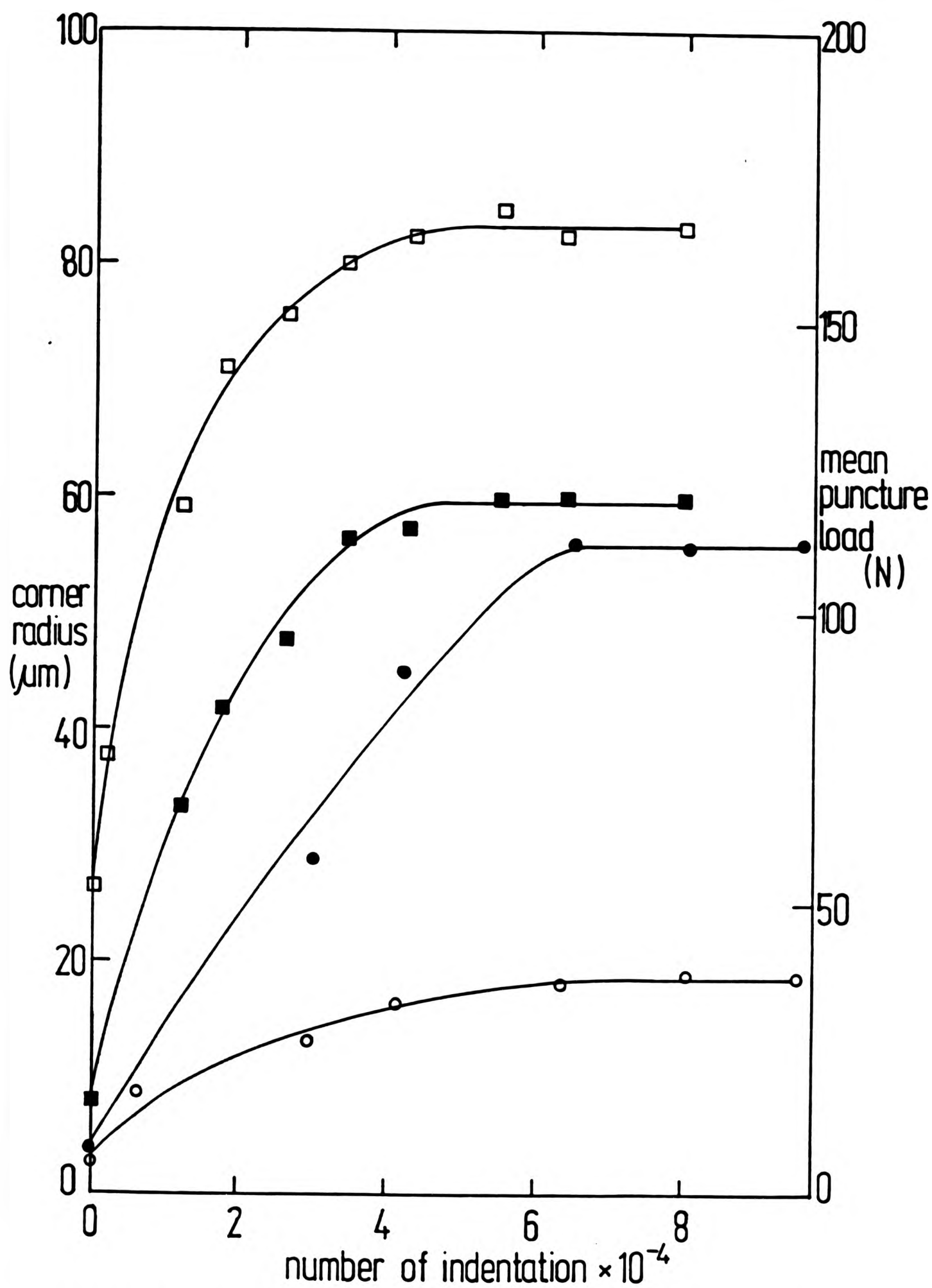


Figure 5.10 Variation of mean puncture load and corner radius with number of indentations on vulcanizate B (lubricated) for 1.5-mm Ti-64 and 0.5-mm Ti-64 indentors: 1.5-mm Ti-64 (puncture load □), (corner radius ■), 0.5-mm Ti-64 (puncture load ○) (corner radius ●).

radius beyond which it decreases slowly. The corner radius can also change due to wear under repeated punctures.

The dependence of puncture load and its reproducibility on the corner radius limits its value as a test parameter despite its convenience. The main work described in this thesis is to analyse the puncture process in terms of fracture mechanics and thus enable results to be derived from a puncture test which are independent of the geometry of the indenter.

CHAPTER SIX
THE MECHANICS OF PUNCTURE

6.1 Introduction

Each puncture test provides information on rubber stiffness and strength - initially in the form of puncture stiffness and puncture load. This and the following chapter will explore the relationship of these measured parameters to more fundamental material properties such as Young's modulus and tearing energy. This however requires an understanding of the mechanisms by which the puncture of rubber occurs.

The main prerequisite for any theory of indentation fracture is a detailed knowledge of the stress field within the loaded system. Given the stress field which accompanies the material deformation caused by the indenter it is possible, in principle, to determine the mechanics of any ensuing fracture. For brittle small strain materials this stress field can be calculated using classical elasticity theory. For rubber, this stress field is more complicated because the strains are large and

elastic behaviour of rubber is non-linear. At the present time a rigorous mathematical solution of this problem is not available; indeed, the problem may be intractable. However, it is possible to develop an empirical model from key features of the puncture process. This model can give insight into the initiation and propagation processes by which crack growth occurs during puncture. This approach is adopted in this chapter, in which an attempt is made to analyse the physics of the puncture process in terms of fracture mechanics.

6.2 Phenomenology of puncture

The puncture of rubber may be usefully considered in stages as follows:-

- stage 1 - deformation
- stage 2 - ring crack
- stage 3 - first puncture
- stage 4 - second deformation
- stage 5 - second puncture
- stage 6 - pull-out

These stages are illustrated in Figures 6.1 and 6.2 by typical force/deformation plots obtained by forcing a cylindrical indenter into unfilled (D) and filled (E) vulcanizates (Table 4.1) respectively. As

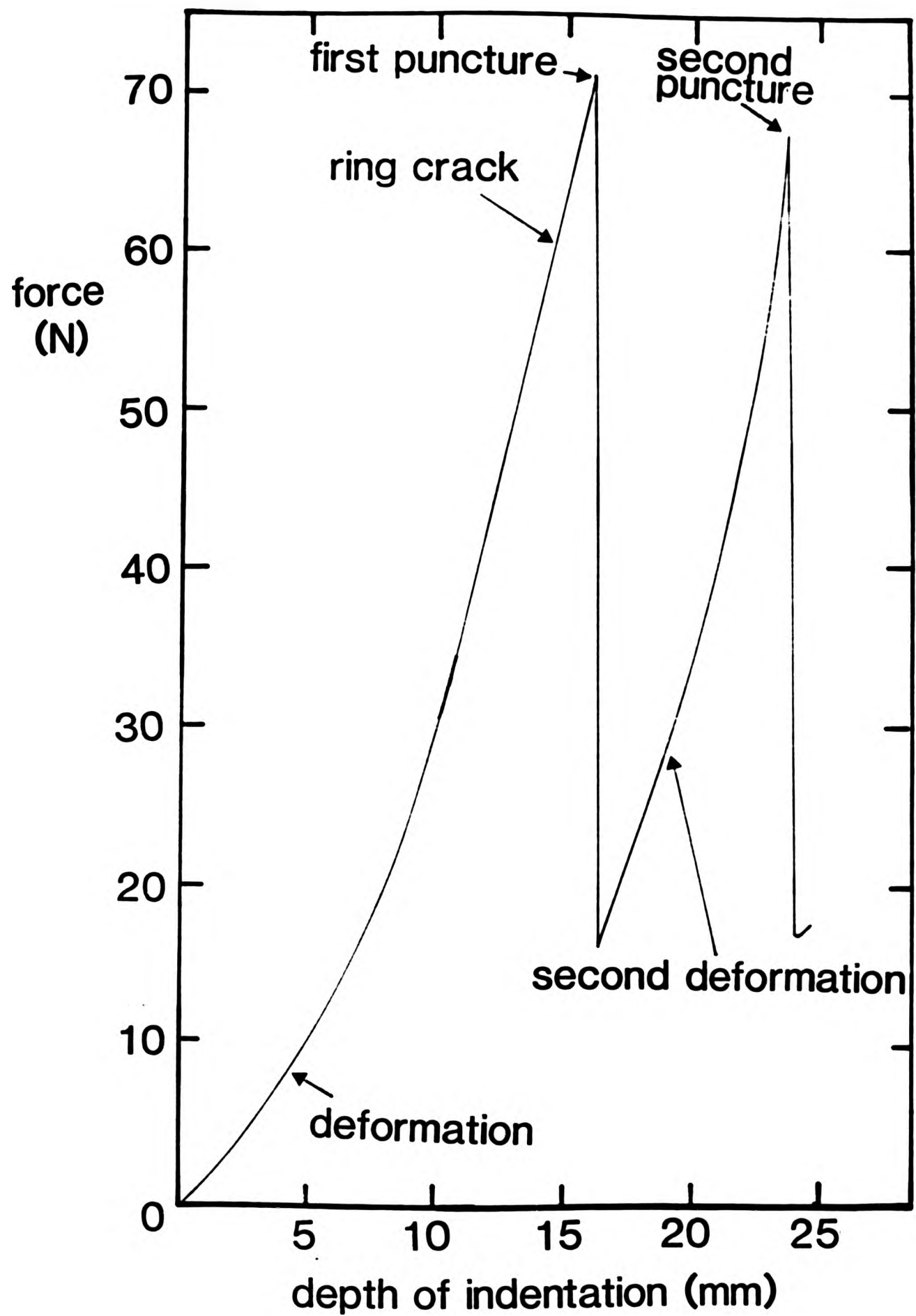


Figure 6.1 A typical force/deformation plot of vulcanizate D.

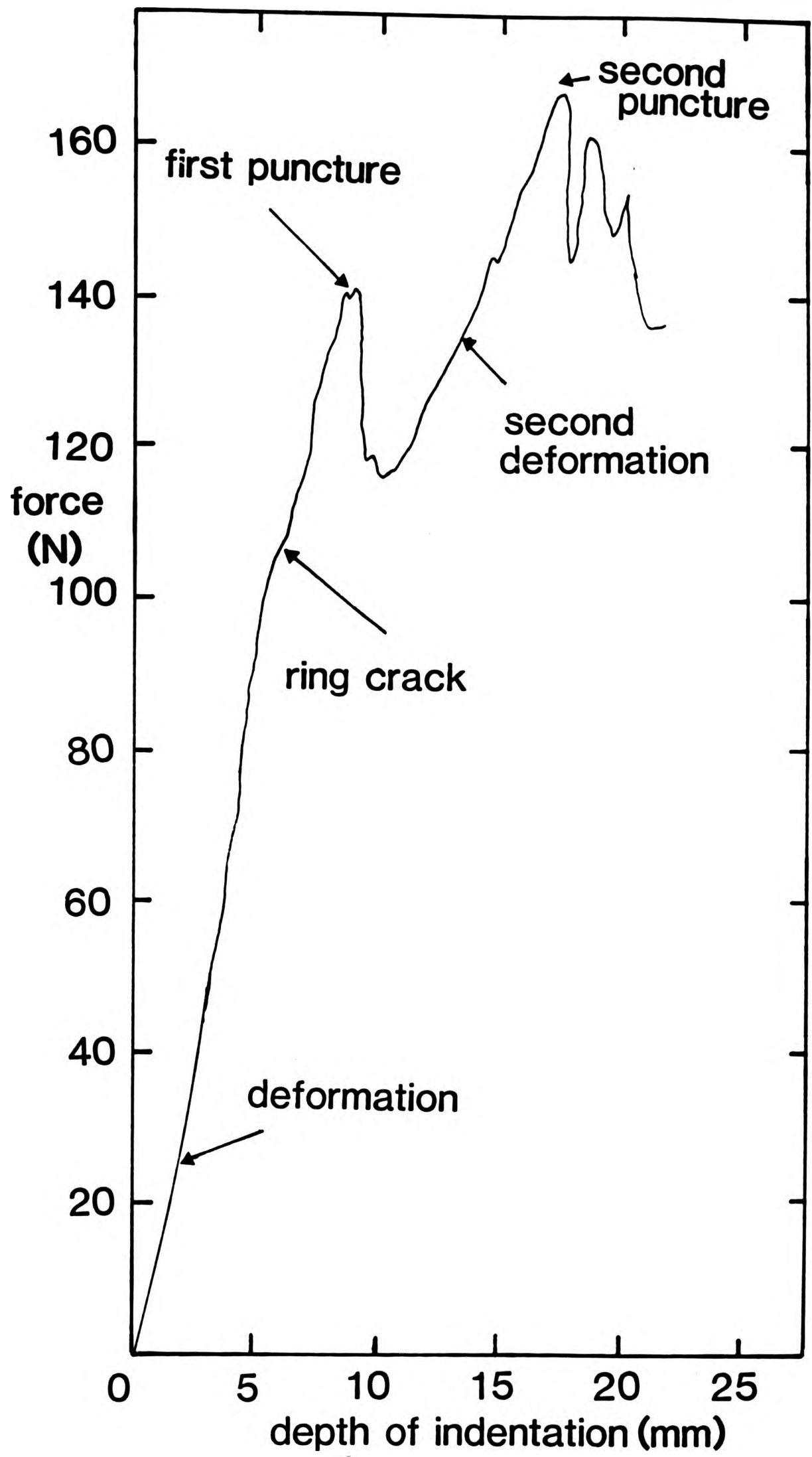


Figure 6.1 A typical force/deformation plot of vulcanizate E.

the indenter makes contact with the rubber surface, the rubber beneath the indenter deforms elastically. As the applied force is increased, indentation increases until, at a certain point, a ring crack develops on the rubber surface beneath the indenter. Further indentation causes the ring crack to grow to a critical length when 'first puncture' occurs. This point is characterised by a sudden drop in puncture force. This drop in force is much greater for an unfilled vulcanizate than for a filled vulcanizate. Further indentation beyond the first puncture causes the load to increase again until a second puncture occurs with another sudden drop in load. For unfilled vulcanizates this again is more sharply defined than for filled vulcanizates. Finally, if the direction of movement of the indenter is reversed, the indenter is pulled out from the rubber. This is accompanied by an instant reduction in load to zero and in some cases a negative 'pull-out' load is experienced as frictional forces have to be overcome in extracting the indenter. 'Pull-out' can be done at any of the stages 1 - 5. The negative 'pull-out' force will be greatest after stage 5.

6.2.1 Ring crack characteristics

If the indenter is pulled out at about 80 - 90% of the expected first puncture load, ring cracks are

invariably observed on the surface of filled vulcanizates. Fig 6.3 shows a ring crack in the surface of the filled vulcanizate E, produced using a 1.5 mm diameter indenter with 10 μ m (sharp) corner radius. An indenter of hemispherical shape (i.e., effectively 750 μ m corner radius) also produces a ring crack, but with a different profile, as can be seen from the micrographs shown in Figure 6.4(a) and 6.4(b). These micrographs show sections of (a) sharp and (b) curved cracks produced by indentors with 10 μ m and 750 μ m corner radii respectively. The ring crack shown in Figure 6.4(a), was produced by a sharp indenter and started with a bell shape in the first 200 μ m. Then the crack became approximately cylindrical in shape. The region where the crack was initiated was well-defined on the rubber surface. The micrograph also shows the asymmetrical start of a sectioned rubber column produced by the ring crack where the crack is deeper on one side (1.6 and 0.9 mm). The reason for this difference is not clear. In addition the column shows a permanent deformation where its length does not fully recover to the surface.

In the case of a hemispherically-shaped indenter, an approximately conical crater with a circular symmetry about the vertical axis is produced. It can be seen from Fig 6.4(c) that the deformed curved surface of the crater is indeed part



Figure 6. 3 Ring crack of vulcanizate E.



Figure 6.4 (a) A section of the ring crack of vulcanizate E produced by a 1.5-mm indenter with sharp (10 μ m) corner radius.



Figure 6.4 (b) A section of the ring crack of vulcanizate E produced by a hemispherical 1.5-mm diameter indenter.

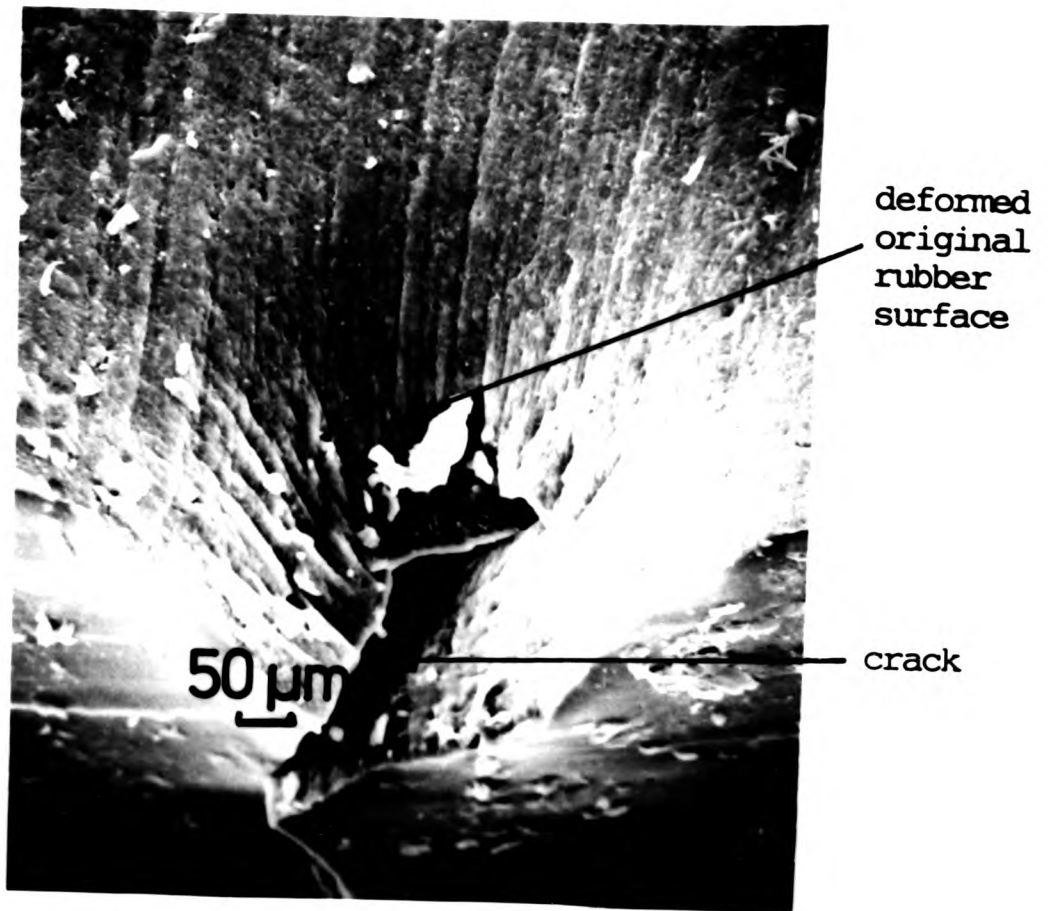


Figure 6.4 (c) Micrograph showing a crater and a crack.

of the original rubber surface and not a fracture surface. The crater is thus attributed to set in the rubber. The crack appears to initiate at the base of the crater which is about 400 μm deep. As can be seen from Figure 6.4(c), the shape of the crack is not well-defined but is approximately 350 μm in length and 10 to 50 μm in width.

The diameter of the surface ring cracks produced by sharp indentors are generally smaller than the diameter of the indentors. Figure 6.5 shows the variation of the diameter of the ring cracks with corner radius for 1.5 mm diameter indentors puncturing blocks of vulcanizate E. The diameter of the ring crack produced by the 750 μm indenter is taken here to be 50 μm - the widest part of the crack.

Ring cracks were more difficult to observe with low-modulus unfilled vulcanizates than with filled vulcanizates. However, when pull-out occurs very near to the expected load at puncture, ring cracks are observed. This degree of precision is difficult to achieve in practice, since puncture loads from replicate tests on the same block can vary by 10%. Figure 6.6 shows a surface ring crack in an unfilled vulcanizate produced using a 1.5 mm diameter indenter with 10 μm corner radius. With an indenter of 750 μm corner radius, surface cracks have not been observed with low-modulus vulcanizates. However,

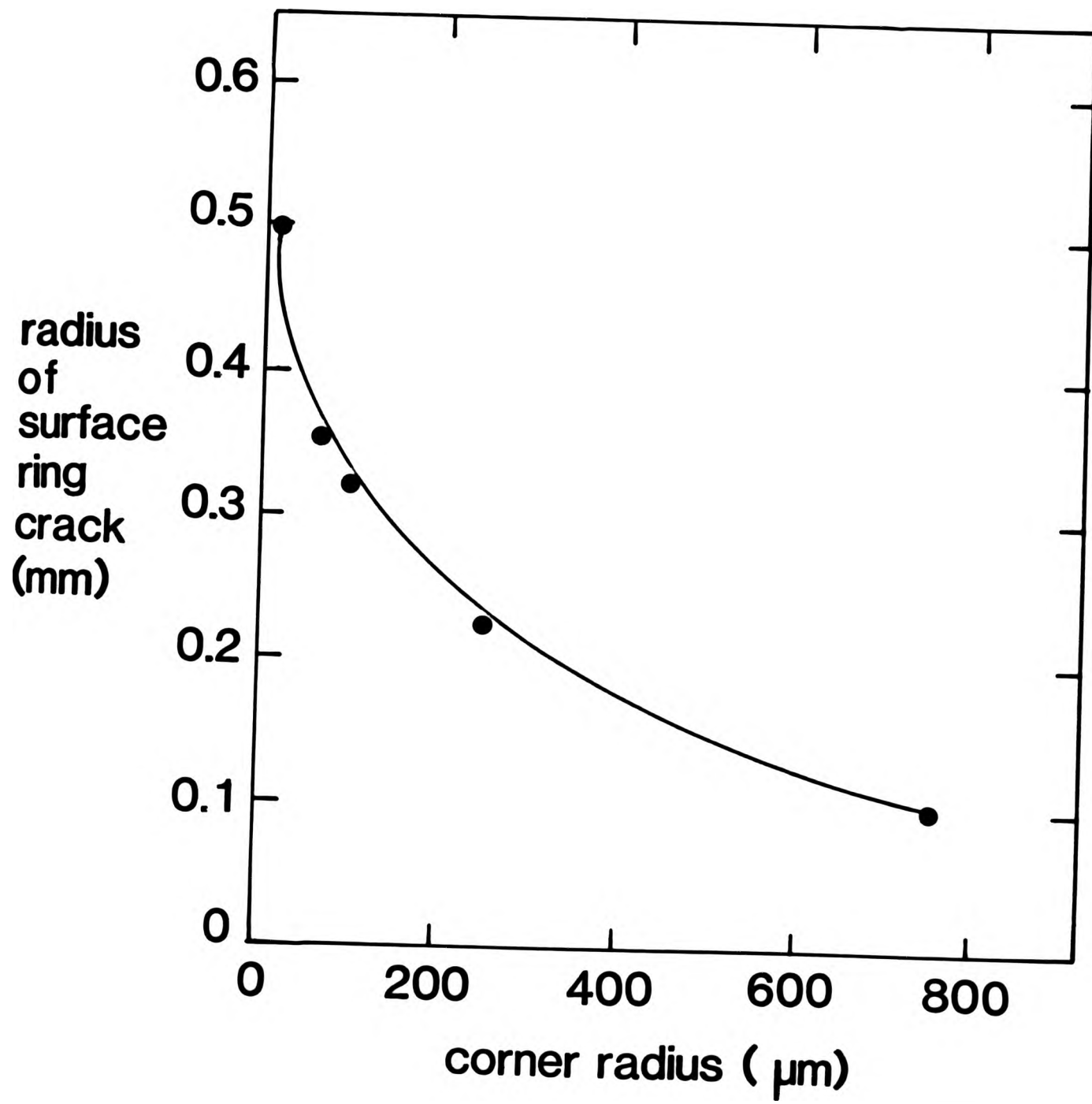


Figure 6.5 Variation of ring crack radius with corner radius.
Vulcanizate E. Indentor: 1.5-mm diameter.

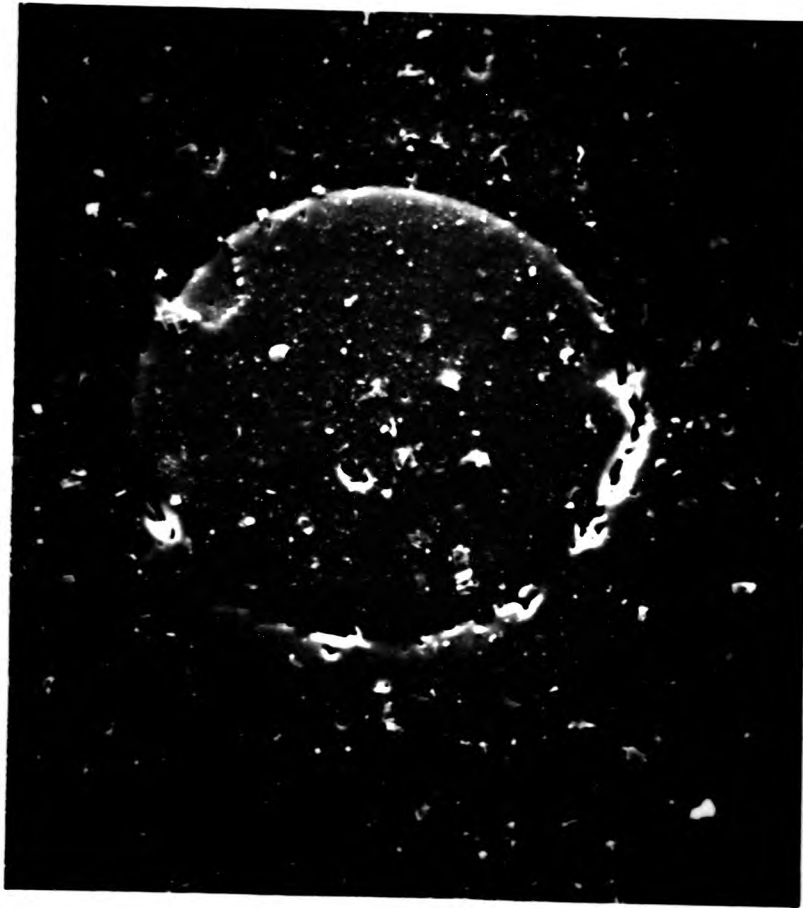


Figure 6.6 A surface ring crack of vulcanizate D produced with a sharp 1.5-mm diameter indenter.

when the modulus of the vulcanizates was increased - for example by increasing the amount of dicumyl peroxide(vulcanizate G) - the cracks developed in the shape of a conical frustum (Figure 6.7) similar to that observed with brittle materials (27) . For the high-modulus vulcanizates G and I, the diameter of the surface ring cracks increased slightly with increasing corner radius (Figure 6.8). In the case of the low-modulus vulcanizates(H and F), the diameter of the surface ring cracks decreased with increasing corner radius. These results suggest that the nature of the puncture initiation process may depend upon both the vulcanizate and the indenter.

6.2.2 Characteristics of puncture

The depth of the ring cracks increases with increasing applied load to a critical value, beyond which puncture occurs. Puncture is accompanied by a sudden increase in crack depth, the crack penetrating into the bulk of the rubber causing the formation of a cylindrical column. This column can be observed if the puncture crack is carefully sectioned into two halves with a razor blade. Figures 6.9(a) and 6.9(b) show typical examples of columns produced with an indenter of 10 μm corner radius in the low-modulus unfilled vulcanizate D and the high-modulus filled vulcanizate E respectively. In the case of the



Figure 6.7 Surface conical frustum crack of vulcanizate G.

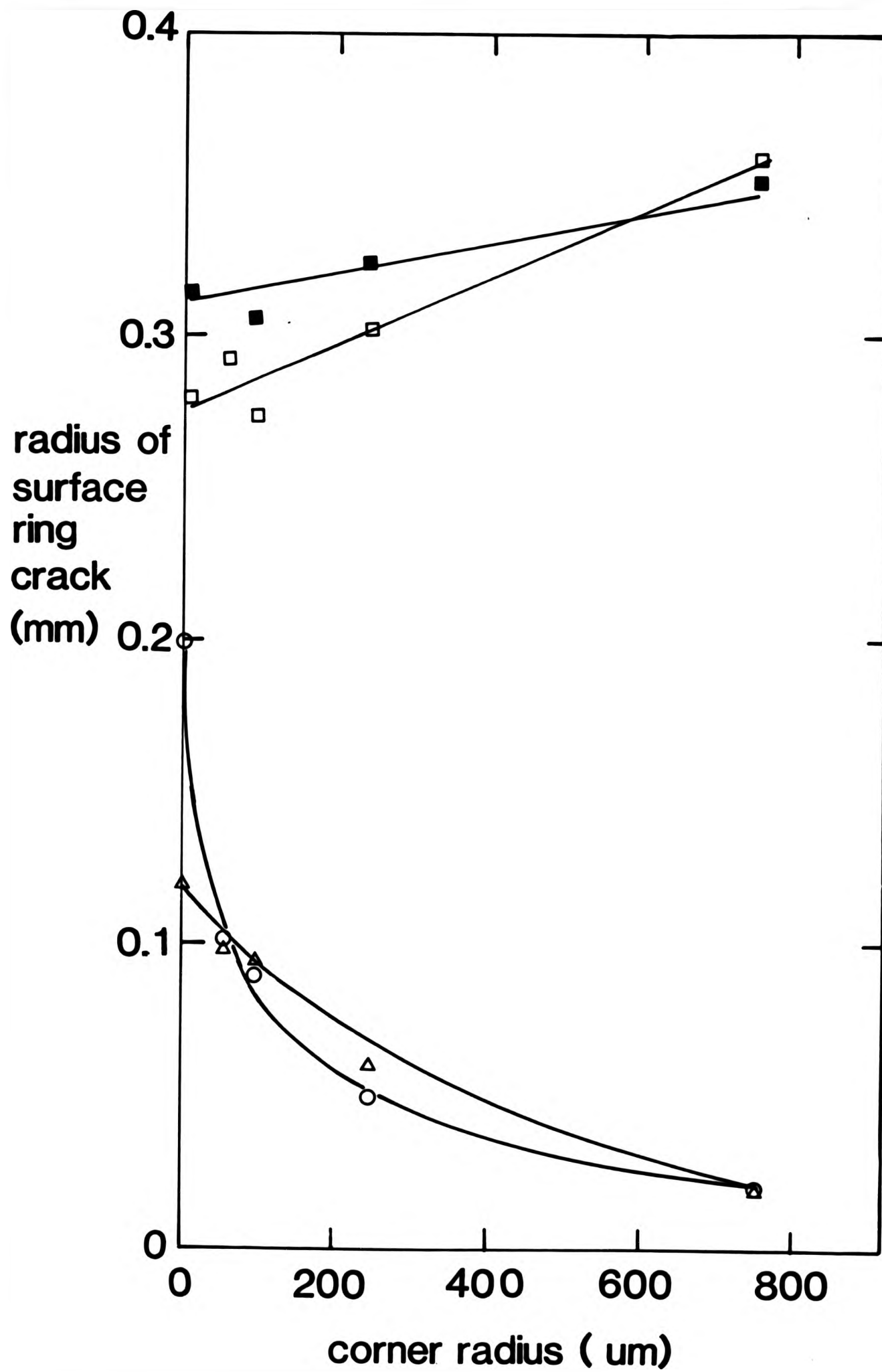


Figure 6.8 Variation of ring crack radius with corner radius produced with 1.5-mm diameter indenter. Vulcanizates: (H O), (FA Δ), (G □), (I ■).

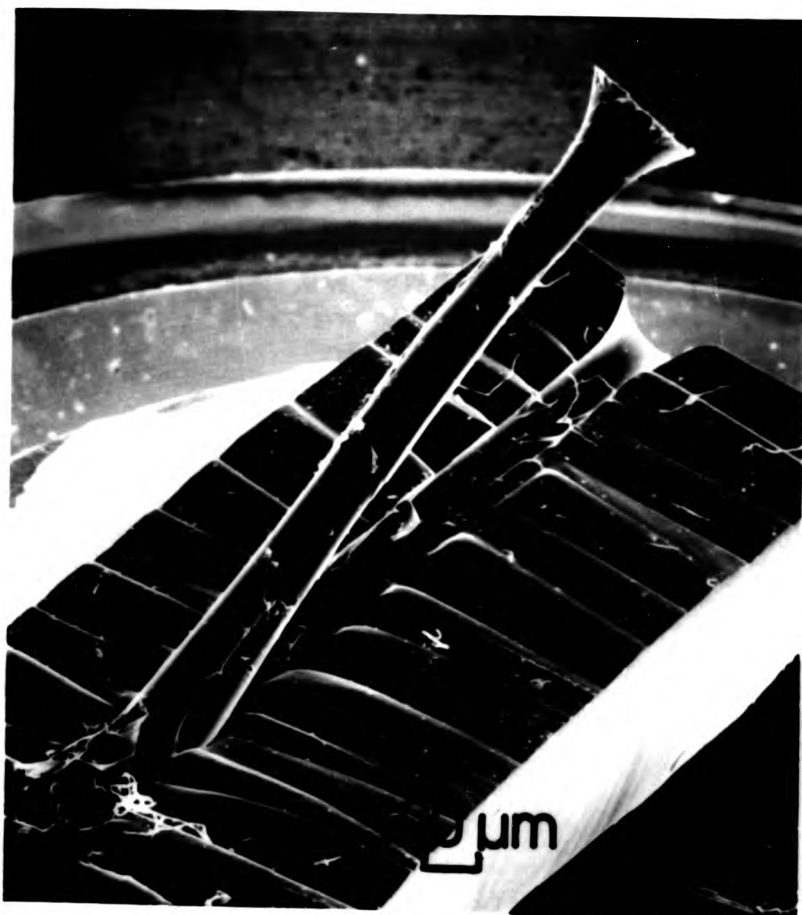


Figure 6.9 (a) A rubber column of vulcanizate D produced by a sharp 1.5-mm diameter indenter.



Figure 6.9 (b) A rubber column of vulcanizate E produced by a sharp 1.5-mm diameter indenter.

low-modulus unfilled vulcanizate, it can be seen that the column is remarkably uniform in the middle, but opens up to a bell shape in the first 300 μm at the top. The top of this column is shown at higher magnification in Figure 6.9(c). The diameter of the top of the column (1.16 mm) is very similar to that of the ring crack (0.98 mm). This is not surprising, since the formation of the ring crack precedes puncture. However, the concordance is not exact in this case, possibly because Figure 6.9(a) and 6.6 (showing a ring crack) were taken at different positions on the rubber, i.e., they refer to two different puncture tests carried out on the same test block using the same indenter.

The diameter of the column appears to increase as the crack grows towards the base. This can be clearly seen in Figure 6.10, where a section of a crack in a translucent vulcanizate is viewed with transmitted light using an optical microscope. A micrograph of the base of the column is shown in Figure 6.11, but in this case the point where the crack terminates is difficult to distinguish. However, Figure 6.11 clearly shows a gradual increase in the diameter of the column with crack depth.

Figure 6.10 also indicates that the crack is deeper on one side of the column than the other. A closer examination (Figure 6.12) suggests that short sections of the column may be helical and therefore

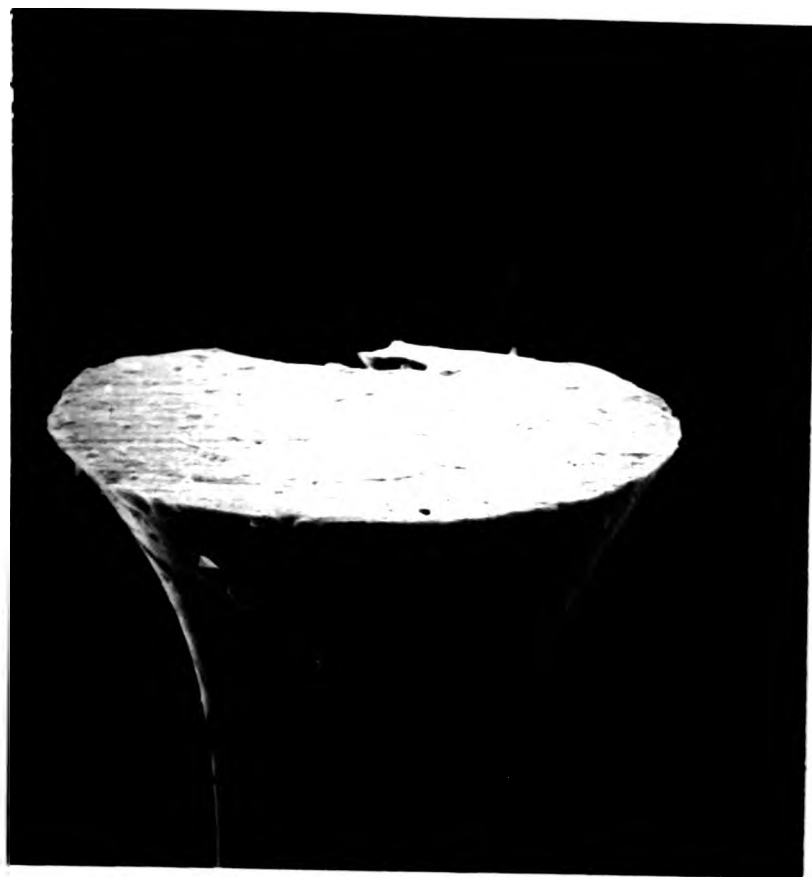


Figure 6.9 (c) A top of the rubber column of the vulcanizate D.



Figure 6.10 A crack section of vulcanizate D viewed with transmitted light using an optical microscope.



Figure 6.11 A micrograph of the base of the rubber column.

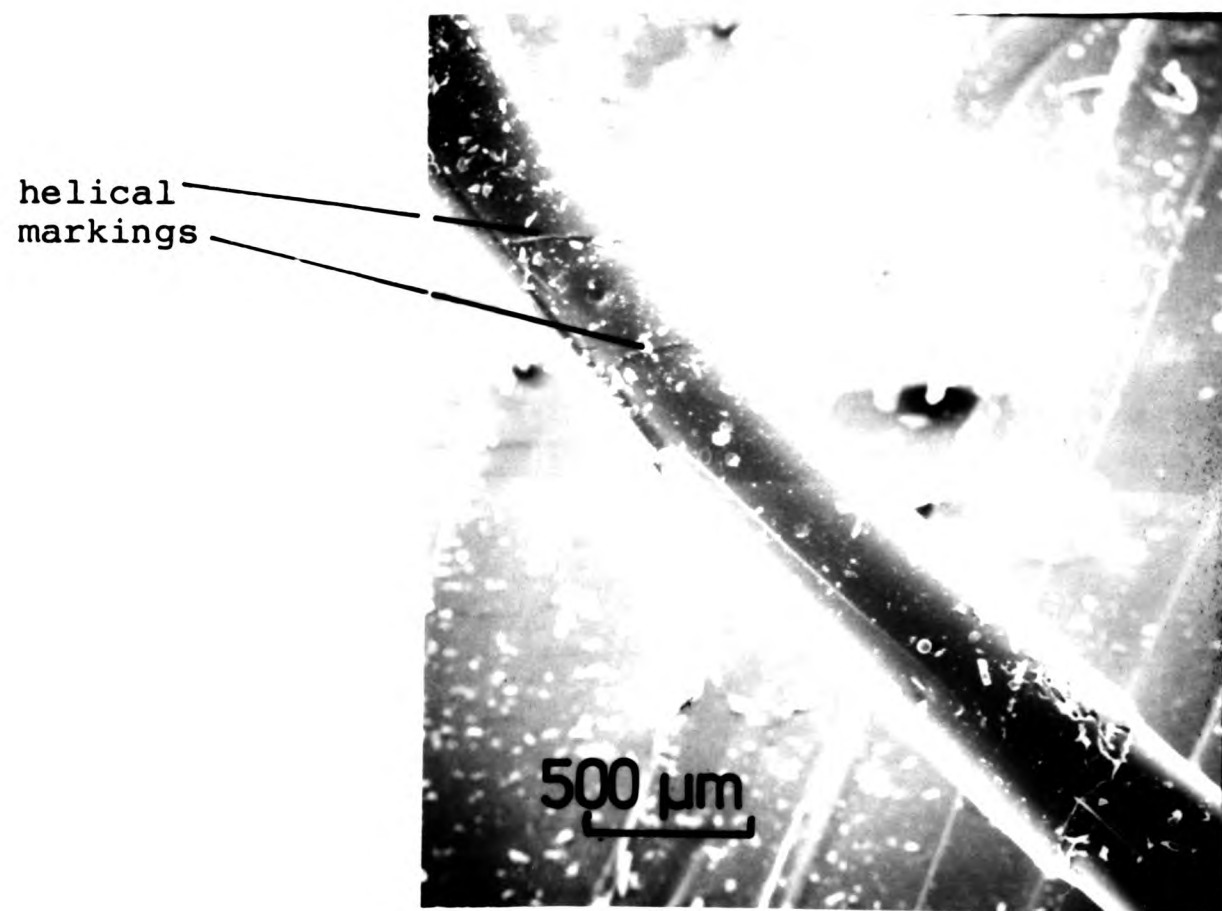


Figure 6.12 Rubber column showing helical rings at some sections.

there is a possibility that the crack grows in a helical form and this may explain the way the crack ends at the base i.e., the crack is deeper on one side of the column than on the other. Incidentally, the diameter of the base AB (see Figure 6.13) is similar to that at the top.

The columns which form in filled vulcanizate E (Figure 6.9(b)) show some similar characteristics. Part of the column was cut off during sectioning. It can be seen that one side of the column has a deeper crack than on the other. However, because the rubber is not translucent, the transmission light microscope could not be used to give the base profile of the crack. Thus the diameter of base of the column is uncertain. No helical features were observed on this column.

The high-modulus vulcanizates G and I produced conical frustum cracks. Figure 6.14 shows a typical cone crack produced with a sharp indenter.

No columns were observed in puncture produced using hemispherical indentors on low-modulus unfilled vulcanizates. Fig 6.15 shows a puncture surface on vulcanizate D formed using a hemispherical indenter. The cracks apparently initiated randomly. As a consequence, a well-characterised crack was not observed. Rather surprisingly, with high-modulus unfilled vulcanizates, the spherical indentors produced cone cracks similar to those observed with the sharp indentors.

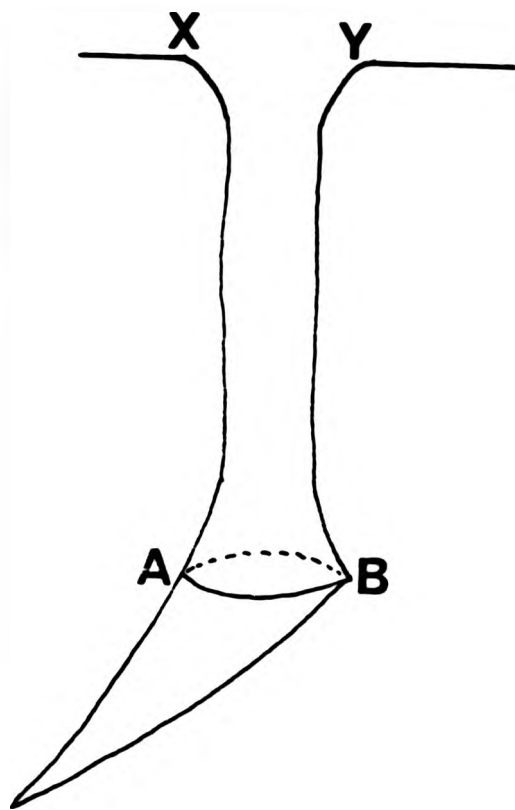


Figure 6.13 Schematic diagram of the rubber column showing that the diameter AB is approximately equal to the surface diameter(XY).



Figure 6.14 Puncture crack of vulcanizate I.

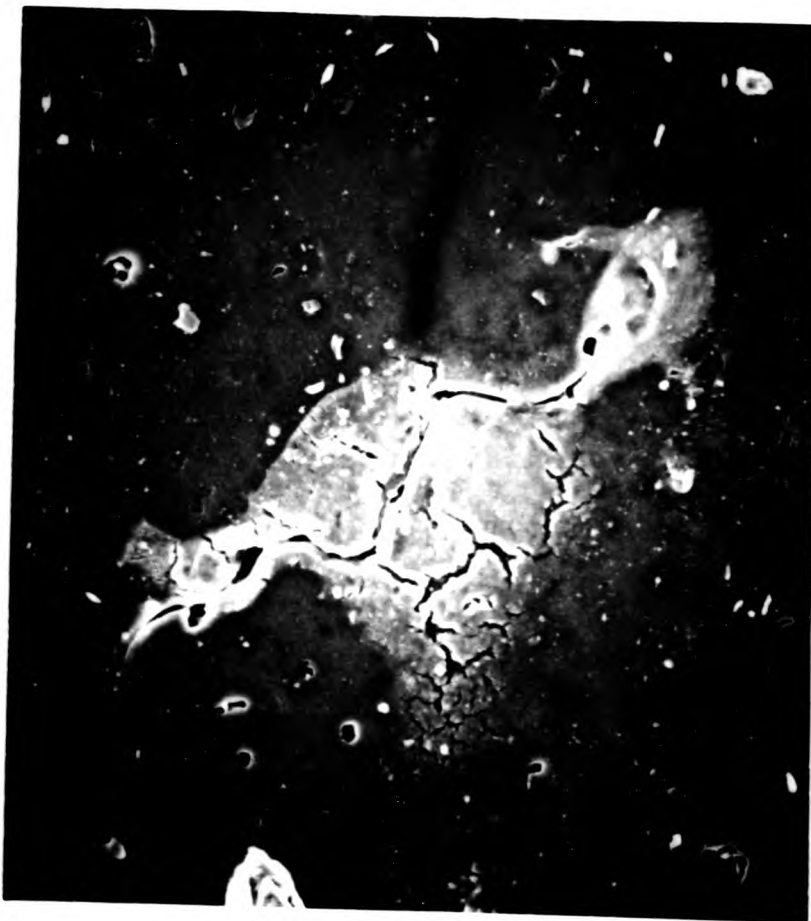


Figure 6.15 Random surface puncture cracks of vulcanizate D produced by a hemispherical indenter.

The results so far show that the characteristics of the puncture cracks and the ring cracks (as discussed in Section 6.2.1) are greatly dependent on the sharpness of the corner radius of the indenter. Figures 5.6 and 5.7 in Chapter Five show that, as the corner radius of the indenter was increased, the puncture load increased to a maximum and then decreased slowly. This suggests different mechanisms of puncture for indentors of very low and very high corner radius. It is important that, if possible, material properties derived from the results of puncture tests should be independent of test variables such as the corner radius of the indenter. With this objective in mind, a fracture mechanics approach has been developed, and is described in the next section.

6.3 Fracture mechanics

In this section, the relationship between puncture load and the catastrophic tearing energy or puncture energy, T_c , will be considered. At the stage during puncture when the ring crack has just developed, the rubber in the column that will eventually separate by crack growth is still intact. At this stage the depth of penetration is x and the unstrained length of the column is c . Figure 6.16 shows schematically the compression of the rubber

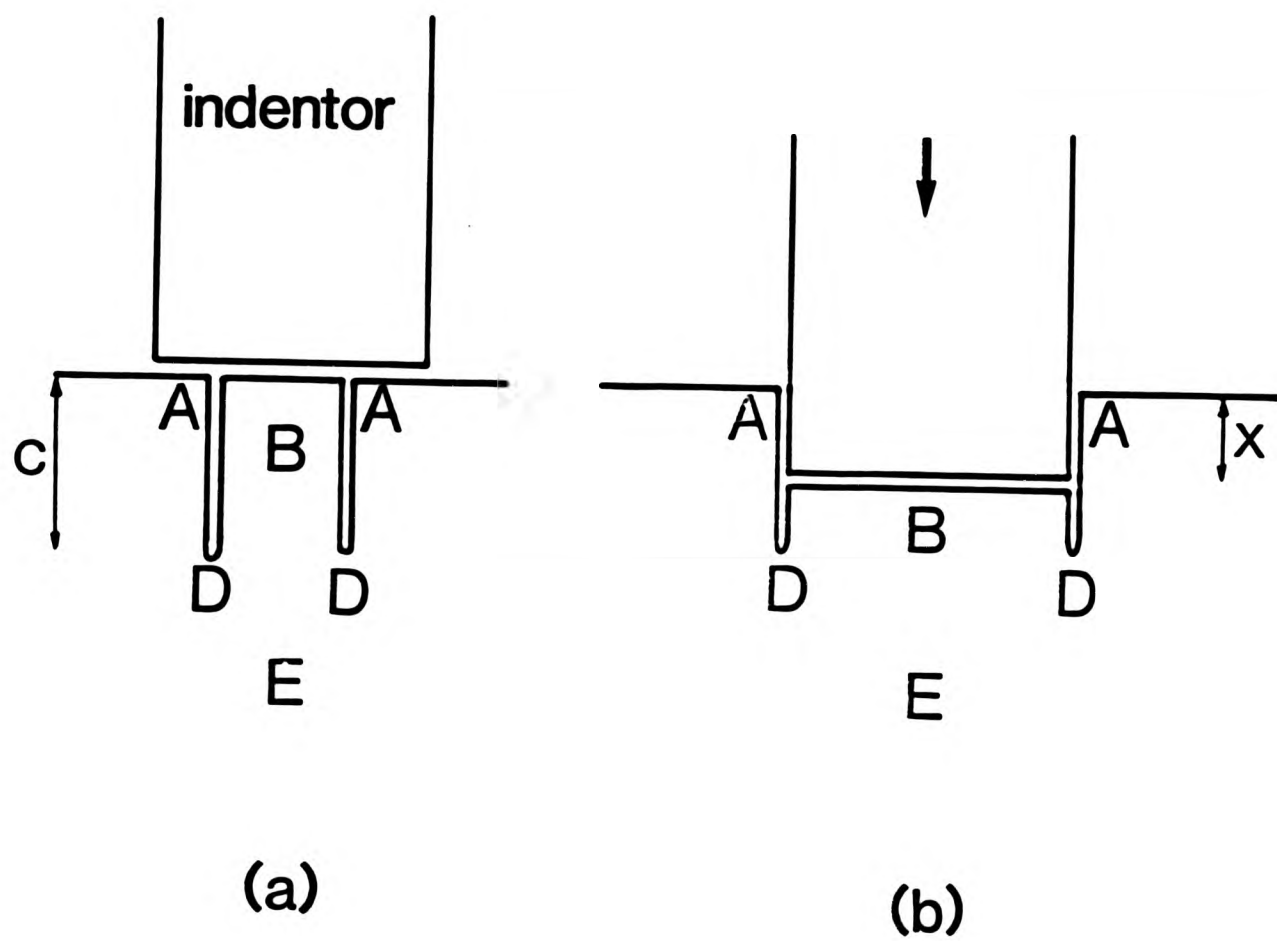


Figure 6.16 Schematic diagram of the compression of the rubber column after the ring crack has developed.

column after the ring crack has developed and the compression ratio is λ_c . At the instant of puncture, T_c can be obtained using equation 2.6. Thus the rate of change of the elastic energy stored in the rubber column, U , with the length of the rubber column, c , can be written as

$$- \frac{1}{2\pi r_0} \left(\frac{\partial U}{\partial c} \right)_x = T_c \quad 6.1$$

where r_0 is the unstrained radius of the rubber column, and the suffix x indicates that the differentiation is carried out under conditions of constant displacement of those parts of the boundary that are not force free, i.e., so that external forces do no work. For simplicity in the analysis, the following assumptions are made:

- (1) that the strain energy involved in region A has no effect on region D;
- (2) that the indenter/rubber interface is perfectly lubricated, so that the column deforms under a simple uniaxial compression; and
- (3) that the rubber column is a uniform cylinder.

The strain distribution in the neighbourhood, D, of the tip of the crack is complicated in character. However, provided there is a sufficiently

thick layer of rubber beneath the crack there is a region E which is substantially undeformed.

A small increase, δc , in the length of the rubber column at constant applied force, F , increases the size of the region B (in simple compression) at the expense of the undeformed region E, while maintaining the strain distribution in the neighbourhood of the column or crack tip unaltered. The increase in volume of the region B is $\pi r_0^2 \delta c$, where r_0 is the radius of the rubber column in its undeformed state. The compression ratio, λ_c , of the rubber column B is unaltered, since it depends only on the applied force F . Thus to maintain a constant force during an increase δc in the crack length, a displacement δx of the indenter must occur. The relationship between δx and δc can be obtained by considering Figure 6.17. For λ_c to remain constant:

$$\frac{x + \delta x}{c + \delta c} = \frac{x}{c} = 1 - \lambda_c$$

$$\begin{aligned} \therefore \delta x &= (1 - \lambda_c)(c + \delta c) - x \\ &= (1 - \lambda_c)(c + \delta c) - c(1 - \lambda_c) \\ &= (1 - \lambda_c)\delta c \end{aligned}$$

$$\left(\frac{\partial x}{\partial c} \right)_F = 1 - \lambda_c \quad 6.2$$

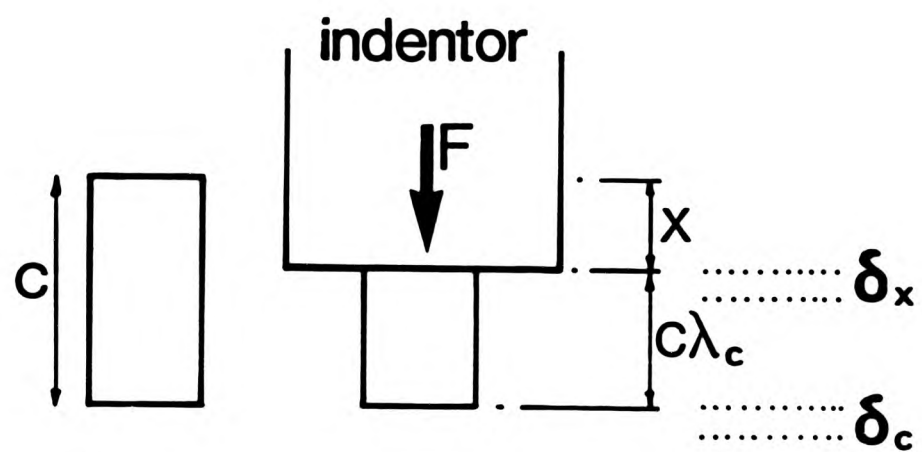


Figure 6.17 Schematic diagram showing relationship between a small increment δx and the corresponding small increment δc at a constant force.

The energy, U , stored elastically in the rubber column is a function of c and x . In general (i.e., when F does not remain constant), c and x vary independently of each other. Therefore, the change, δU , in this energy, accompanying changes δc and δx in c and x respectively is given by

$$\delta U = \left(\frac{\partial U}{\partial c} \right)_x \delta c + \left(\frac{\partial U}{\partial x} \right)_c \delta x \quad 6.3$$

But,

$$F = \left(\frac{\partial U}{\partial x} \right)_c$$

Hence equation 6.3 at constant F becomes

$$\left(\frac{\partial U}{\partial c} \right)_F = \left(\frac{\partial U}{\partial c} \right)_x + F \left(\frac{\partial x}{\partial c} \right)_F \quad 6.4$$

$$\therefore \left(\frac{\partial U}{\partial c} \right)_x = \left(\frac{\partial U}{\partial c} \right)_F - F \left(\frac{\partial x}{\partial c} \right)_F \quad 6.5$$

Substituting equation 6.5 into 6.1 yields,

$$T_c = \frac{F}{2\pi r_o} \left(\frac{\partial x}{\partial c} \right)_F - \frac{1}{2\pi r_o} \left(\frac{\partial U}{\partial c} \right)_F \quad 6.6$$

Equation 6.6 yields, with equation 6.2,

$$T_c = \frac{F(1 - \lambda_c)}{2\pi r_o} - \frac{1}{2\pi r_o} \left(\frac{\partial U}{\partial c} \right)_F \quad 6.7$$

The term $\left(\frac{\partial U}{\partial c} \right)_F$ in equation 6.7 refers to the rate of change with c of the energy stored elastically in the system as the crack length increases under conditions of constant applied force, F . The change in energy δU occurs in two regions and they are:

- (1) the rubber beneath the indenter, and
- (2) the rubber surrounding the indenter.

When the crack length increases by δc , there is a transfer of volume of rubber $\pi r_o^2 \delta c$ beneath the indenter from the undeformed state to a state of simple compression. The change in energy δM stored elastically beneath the indenter is thus $W \pi r_o^2 \delta c$, where W is the elastic stored energy per unit volume. This is associated with the lateral (biaxial) extension of rubber beneath the indenter when a simple uniaxial compression occurs. The change in stored energy δN in the rubber surrounding the indenter is due to the extension of the rubber. The crack grows at the boundary of the compressed region in response to the local strain

distribution. When the crack hole is formed it is immediately filled by the indenter which 'locks-in' the strain in the rubber surrounding the indenter. Then,

$$\begin{aligned} \left(\frac{\partial U}{\partial c}\right)_F &= \left(\frac{\partial(M + N)}{\partial c}\right)_F \\ &= \left(\frac{\partial M}{\partial c}\right)_F + \left(\frac{\partial N}{\partial c}\right)_F \end{aligned}$$

Putting this value of $\left(\frac{\partial U}{\partial c}\right)_F$ in equation 6.7, gives

$$T_c = \frac{F(1 - \lambda_c)}{2\pi r_o} - \frac{Wr_o}{2} - \frac{1}{2\pi r_o} \left(\frac{\partial N}{\partial c}\right)_F \quad 6.8$$

The values of F and r_o can be easily obtained from the puncture test. Values of W and $\left(\frac{\partial N}{\partial c}\right)_F$, however,

are not directly measurable. The contributions of W and $\left(\frac{\partial N}{\partial c}\right)_F$ are evaluated in the next chapter. The

method of measuring the compressive ratio, λ_c , will also be discussed in the next chapter.

6.4 A direct determination of catastrophic tearing energy T_c

The puncture energy can also be determined empirically from the energy loss measured from force-deflection curves such that shown in Fig.6.18. At point B, all the energy available for the crack growth has dissipated. If at this point the indenter is immediately withdrawn from the rubber and then again inserted into the same crack, the force-deflection curve will follow the line OB. The area under OB represents the energy stored in the compressed rubber column and the energy stored in the expanded rubber surrounding the column. The area OAB represents the energy (J) expended for the crack growth. The catastrophic tearing energy is then, assuming no distortion caused by frictional forces, given by:

$$T_c = \frac{J}{2\pi r_0 c} \quad 6.9$$

where $2\pi r_0 c$ is the area of the crack. However, this method poses problems when determining the length of the puncture crack. Sectioning the crack is possible, but the measurement of puncture energy this way is laborious because every puncture crack has to be sectioned in order to measure the length of

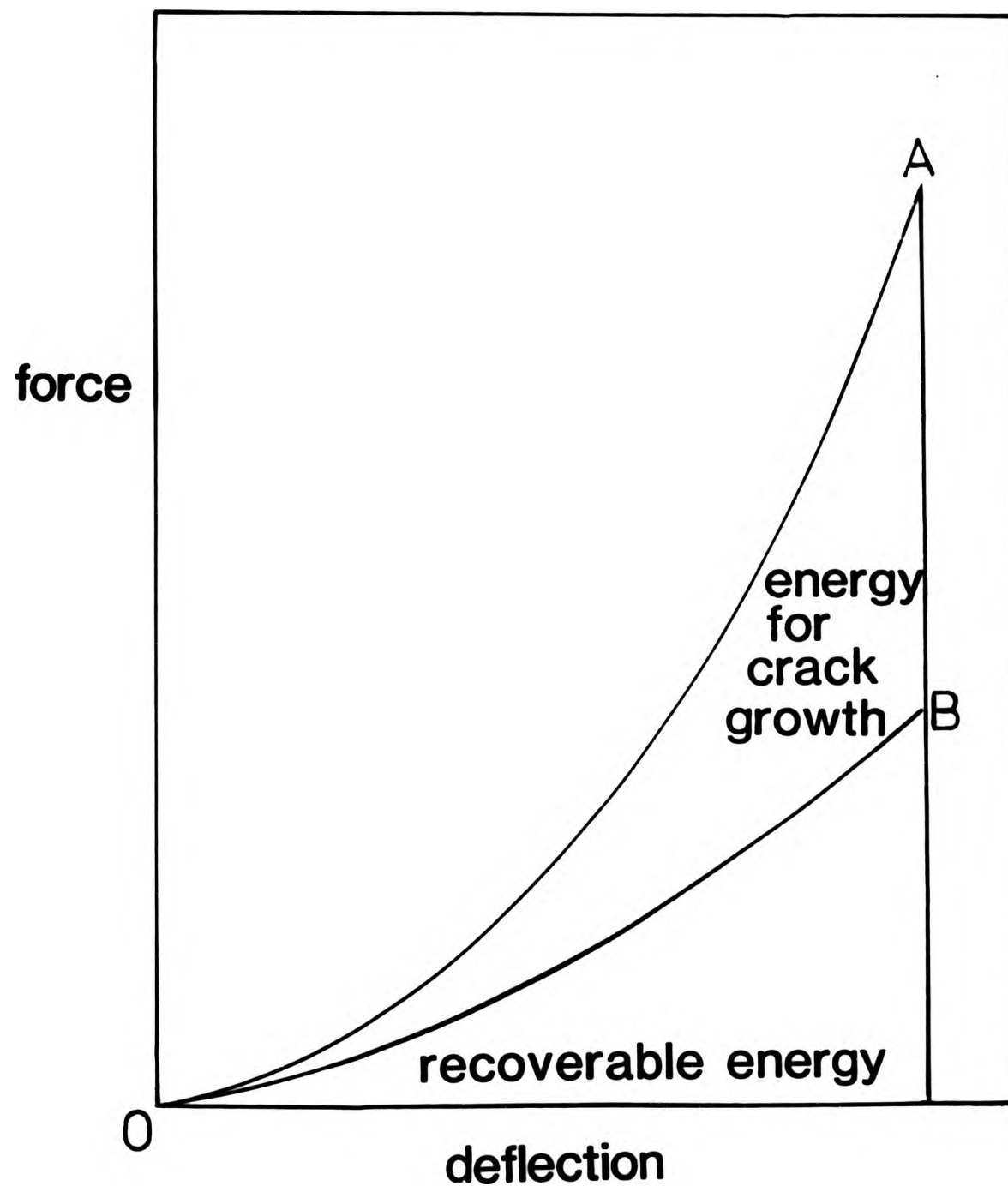


Figure 6.18 Force/deflection curve showing energy available for crack growth and energy stored in the rubber.

the crack. Routine checks on rubber components in service would be out of question because sectioning would destroy them.

Table 6.1 shows the results of experimentally measured puncture tearing energy, T_c , of peroxide cured vulcanizates. The indenter used was 1.5 mm in diameter and had a corner radius of 10 μm . T_c appears to agree well with the tearing energy measured by the trouser tear test.

6.5 Discussion

During each puncture event, the point at which rupture of the rubber occurs will be determined by the stress distribution on the the rubber surface in contact with the indenter. This stress distribution will itself strongly depend on the extent of any slip between the rubber and indenter surfaces. Obviously the higher the stress concentration, the easier will it be for puncture to occur, i.e., the lower will be the puncture force.

The rubber surface contains flaws which are randomly distributed and act as initiation sites for subsequent crack growth. As the applied force is increased, the stresses on the flaws increase proportionally until the flaws propagate along the circular edge of the sharp indentors to form a ring crack, i.e., along the locus of the highest

Table 6.1 Experimental puncture energy compared with trouser tear test results

Vulcanizate	T_c kJ/m ²	T(Trouser tear test) kJ/m ²
D(1 pphr DICP)	9.5	12.5
H(2 pphr DICP)	5.5	6.5
F(3 pphr DICP)	2.4	3.0
G(4 pphr DICP)	0.9	0.8

DICP = dicumyl peroxide

stress concentration. However, in the case of blunt indentors (e.g. those which are hemispherically-shaped), ring cracks sometimes cannot be observed for a low-modulus rubber. This may be because a large equibiaxial extension has taken place. In this case, the locus of the highest stress concentration does not appear to follow a characteristic pattern.

The experimental results (Figures 5.6 and 5.7) have shown that as the indenter corner radius increases, the puncture force increases sharply to a maximum and then decreases slowly. This observation suggests that there are two possible mechanisms of failure. These mechanisms are as follows:

(1) The sharp corner of the indenter causes a high stress concentration which will be strongly dependent on the corner radius.

(2) Equibiaxial extension of the rubber over the base of the indenter occurs during slip.

Consider two extreme hypothetical cases for an indenter with a sharp corner. In the first case is when the friction is sufficiently high to prevent slip between the rubber and the base of the indenter. In the second case is where there is a very minimal friction between the rubber surface and the base of the indenter, and thus allows complete slip to occur.

Figure 6.19(a) and (b) respectively illustrate these two cases.

In the absence of slip, the rubber surface between A and B(Figure 6.19(a) suffers no strain. The regions at A and B, however, at the indenter corners, experience high stress concentrations which will lead to local microscopic cracking and eventually puncture when the naturally-occurring flaws on the rubber surface reach a critical size. If complete slip occurs, the surface AB will become equibiaxially stressed. This is likely to enhance the tendency for rupture from naturally-occurring flaws in the rubber and will also enhance the effect of a stress concentration from the sharp corner of an indenter. It is known, for example, that rubber cuts at much lower forces when it is highly extended(60,61). As a result, failure occurs at a lower forces under lubricated conditions than without lubrication.

In practice, both these mechanisms of failure may occur together to extents that vary, particularly, with the sharpness of the indenter corner and the effectiveness of any lubrication in reducing the rubber/indenter interfacial coefficient of friction.

Thus, the qualitative model proposed is that, in the absence of slip, decreasing corner radius will increase the stress concentration at the indenter corners, and so lead eventually to a decrease in

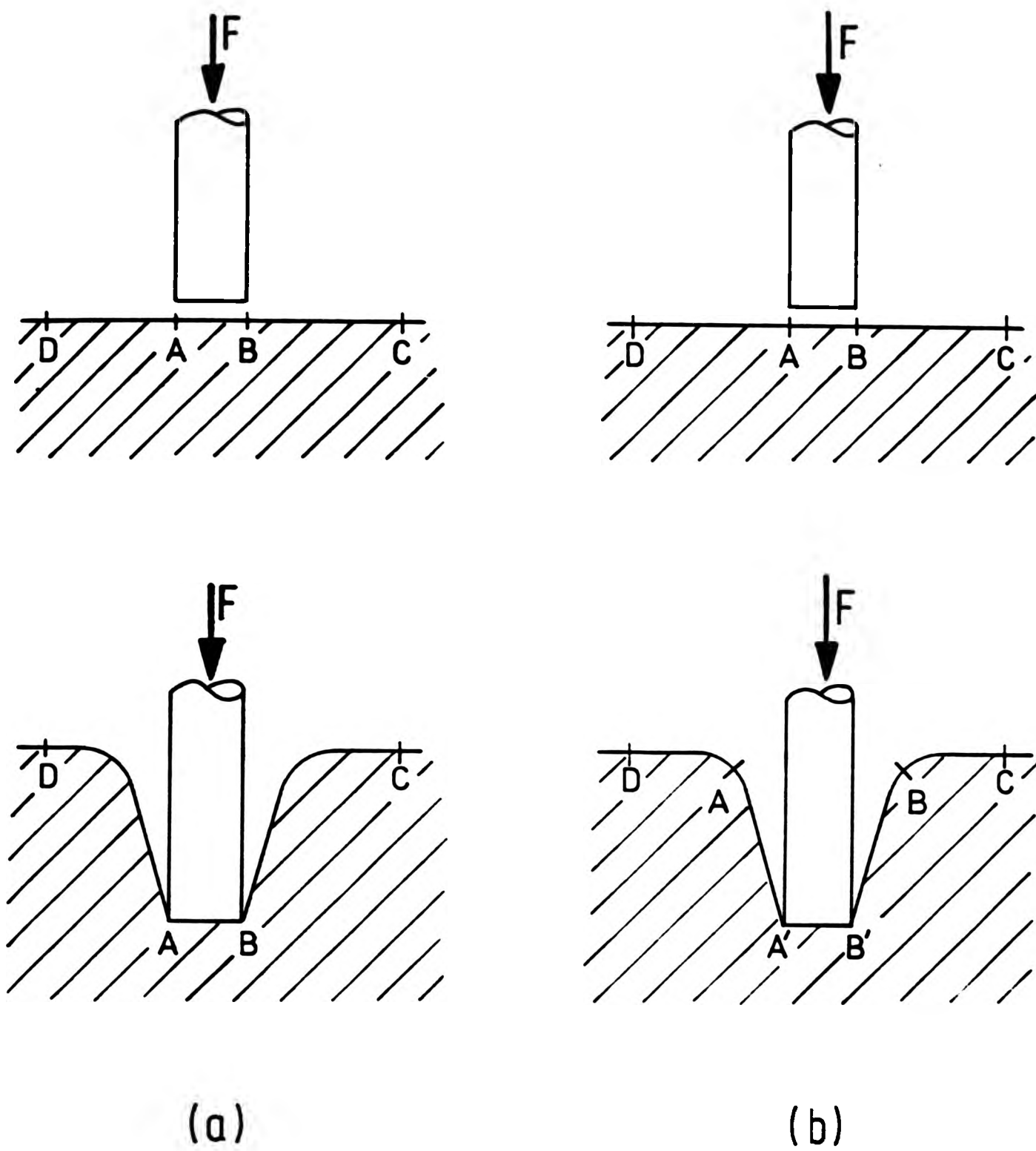


Figure 6.19 Strain on rubber/indenter interface during indentation: no slip (a); lubricated interface - complete slip (b).

puncture force which becomes marked at small corner radii only. In the presence of slip, this same phenomenon will be superimposed on a biaxially stress distribution in the rubber surface. The effect of the slip will be to concentrate the stress distribution over a reduced area of rubber in the unstrained state. Slip caused by lubrication may thus lower puncture force, as is observed.

In spite of the complexity of the mechanisms involved, puncture is ultimately a fracture process which involves tearing of a rubber surface. A major problem in applying the fracture mechanics approach in practice is to determine the relation between the tearing energy, crack size and overall forces or deformations for the rubber. Section 6.3 has shown that a fracture mechanics approach yields an expression for the puncture energy T_c (equation 6.8). Even though some parameters in the puncture energy equation can be easily obtained (i.e., F and r_0), λ_c and two more terms which involve the energy stored in and surrounding the rubber column are not obviously measurable, and their determinations and significance will be discussed in the next chapter.

In the analysis which has been given in this chapter, the ring crack is assumed to form in the initial stages of deformation. Probably, this is the stage where a high stress concentration at the corner is important, leading to microscopic cracking.

Subsequent deformation may then take place by a uniaxial compression of the initial rubber column. Thus for the analysis to be valid, a puncture must first form a ring crack of non-zero depth. With a hemispherical indenter, difficulty may occur in forming a ring crack; if so, some aspects of the theoretical analysis will not apply.

CHAPTER SEVEN
EVALUATION OF THE TERMS WHICH CONTRIBUTE TO
PUNCTURE ENERGY

7.1 Introduction

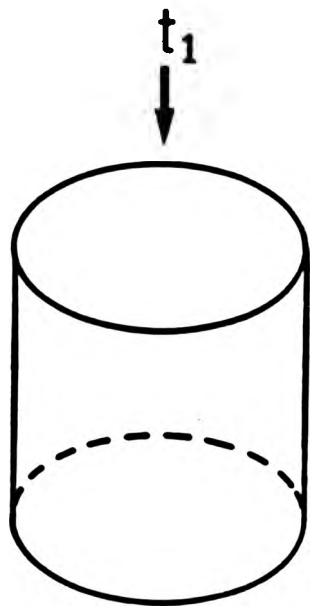
In Chapter Six, equation 6.8 for the tearing energy at puncture, T_c , (i.e., the puncture energy) was derived. Several terms, namely W (elastic stored energy per unit volume), λ_c (compressive ratio) and $\left(\frac{\partial N}{\partial c}\right)_F$ (the rate of change of energy stored surrounding the rubber column with the crack length) are not directly measurable. This chapter describes model experiments designed to evaluate λ_c and W and an analytical method of determining $\left(\frac{\partial N}{\partial c}\right)_F$.

7.2 Energy stored in rubber beneath indenter

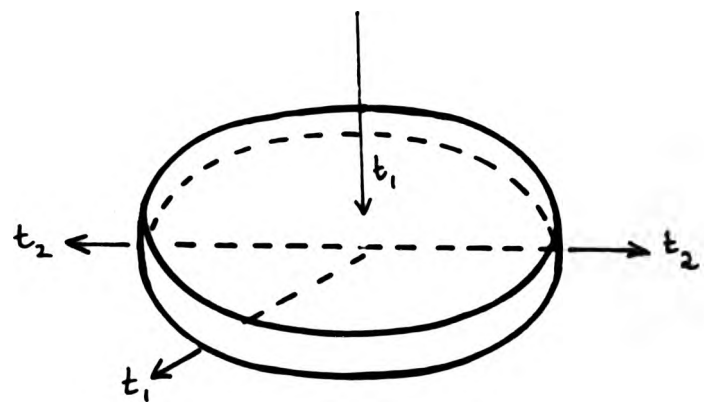
7.2.1 Theory

The uniaxial compression of a rubber column can be considered equivalent in strain terms to equibiaxial extension. Under the application of a

compressive stress t_1 , the deformation of rubber column may thus be considered in strain terms to be equivalent to equibiaxial extension as shown in Figure 7.1. The stresses t_2 and t_3 in the force-free area of the deformed column are zero. Superposition of a hydrostatic pressure $-t_1$ will reduce the compressive stress t_1 to zero and produces equivalent tensile stresses t_2 and t_3 to the effect of t_1 on the previously force-free surface. This state of strain of simple compression of the rubber column thus corresponds to that produced by equibiaxial extension of an inflated circular rubber sheet clamped around its circumference. Thus some indications of the stress-strain behaviour of the rubber immediately beneath the indenter can thus be obtained from a model equibiaxial experiment which avoids a direct analysis of the complex stress-strain behaviour of the rubber underneath the indenter. However, this model equibiaxial experiment will not represent the full state of strain in the compressed rubber column because the bottom end of the column is part of the bulk of the rubber, is under compression and cannot move freely. These considerations limit the validity of this model. However the model can be considered to provide a reasonable approximation to the behaviour of the rubber column under a simple compression.



undeformed



deformed

Figure 7.1 A rubber column undergoing a simple uniaxial compression.

Consider a small section of an inflated rubber sheet, as shown in Fig 7.2. The inflation pressure, P , the radius of curvature, a , and the tensile force, f , per unit length of section of the rubber are related(64) by the equation,

$$P = 2f/a \quad 7.1$$

If λ_2 and λ_3 are the extension ratios in the plane of the sheet, and the rubber does not change its volume during deformation, then

$$\lambda_2 = \lambda_3 = 1/\sqrt{\lambda_1}$$

where λ_1 is the extension ratio in the thickness direction. If h_0 is the original thickness, the area on which the force f per unit length acts is $\lambda_1 h_0$, hence

$$f = t_2 \lambda_1 h_0 = t_2 h_0 \lambda_2^{-2}$$

where t_2 is the true stress which is equal to t_3 . Thus the true stress t_2 is given by

$$t_2 = \lambda_2^2 f / h_0$$

Here again superposition of a hydrostatic pressure $-t_2$ will reduce tensile stresses t_2 and

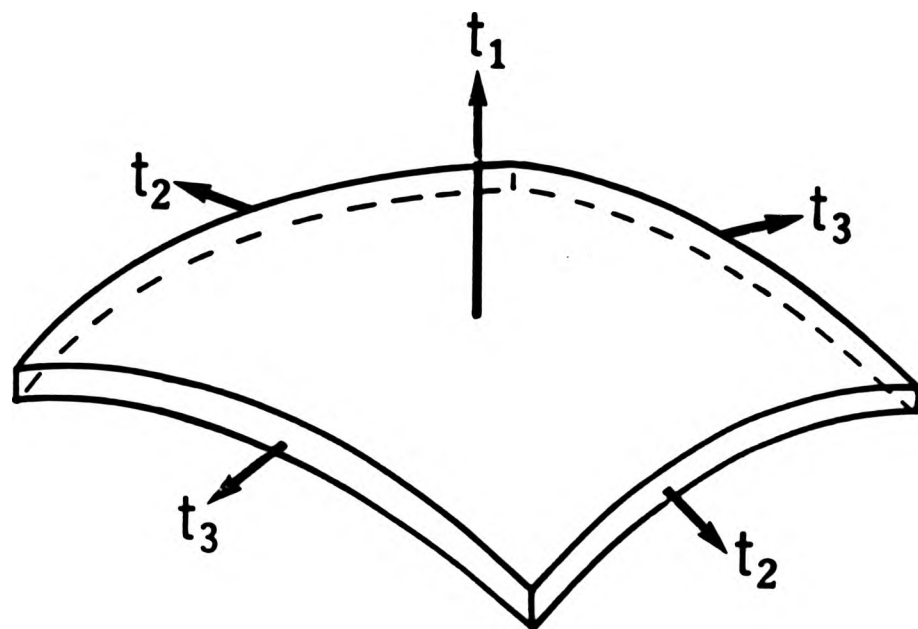


Figure 7.2 Inflation of rubber sheet.

t_3 to zero to give an equivalent value of t_1 which is the true compressive stress normal to the surface the rubber sheet. Hence,

$$t_1 = \lambda_2^2 f / h_0 \quad 7.2$$

The change in energy per unit volume, δW , with a small change in $\delta \lambda_1$ is $t_1 \lambda_2^2 \delta \lambda_1$ or $t_1 \lambda_1^{-1} \delta \lambda_1$. Thus the value of W , as λ_1 changes from the value of 1 to λ_1' , is given by the following equation;

$$W = \int_{\lambda_1=1}^{\lambda_1=\lambda_1'} t_1 \lambda_1^{-1} d\lambda_1 \quad 7.3$$

where λ_1' is the value of λ_1 when the rubber sheet ruptures. λ_1' must therefore be equal to the compression ratio (λ_c) at puncture. The value of W thus obtained is approximately equal to W in the rubber column at the state of strain λ_1' . W is, in principle, readily obtained from the area of the curve of the plot of $t_1 \lambda_1^{-1}$ versus λ_1 .

Knowing W and λ_c , the terms $W r_0 / 2$ and $F(1 - \lambda_c) / 2\pi r_0$ in the puncture energy equation can now be calculated.

As discussed in Chapter Six, ring crack formation precedes puncture which results in the increase in the length of the rubber column. For a very sharp indenter, the rubber will experience the

highest stress concentration at the circular edge of the indenter. As observed, the ring crack is indeed circular. It is reasonable to assume that the diameter of the ring crack in the strained state will be equal to the diameter of the indenter. It follows that the elongation ratio (λ_2 and λ_3) in the equibiaxial direction is equal to;

$$\frac{\text{diameter of the indenter}}{\text{unstrained diameter of the ring crack}}$$

Knowing λ_2 and hence λ_3 , λ_1 can be calculated and it can be compared with λ_c , measured by the equibiaxial method and this will indicate the applicability of the theory.

However, the method of obtaining the compression ratio by measuring the diameter of the ring crack may not give the exact value of the compression ratio at puncture because the diameter of column where the crack starts to propagate may not correspond exactly to the diameter of the ring crack. In any case, this method is considered to be a reasonable first approximation but may not be precise value of the compression ratio at puncture because slip can occur between ring crack formation and puncture.

7.2.2. Model experiment for equibiaxial tearing

Square test-pieces of 7cm edge were cut from sheets of vulcanizates D,H,F,J and K (Table 4.1) of uniform thicknesses varying from 0.6 to 1.5 mm. Each test-piece was clamped horizontally on its major surfaces between metal plates, the upper of which had in it a circular hole of radius 25mm and the lower of which carried a tube. By passing compressed air into this tube, the sheet could be inflated, the air pressure being measured by a mercury manometer. The experimental arrangement is shown schematically in Figure 7.3 .

Measurements were made as follows on the rubber sheets until bursting occurred. Initially, a circular grid(25mm radius) and two perpendicular lines were drawn centrally with a silver pen such as shown in Fig 7.4(a). For each inflated pressure, two photographs were taken. One was a planar view, as shown in Fig 7.4, and the other a profile view, as shown in Fig 7.5. From the photographs, the lengths X and Y(Fig 7.6) could be obtained. The radius of curvature of the inflated sheet is thus,

$$a = \frac{1}{2} \left(\frac{x^2}{4Y} + Y \right)$$

and the length of the arc AOB = $2a\theta$, where θ is in

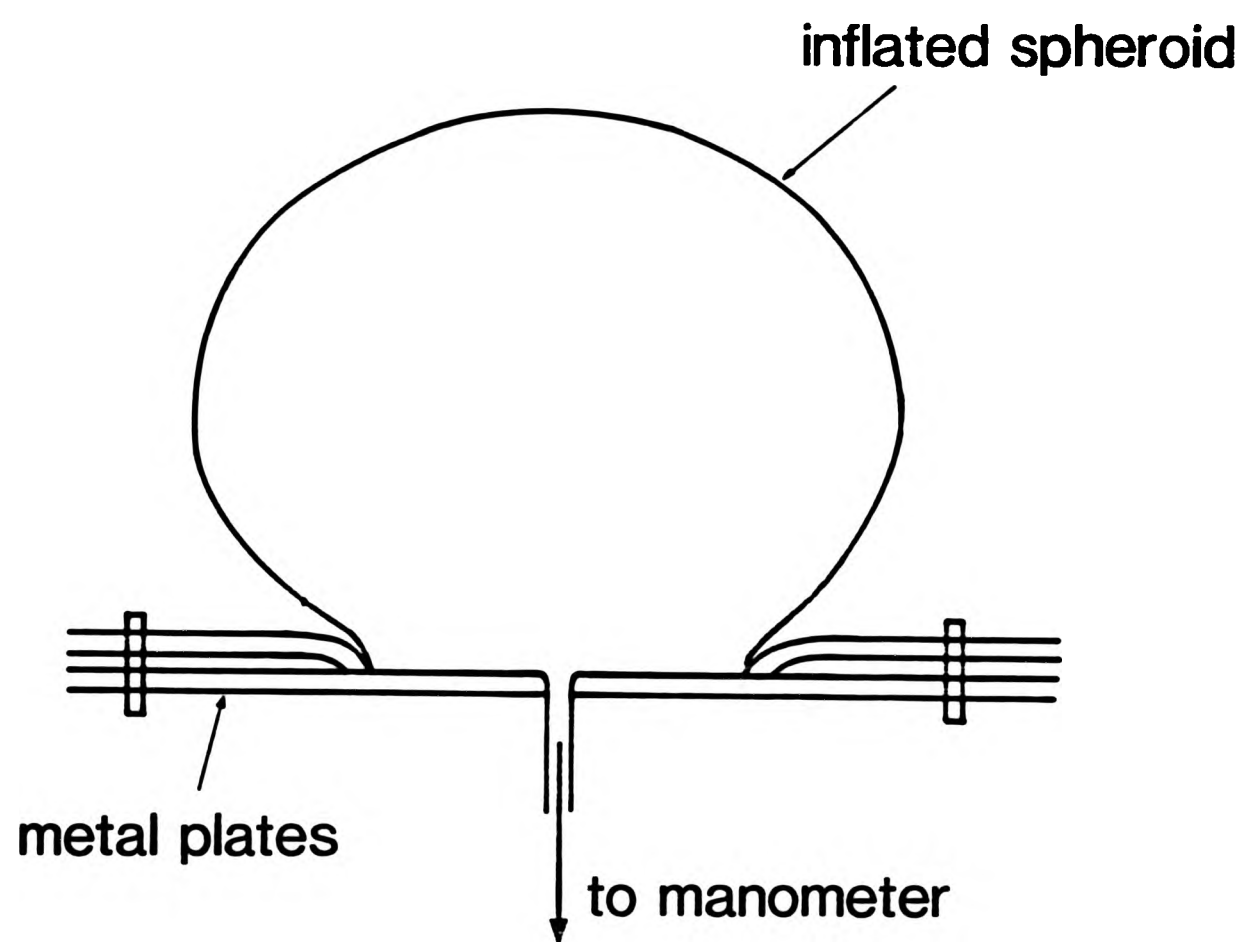
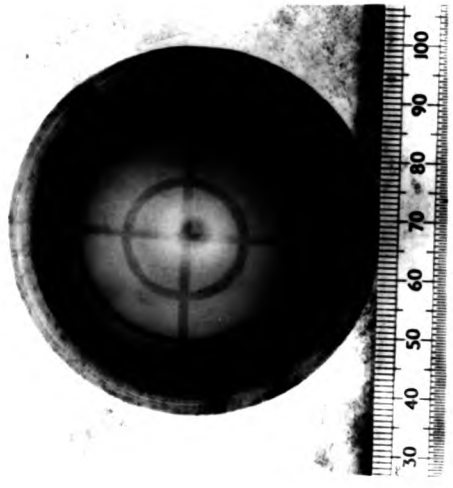


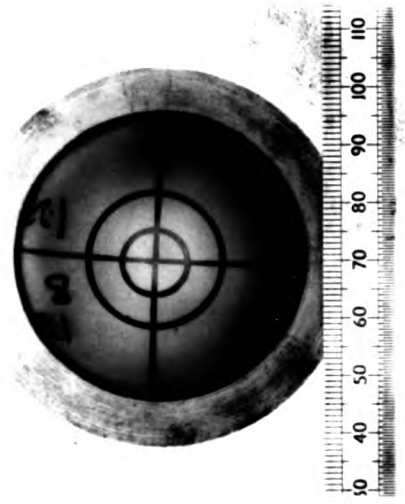
Figure 7.3 Experimental arrangement of rubber inflation.



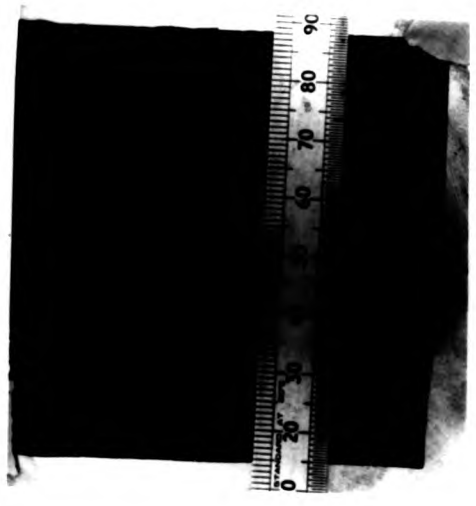
(d)



(c)



(b)



uninflated
(a)

← increasing pressure

Figure 7.4 Photographs showing progressive inflation of the rubber sheet with increasing pressure(planar views).

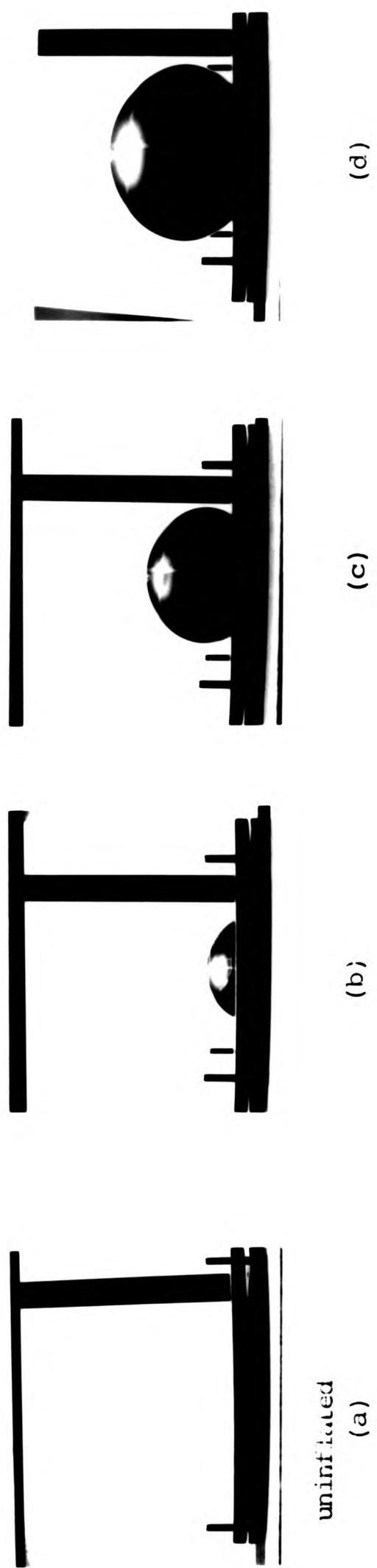


Figure 7.5 Photographs showing progressive inflation of the rubber sheet with increasing pressure (profile view).

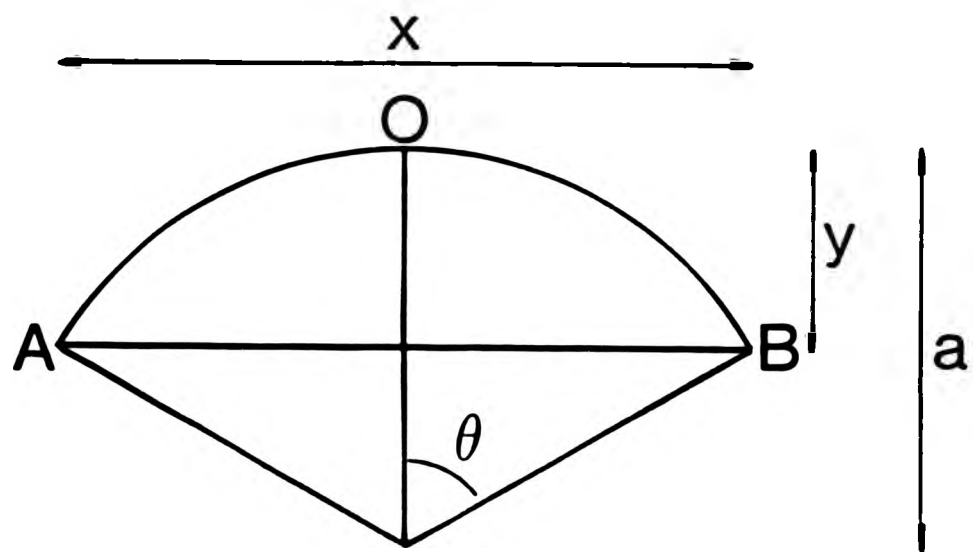


Figure 7.6 Schematic diagram of inflated rubber sheet showing X , Y and θ .

radians. Knowing that

$$\lambda_2 = \frac{\text{arc AOB}}{AB}$$

and also knowing the radius of curvature, a , and the inflation pressure, P , the value of f can be calculated using equation 7.1. Then having found f , and knowing λ_2 and h_0 , t_1 can then be obtained from equation 7.2.

Table 7.1 gives the relevant experimental data and the results obtained for f and t_1 for various extents of inflation up to the bursting point, for sheets of vulcanizates D, H, F, J and K. Fig 7.7 shows the plot of $t_1 \lambda_1^{-1}$ versus λ_1 for these vulcanizates. The areas under the curves which were calculated using trapezoidal rule are the values of the W ; and they are given in table 7.2. These are not strictly the value of W at bursting because no measurement could be made when the sheet bursted. However, these results were obtained at the inflating pressure very close to the bursting pressure. The vulcanizate F showed a lower value of W than vulcanizates D and H because, being a weaker rubber, it tore at the clamp before bursting took place at the pole of the inflated spheroid.

Table 7.3 shows the comparison of the values of compression ratios at puncture obtained by the equibiaxial experiment and by the measurement of the

Table 7.1 Results of equibiaxial strain experiments

Vulcanizate D

Thickness 1.5 mm

pressure kN/m ²	a mm	λ_2	λ_1	f N/m	t_1 MPa	$t_1 \lambda^{-1}$ MPa
1.96	21.7	1.21	0.680	21.3	0.02	0.03
1.91	18.5	1.27	0.620	17.7	0.02	0.04
2.60	17.6	1.58	0.400	22.9	0.05	0.12
2.69	42.9	3.38	0.087	57.7	0.53	6.02
2.64	44.0	4.27	0.055	58.1	0.85	15.50
2.60	53.9	4.83	0.043	70.0	1.35	31.50
2.70	60.5	5.12	0.038	81.6	1.52	39.80
2.99	73.9	6.03	0.027	110.5	3.10	111.80

Vulcanizate H

thickness: 0.75 mm

2.28	20.5	1.15	0.756	21.4	0.04	0.05
2.42	24.6	1.22	0.672	22.1	0.05	0.07
2.75	28.9	1.28	0.610	23.9	0.06	0.10
3.01	35.4	1.80	0.308	46.7	0.21	0.68
3.25	41.3	2.25	0.197	58.1	0.41	2.10

3.54	46.3	3.50	0.081	60.0	1.02	12.51
3.82	55.1	4.25	0.055	65.0	1.63	29.45
4.40	63.5	5.05	0.039	88.0	3.12	79.49

vulcanizate F

thickness: 0.77 mm

1.58	25.1	1.04	0.916	19.8	0.03	0.03
2.16	27.7	1.10	0.824	29.9	0.04	0.05
2.38	26.7	1.12	0.800	31.8	0.05	0.06
2.90	25.5	1.13	0.784	37.0	0.06	0.08
3.54	23.7	1.16	0.748	42.0	0.07	0.10
4.44	21.2	1.32	0.578	47.1	0.10	0.18
5.42	26.2	1.91	0.273	71.0	0.34	1.23

Vulcanizate J

thickness: 0.63 mm

1.36	33.0	1.09	0.841	22.4	0.04	0.05
2.03	49.1	1.62	0.382	49.7	0.21	0.55
2.31	80.0	2.31	0.187	92.2	0.79	4.21
2.52	58.9	2.51	0.159	74.2	0.75	4.73
2.59	39.0	3.76	0.070	50.4	1.15	16.27
2.92	55.6	3.82	0.068	81.1	1.91	27.87

Vulcanizate K

thickness:0.75 mm

2.24	35.1	1.07	0.875	39.4	0.06	0.07
2.81	36.8	1.18	0.712	51.7	0.10	0.14
3.36	32.5	1.31	0.500	54.6	0.13	0.23
3.96	30.4	1.69	0.350	60.0	0.24	0.70
4.26	29.6	1.90	0.277	63.13	0.32	1.17
4.55	33.7	2.18	0.210	76.47	0.52	2.46
4.78	35.9	2.41	0.172	85.90	0.71	4.14
5.13	41.2	2.72	0.135	105.78	1.11	8.27
5.52	45.6	2.99	0.111	125.94	1.61	14.38
5.85	47.8	3.17	0.099	139.84	2.00	20.17
6.40	54.4	3.45	0.084	174.05	3.00	35.63

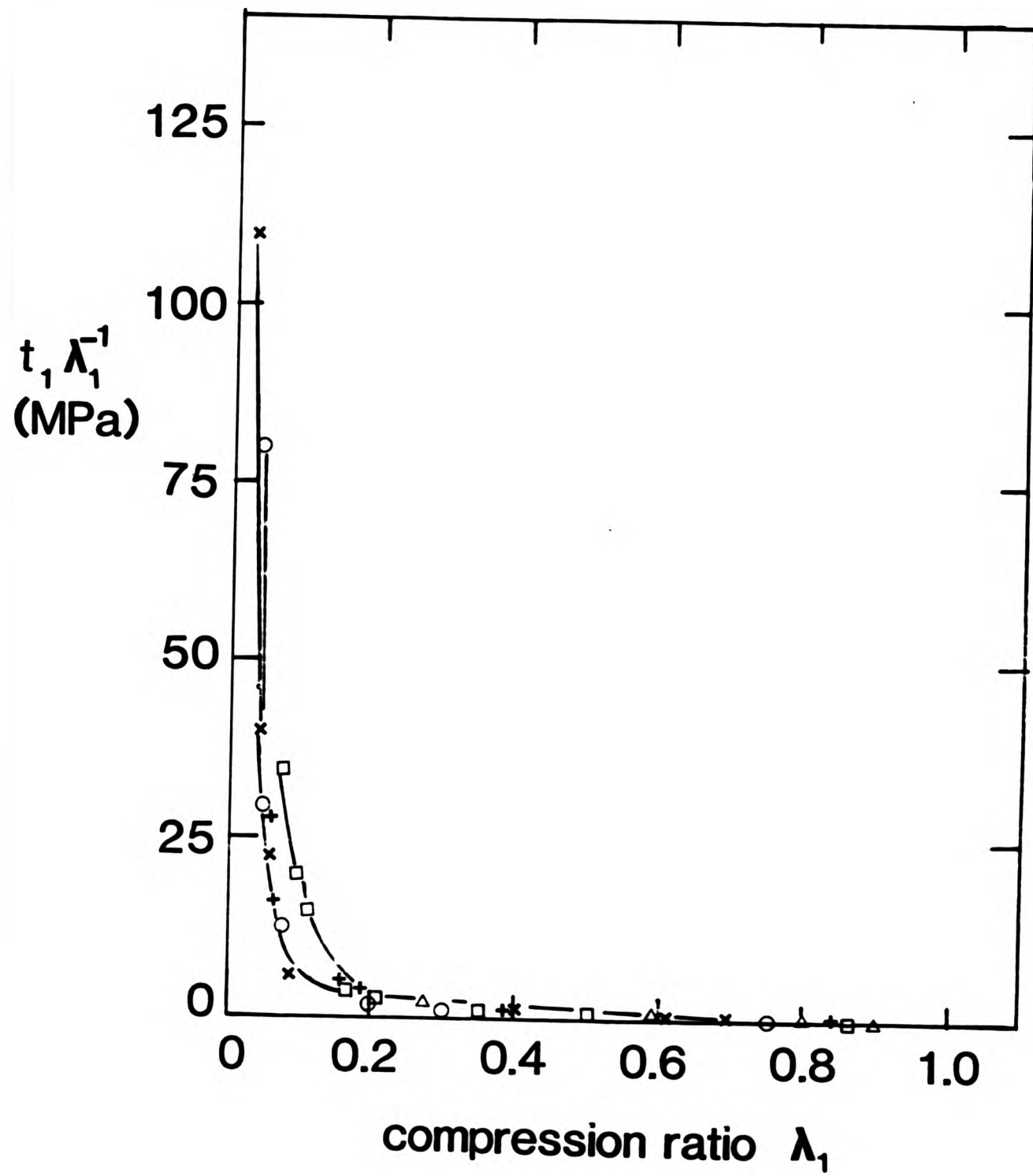


Figure 7.7 Plots of $t_1 \lambda_1^{-1}$ versus λ_1 : (vulcanizate D \times), (vulcanizate H \circ), (vulcanizate F Δ), (vulcanizate J $+$) and (vulcanizate K \square)

Table 7.2 Results for energy stored per unit volume at point of rupture, W, obtained from equibiaxial strain experiments.

Vulcanizates	W J/m^{-3}
D	3.80×10^6
H	2.79×10^6
F	0.53×10^6
J	1.89×10^6
K	2.09×10^6

Table 7.3 Comparison of compression ratios at the point of rupture obtained by equibiaxial method and surface crack measurement.

Vulcanizates	Equibiaxial	Surface crack	
		1.5 mm indenter 10 μ m	750 μ m
D	0.03	0.44	0.07
H	0.04	0.28	0.02
F	0.27	0.20	0.01
J	0.07	0.16	0.01
K	0.08	0.21	0.02

surface cracks produced by indentors of different corner radii. The compression ratios obtained from the latter were the mean value of five puncture tests. The diameter of the surface cracks was measured using an optical microscope with a graduated scale with an accuracy of $\pm 0.01\text{mm}$. The coefficient of variations of the diameter of the cracks increases from 10% for $10\mu\text{m}$ corner radius to 25% for $750\mu\text{m}$ corner radius. It can be seen that the compression ratios obtained from the hemispherical indenter agree broadly with those obtained from the equibiaxial experiment except in the case of vulcanizate F. But compression ratios obtained using the sharp indenter differ greatly from those obtained by equibiaxial straining.

7.2.3 Bursting of the rubber sheet

The compressive ratios at bursting were difficult to obtain accurately. This is because the point at which the rubber burst cannot be predicted. Therefore the compressive ratios were obtained at the strain just before bursting occurred. But the compressive ratios obtained in this way should not be very much different from the true bursting compressive ratios.

More useful information from the bursting rubber sheet is the pattern of the ruptured rubber sheet, which showed biaxial rupture characteristics.

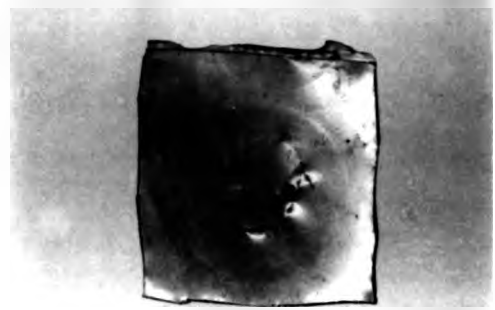
Common to all the vulcanizates tested (D, H, F, J and K) is the random petal type bursting at the pole of the inflated sheet, as shown in Fig 7.8. However there were more petals for vulcanizates J and K than for vulcanizates D and H. In the latter cases, the petals were kidney-shaped. Bursting could not be observed with vulcanizate F because, being a weaker vulcanizate, it broke at the grip before bursting.

In some ways, the random petal-like bursting pattern resembles the puncture surface crack (Fig 6.14 section 6.2.3) obtained using the hemispherical indenter (750 μ m corner radius). This suggests that, for this particular indenter, equibiaxial rupture may be a mechanism in the puncture process which explains a broad agreement between compression ratios at rupture obtained using a hemispherical indenter and from equibiaxial extension measurement.

The experimental results shown in Figures 5.6 and 5.7 of Chapter Five for the effect of corner radius on puncture force show that, as the indenter corner radius increases, the puncture force increases sharply to a maximum and then decreases slowly. This suggests that, for indentors having small radii, the puncture process depends more on the sharpness of the corner of the indenter causing a high stress concentration than on the equibiaxial extension of the rubber. This might explain the discrepancy between compression ratios at rupture obtained using



D



H



J



K

Figure 7.8 Random petal type bursting of vulcanizates D, H, J and K.

a sharp indenter and from equibiaxial strain experiment.

7.3 Energy stored in the rubber surrounding the column.

7.3.1 Theory

The energy N arising from the expansion of the puncture crack (see Section 6.4) can be calculated if the internal pressure, P , or stress, t_2 , acting on the inner wall of the cylinder surrounding the rubber column is known.

Consider in Figure 7.9 a cylindrical puncture hole of radius r_0 , subjected to internal pressure P , and the radius of the puncture hole increases to r . As a result of the expansion of the puncture hole, the thickness of the small element ABCD decreases from δr_0 to δr . In addition, the element ABCD now supports the radial stress t_2 (compressive) and the circumferential stress t_1 (tensile). If it is assumed that there is no vertical strain, then $\lambda_3 = 1$.

The extension ratios after expansion can be derived by considering the enlargement of the circumference. These ratios are

$$\lambda_1 = 2\pi r / 2\pi r_0 = r / r_0 \quad 7.4$$

$$\text{and } \lambda_2 = \delta r / \delta r_0 \quad 7.5$$

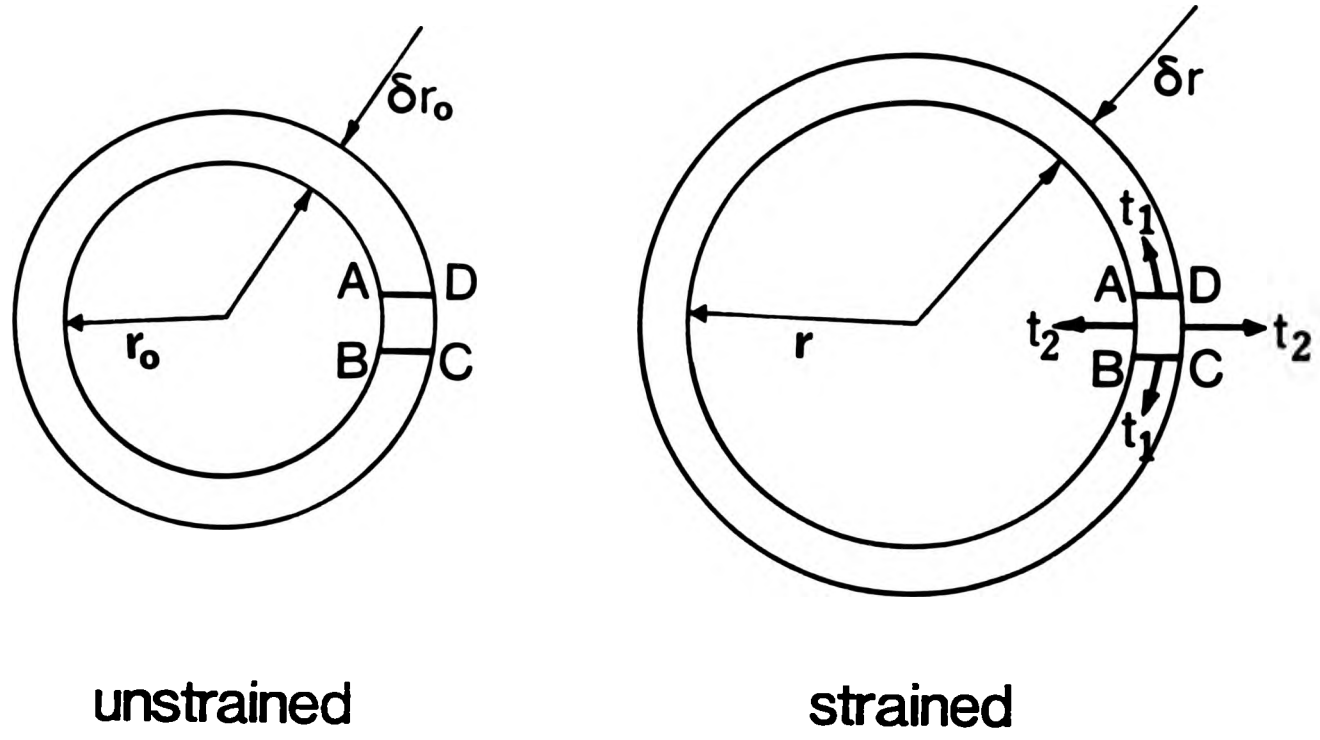


Figure 7.9 Stresses set up in a small element ABCD as the hole increases in radius from r_0 to r .

If it is assumed that rubber is incompressible, then $\lambda_1 \lambda_2 \lambda_3 = 1$, so that $\lambda_1 \lambda_2 = 1$. Therefore

$$\frac{\delta r}{\delta r_0} = \frac{r_0}{r}$$

i.e., $r \delta r = r_0 \delta_0$

Integration of each side of this equation gives

$$\frac{1}{2} r^2 = \frac{1}{2} r_0^2 + \text{constant} \quad 7.6$$

Let the values of r and r_0 be b and b_0 respectively at a particular deformation. Equation 7.6 then becomes

$$\frac{1}{2} b^2 = \frac{1}{2} b_0^2 + \text{constant}$$

and the value of the constant in equation 7.6 is

$$\frac{1}{2} b^2 - \frac{1}{2} b_0^2$$

Thus equation 7.6 becomes

$$r^2 = r_0^2 + b^2 - b_0^2 \quad 7.7$$

By dividing equation 7.7 by r_0^2 we get

$$\lambda_1^2 = 1 + b^2/r_0^2 - b_0^2/r_0^2$$

Using equation 7.4, this can be rearranged to give

$$r^2 = (b^2 - b_0^2) \left(\frac{\lambda_1^2}{\lambda_1^2 - 1} \right) \quad 7.8$$

Differentiation of equation 7.8 with respect to λ_1 gives

$$\frac{dr}{d\lambda_1} = \frac{-\lambda_1(b^2 - b_0^2)}{r(\lambda_1^2 - 1)^2} \quad 7.9$$

Combining this equation with equation 7.8 gives

$$\frac{\delta r}{r} = - \frac{1}{\lambda_1^2 - 1} \cdot \frac{\delta \lambda_1}{\lambda_1} \quad 7.10$$

The stress-strain relation for a rubber which obeys the Mooney-Rivlin equation are(65)

$$\begin{aligned} t_2 &= 2(\lambda_2^2 C_1 - \frac{1}{\lambda_2^2} C_2) + p \\ t_1 &= 2(\lambda_1^2 C_1 - \frac{1}{\lambda_1^2} C_2) + p \\ t_3 &= 2(\lambda_3^2 C_1 - \frac{1}{\lambda_3^2} C_2) + p \end{aligned} \quad 7.11$$

where p is an arbitrary hydrostatic pressure for constant volume deformation and C_1 and C_2 are elastic constant.

Since $\lambda_3 = 1$, on substitution into equation 7.11 we get,

$$\begin{aligned} t_2 - t_1 &= 2C_1 \left(\frac{1}{\lambda_1^2} - \lambda_1^2 \right) + 2C_2 \left(\frac{1}{\lambda_1} - \lambda_1 \right) \\ &= 2(C_1 + C_2) \left(\frac{1}{\lambda_1^2} - \lambda_1^2 \right) \end{aligned} \quad 7.12$$

In addition, the equation of equilibrium for the element ABCD is (66),

$$dt_2/dr = (t_2 - t_1)/r \quad 7.13$$

On rearrangement, this becomes

$$\delta t_2 \cong (t_2 - t_1) \delta r / r \quad 7.14$$

Substituting the value of $t_2 - t_1$ from equation 7.12 and that of $\delta r / r$ from equation 7.10 into equation 7.14, we get

$$\begin{aligned} \delta t_2 &\cong 2(C_1 + C_2) \left(\lambda_1^2 - \frac{1}{\lambda_1} \right) \left(\frac{\delta \lambda_1}{\lambda_1 (\lambda_1^2 - 1)} \right) \\ &\cong 2(C_1 + C_2) \left(\frac{\lambda_1^2 + 1}{\lambda_1^3} \right) \delta \lambda_1 \end{aligned} \quad 7.15$$

Hence the stress t_2 or pressure P required to increase the radius of a cylindrical cavity by a factor of r/r_0 can be obtained by integrating equation 7.15 over the range $\lambda_1 = 1$ to $\lambda_1 = r/r_0$. The result obtained for P is

$$P = (C_1 + C_2) \left[1 - \frac{r_0^2}{r^2} + \ln\left(\frac{r^2}{r_0^2}\right) \right] \quad 7.16$$

Having obtained an expression for P , we now can derive an expression for the stored energy, N , surrounding the rubber column and subsequently the rate of change of this energy with the crack length c at constant applied force, i.e., $\left(\frac{\partial N}{\partial c}\right)_F$.

Consider a cylindrical puncture in an unstrained state and the radius is r_0 as shown in Figure 7.10 (a). As the indenter penetrates the hole, the indenter exerts a pressure on the inner wall of the hole which subsequently expands to a new radius r_1 as shown in Figure 7.10(b). The work done or the energy stored in the rubber during this expansion can be calculated as follows. Consider an increment δr of the radius r of the cylindrical cavity and r is an arbitrary radius between r_0 and r_1 . The change in energy stored in the rubber is $P\delta V$ where δV is equal to $2\pi r c \delta r$. Hence the energy stored in

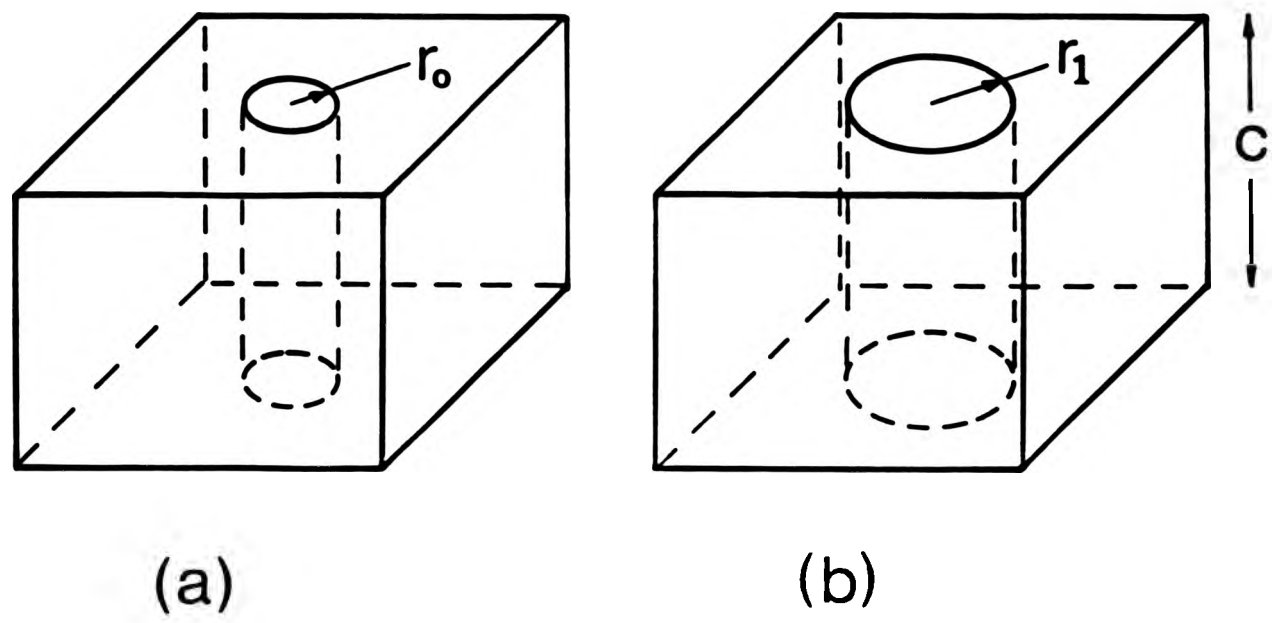


Figure 7.10 Expansion of puncture hole from radius r_0 to r_1 .

the surrounding rubber column as the puncture hole expands from unstrained radius r_0 to r_1 is given by

$$N = \int_{r_0}^{r_1} P 2\pi r c dr \quad 7.17$$

The term to be determined in the puncture energy equation is $\frac{1}{2\pi r_0} \left(\frac{\partial N}{\partial c} \right)_F$. Dividing equation 7.17

by r_0 and on rearrangement we get,

$$\frac{1}{2\pi r_0} \left(\frac{\partial N}{\partial c} \right)_F = \frac{1}{r_0} \int_{r_0}^{r_1} r P dr \quad 7.18$$

Substitution of equation 7.16 into equation 7.18, gives,

$$\begin{aligned} \frac{1}{2\pi r_0} \left(\frac{\partial N}{\partial c} \right)_F &= \frac{C_1 + C_2}{r_0} \int_{r=r_0}^{r=r_1} r \left(1 - \frac{r_0^2}{r^2} + 2 \ln \frac{r}{r_0} \right) dr \\ &= \left(\frac{C_1 + C_2}{r_0} \right) \left(r_1^2 - r_0^2 \right) \ln \left(\frac{r_1}{r_0} \right) \quad 7.19 \end{aligned}$$

In this case, r_1 is equal to the radius of the indenter and r_0 is the radius of the unstrained puncture crack. Both radii are readily obtainable.

The method of determining C_1 and C_2 is described in the next section.

7.3.2 Determination of C_1 and C_2 : results

The quantities C_1 and C_2 in the equation 7.19 are constants in the equation which describes the stress-strain behaviour of rubber in simple extension(65), i.e.,

$$f = 2A_0(\lambda_a^{-2} - \lambda_a^{-1})(C_1 + \lambda_a C_2) \quad 7.20$$

where f is the force required to extend a sample of rubber of unstrained cross-sectional area A_0 to an extension ratio λ_a .

Measurements of the constant C_1 and C_2 of the vulcanizates D,H,F,J and K in simple extension were made using an instrument devised by Greensmith(67) for this purpose. A parallel-sided specimen of approximately 3 x 1 x 110 mm is clamped in the sample holder and its length is determined in a preliminary experiment in which a stress-strain curve is constructed at strains up to 2%, allowing 1 minute relaxation at each strain. The unstrained length is then estimated by extrapolating the stress-strain curve to zero stress. After allowing the specimen to recover for 5 minutes, the specimen is then extended in a series of strains from

λ_a^{-1} of 0.95 to ca 0.35 in intervals of 0.05. At each strain a relaxation time of 3 minutes is allowed before measuring the force of retraction, f . The Mooney-Rivlin coefficients can then be estimated from a graph of $f/2A_0(\lambda_a - \lambda_a^{-2})$ against λ_a^{-1} . The intercept is equal to the coefficient C_1 and the slope is equal to the coefficient C_2 .

Figure 7.11 shows plots of $f/2A_0(\lambda_a - \lambda_a^{-2})$ against λ_a^{-1} for the vulcanizates D, H, F, J and K. The curves show that at low and moderate extensions there is a linear region. At higher extensions (smaller λ_a^{-1}), departures from linearity occur. Each curve goes through a minimum, the value of $f/2A_0(\lambda_a - \lambda_a^{-2})$ thereafter increasing rapidly with further extension. From the slopes and intercepts of the linear portions of the curve, the values of C_1 and C_2 were obtained. These values are given in Table 7.4.

7.4 Effect of corner radius on puncture energy

The results presented in Figures 5.6 and 5.7 of Chapter Five show that the puncture force is dependent on the corner radius of the indenter. Inevitably, this corner radius will greatly influence the puncture energy. Table 7.5 and 7.6 show the results on vulcanizate D for the effect of corner radius on the three terms in the puncture energy

$f/2A_0(\lambda_a - \lambda_a^{-2})$ (MPa)

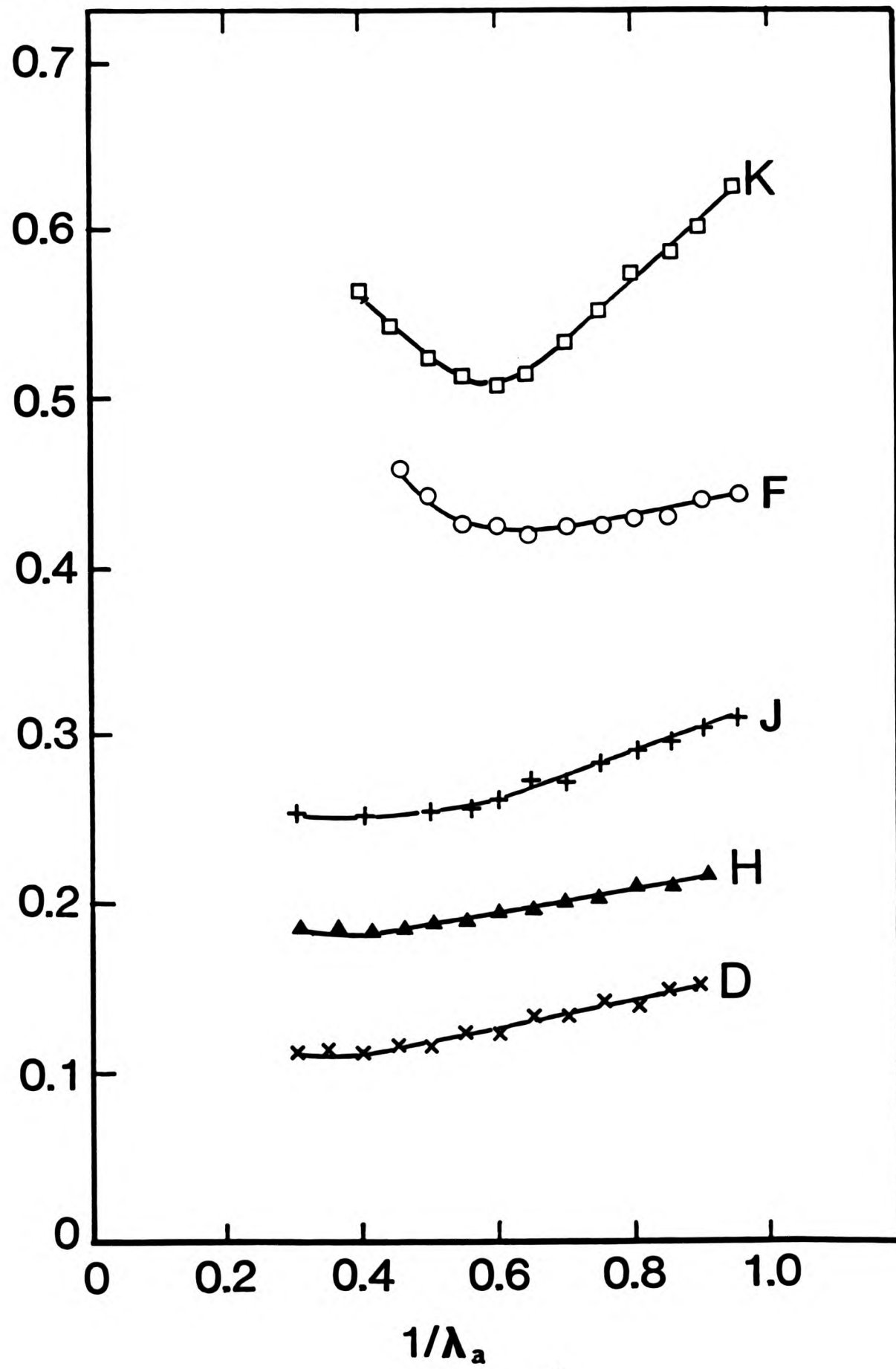


Figure 7.11 A plot of $f/2A_0(\lambda_a - \lambda_a^{-2})$ versus $1/\lambda_a$.

Table 7.4 Values of C_1 and C_2

Vulcanizate	C_1 MPa	C_2 MPa
D	0.09	0.07
H	0.15	0.07
F	0.37	0.07
J	0.18	0.14
K	0.27	0.37

Table 7.5 Effect of corner radius on various terms in the puncture energy equation.

Vulcanizate D

1.5-mm indenter

Tearing energy from trouser tear test: 12.5kJ/m²

corner radius μm	r _o mm	$\frac{W r_o}{2}$ kJ/m ²	$\frac{1}{2\pi r_o} \left(\frac{\partial N}{\partial c} \right) F$ kJ/m ²	$\frac{F(1 - \lambda_c)}{2\pi r_o}$ kJ/m ²	T ^o kJ/m ²
10	0.50	0.95	0.04	10.5	9.5
60	0.30	0.57	0.23	38.0	11.0
100	0.30	0.57	0.23	42.0	9.0
250	0.25	0.47	0.35	43.0	18.0
750	0.20	0.38	0.55	57.0	16.0

T^o = tearing energy obtained from a direct determination using the force/deflection curve and the total crack area.

r_o = radius of surface crack

λ_c = compression ratio at rupture based on the surface crack

Table 7.6 Effect of corner radius on various terms in the puncture energy equation.

Vulcanizate D

0.5-mm indenter

Tearing energy from trouser tear test: 12.5kJ/m²

corner radius μm	r _o mm	$\frac{W r_o}{2}$ kJ/m ²	$\frac{1}{2\pi r_o} \left(\frac{\partial N}{\partial c} \right) F$ kJ/m ²	$\frac{F(1 - \lambda_c)}{2\pi r_o}$ kJ/m ²	T ^o kJ/m ²
5	0.14	0.27	0.02	13.0	10.0
50	0.12	0.24	0.04	13.5	11.5
100	0.09	0.18	0.09	13.0	12.0
250	0.06	0.12	0.22	12.0	17.0

T^o-tearing energy obtained from a direct determination using the force/deflection curve and the total crack area.

r_o-radius of surface crack

λ_c-compression ratio at rupture based on the surface crack

equation. These three terms are $F(1 - \lambda_c)/2\pi r_o$, $W r_o/2$ and $\frac{1}{2\pi r_o} \left(\frac{\partial N}{\partial c} \right) F$. The latter was evaluated using equation 7.19. The results in Table 7.5 and 7.6 are based on 1.5-mm and 0.5-mm diameter indentors respectively. Figure 7.12 shows the plot of the various terms versus corner radius. The values of the terms $W r_o/2$ and $\frac{1}{2\pi r_o} \left(\frac{\partial N}{\partial c} \right) F$ are not plotted because they are too small to be relevant.

It can be seen that, for a 1.5-mm diameter indenter with 10 μm corner radius, the $F(1 - \lambda_c)/2\pi r_o$ term shows good agreement with the value of tearing energy obtained from the direct measurement using the force/deflection curve and the total area of the crack, and with the value of tearing energy obtained from the trouser tear test (12.5 kJ/m^2). However, as the corner radius increases, $F(1 - \lambda_c)/2\pi r_o$ becomes very high. The value of T_c obtained by direct measurement appears not to increase substantially with increasing corner radius. The values for the term $W r_o/2$ do not appear to change with increasing corner radius, and are 1 kJ/m^2 or less. The values of $\frac{1}{2\pi r_o} \left(\frac{\partial N}{\partial c} \right) F$ are very small indeed (less than 0.55 kJ/m^2), and are unaffected by corner radius.

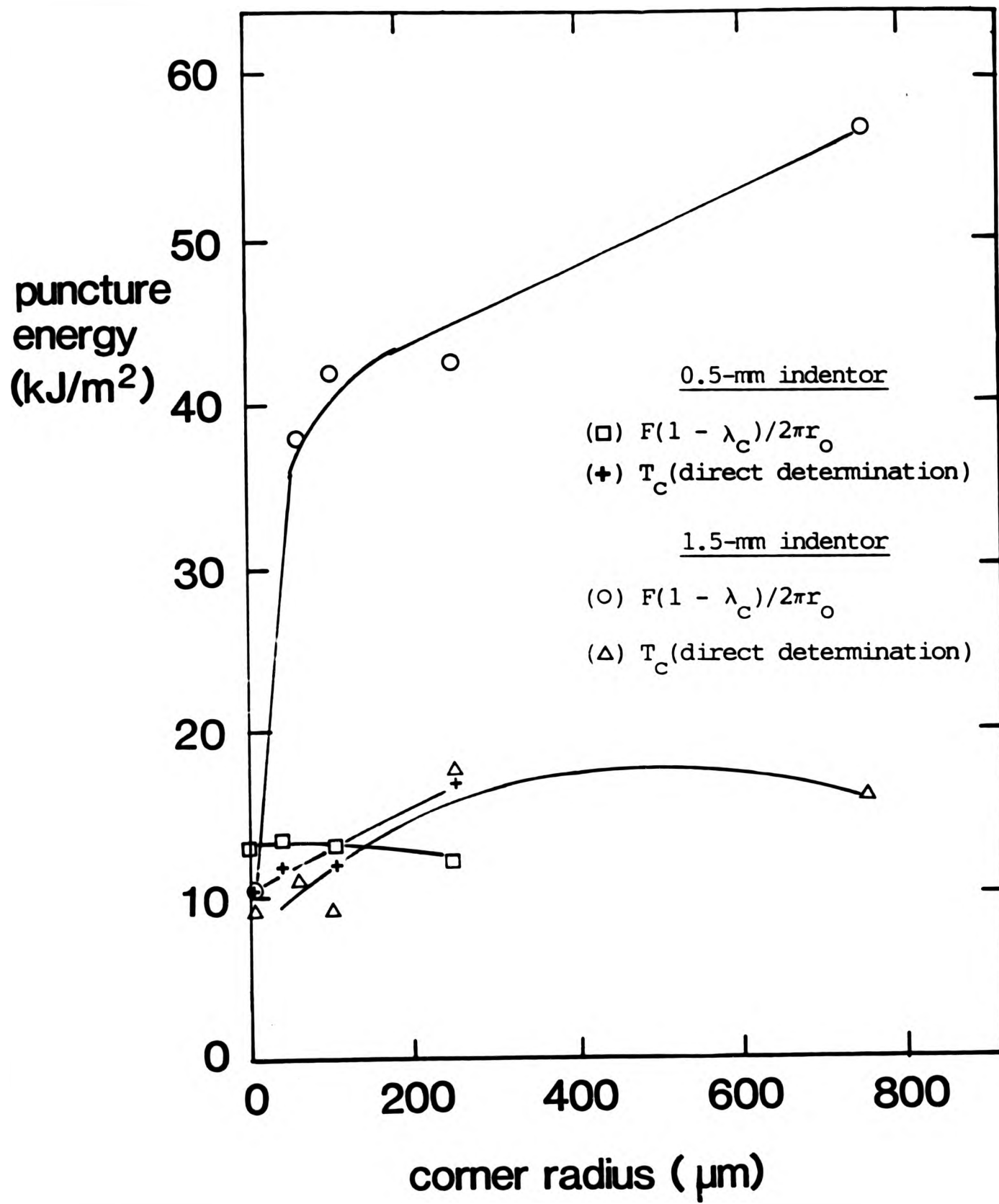


Figure 7.12 Effect of corner radius on contributions to puncture energy of vulcanizate D.

For a 0.5-mm diameter indenter with 10 μm corner radius, the values of the terms $Wr_0/2$ and $\frac{1}{2\pi r_0} \left(\frac{\partial N}{\partial c} \right) F$ are both very low. The $F(1 - \lambda_c)/2\pi r_0$ term at low corner radius shows good agreement with the tearing energy obtained from the trouser tear test and the value of T_c obtained by direct measurement. With increasing corner radius, the value of the term $F(1 - \lambda_c)/2\pi r_0$ does not vary greatly, suggesting that for a 0.5-mm diameter indenter the puncture energy equation can give a reasonably accurate value of tearing energy which is independent of corner radius.

Observations on the puncture columns reported in Chapter Six show that the diameter of the columns varies at different depths. The results shown in Fig 7.12 were based on the value of r_0 measured at the surface. Table 7.7 shows the effects of base radius crack on puncture energy of vulcanizate D using 1.5-mm diameter indentors of various corner radii. Figure 7.13 shows the comparison of the effect of base and surface diameter crack on the various terms in the puncture energy equation. The data based on surface crack were obtained from the Table 7.5.

Again, the values of $Wr_0/2$ and $\frac{1}{2\pi r_0} \left(\frac{\partial N}{\partial c} \right) F$ are not

included since these values are very small compared to other terms. It can be seen that at, 10 μm

Table 7.7 The dependence of various terms in the puncture energy equation on the diameter of the base crack

Vulcanizate D

1.5-mm indenter

Tearing energy from trouser tear test: 12.5kJ/m²

corner radius μm	r _b mm	$\frac{W r_b}{2}$ kJ/m ²	$\frac{1}{2\pi r_b} \left(\frac{\partial N}{\partial c} \right) F$ kJ/m ²	$\frac{F(1 - \lambda_c)}{2\pi r_b}$ kJ/m ²	T ⁰ kJ/m ²
10	0.50	0.95	0.04	10.5	9.5
60	0.60	1.14	0.01	8.0	11.0
100	0.50	0.95	0.04	17.0	9.0
250	0.45	0.85	0.06	17.0	18.0
750	0.40	0.76	0.10	27.0	16.0

T⁰=tearing energy obtained from a direct determination using the force/deflection curve and the total crack area.

r_b=radius of base crack

λ_c=compression ratios obtained from the radius of base crack.

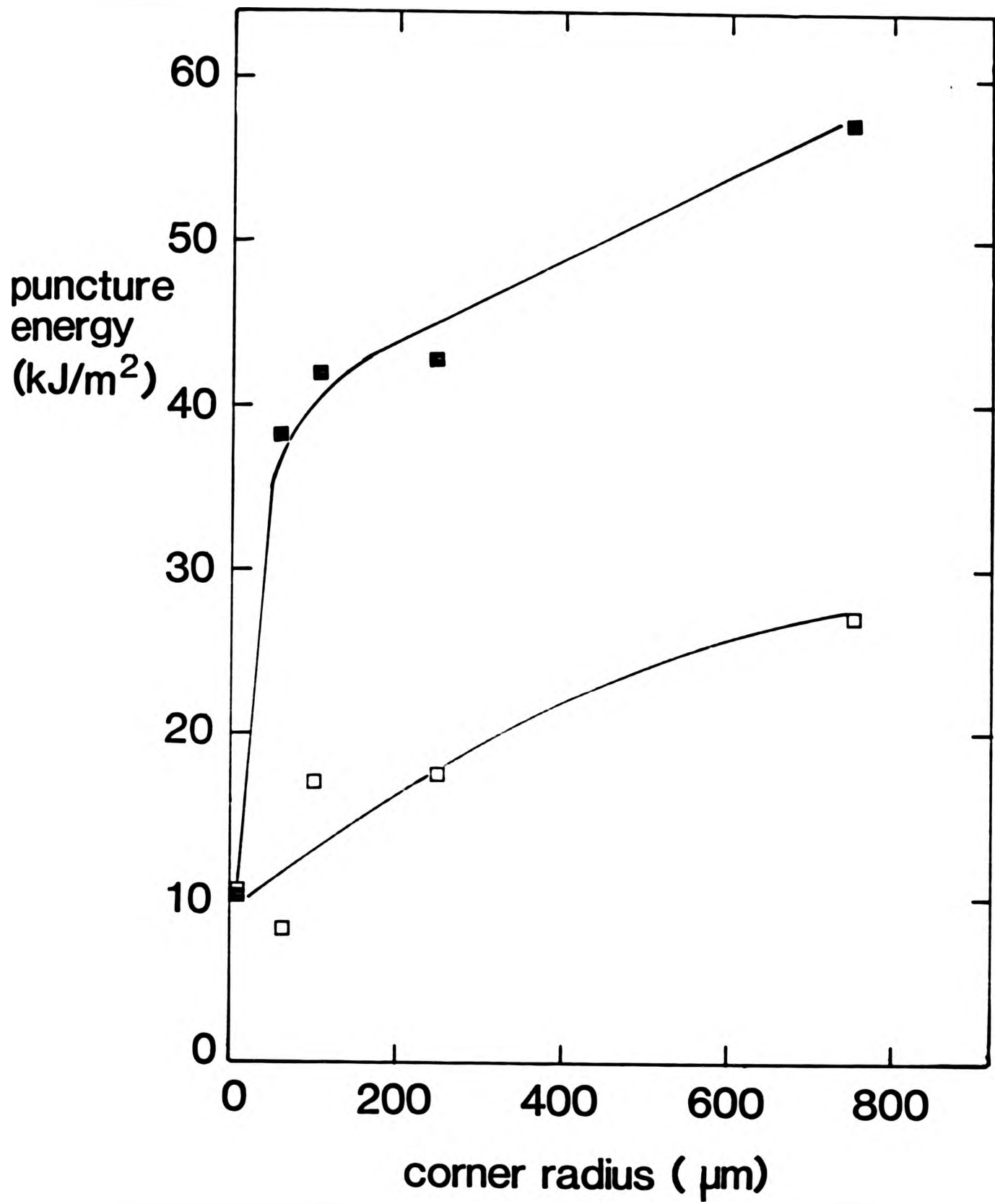


Figure 7.13 Effect of base and surface radius crack on puncture energy: (■) - surface radius, (□) - base radius. Indentor: 1.5-mm diameter indenter.

corner radius, the values of $F(1 - \lambda_c)/2\pi r_o$ for both base and surface diameters are equal. However, as expected, the value $F(1 - \lambda_c)/2\pi r_o$ increases with increasing corner radius for both the base and surface cracks.

Table 7.8 shows values of $F(1 - \lambda_c)/2\pi r_o$, $Wr_o/2$ and $\frac{1}{2\pi r_o} \left(\frac{\partial N}{\partial c} \right) F$ for vulcanizates D, H, F, J and K.

The indentors used were sharp-cornered (10 μ m corner radius). In all these cases, r_o is the surface value. It can be seen that the values of $F(1 - \lambda_c)/2\pi r_o$ for these vulcanizates agree well with values of T_c measured by the trouser tear test and with the puncture energy obtained by direct measurement. In addition, the values of $Wr_o/2$ and $\frac{1}{2\pi r_o} \left(\frac{\partial N}{\partial c} \right) F$ obtained using 0.5-mm indenter were lower than those obtained using the 1.5-mm indenter.

7.5 Conclusions concerning relative importance of terms in puncture energy equation

The results shown so far indicate that the contribution made to the puncture energy by the terms $Wr_o/2$ and $\frac{1}{2\pi r_o} \left(\frac{\partial N}{\partial c} \right) F$ is minimal regardless of the corner radius. In addition, these two terms appear to become much lower when a 0.5-mm diameter indenter is

Table 7.8 Comparison of various puncture energy terms

Vulcanizates	r_o	$\frac{W r_o}{2}$	$\frac{1}{2\pi r_o} \left(\frac{\partial N}{\partial c} \right)_F$	$\frac{F(1 - \lambda_c)}{2\pi r_o}$	T^*	T^d
	mm	kJ/m ²	kJ/m ²	kJ/m ²	kJ/m ²	kJ/m ²
D						
1.5-mm indenter	0.50	1.00	0.04	10.5	12.5	9.5
0.5-mm indenter	0.14	0.27	0.02	13.0		
H						
1.5-mm indenter	0.40	0.56	0.14	7.0	6.5	5.5
0.5-mm indenter	0.12	0.16	0.06	3.5		
F						
1.5-mm indenter	0.32	0.08	0.54	4.0	3.0	2.4
J						
1.5-mm indenter	0.24	0.22	0.76	10.0	12.0	8.0
0.5-mm indenter	0.07	0.06	0.34	9.0		
K						
1.5-mm indenter	0.35	0.36	0.61	25.0	22.0	18.0
0.5-mm indenter	0.07	0.07	0.67	21.0		

T^* = tearing energy measured from trouser tear test

r_o = surface crack radius

λ_c = compression ratio based on surface crack

T^d = tearing energy determined directly

used. As a result, the expression for the puncture energy, T_c , is effectively $F(1 - \lambda_c)/2\pi r_0$. In addition, at low corner radius, the value of $F(1 - \lambda_c)/2\pi r_0$ agrees well with the puncture energy obtained by direct measurement, and with the tearing energy measured by the trouser test method. This agreement is not unexpected since, as discussed in Chapter Six, ring cracks are much easier to initiate with sharp corner indentors than with blunt indentors, because the circular edge of the former is the locus of the highest stress concentration. The initial ring crack is a prerequisite to the successful fracture mechanic analysis.

Once a ring crack forms, it will be compressed uniaxially under an increasing applied force. Moreover, the tip of the crack is well-defined, and subsequent crack growth will increase the length of the crack or of the column. Therefore, as expected, a petal-like surface crack, characteristic of equibiaxial fracture, was not observed when an indenter having a sharp edge was used. However, for the blunt indenter, a surface crack characteristics of equibiaxial petal-like tear was observed. This suggests that under these circumstances puncture proceeds by equibiaxial fracture and with no initial ring cracking. As a result, the compression ratios, based on the diameter of the ring crack, produced by the hemispherical indenter agree well with the

compression ratios obtained from the equibiaxial experiment. For the sharp indenter, the agreement is not as good. However, the use of the compression ratios based on the diameter of the crack in the puncture energy equation, $F(1 - \lambda_c)/2\pi r_0$, gives satisfactory agreement with the puncture energy obtained by direct measurement, and with the catastrophic tearing energy as measured by the trouser tear test method.

CHAPTER EIGHT

APPLICATION OF PUNCTURE TEST TO A STUDY OF AGEING

8.1 Introduction

Rubber engineering components are frequently bulky and include thick layers of rubber. These components are sometimes expected to last for a very long time - e.g. over 100 years for civil engineering applications. Therefore it is necessary to have some method of assessing the probable lifetimes of these rubber components at the design stage before the components are subjected to service conditions. In this chapter, the use of puncture test to investigate changes in thick rubber blocks subjected to elevated temperatures and long term ageing is described.

The strength of rubber can be seriously affected by oxidation and the effect becomes worse when the rubber is subjected to high temperatures. It is known that a small amount of oxygen (ca. 1%) absorbed by a natural or synthetic rubber can have a deleterious effect on its physical properties(68). Much research has been concerned with the mechanisms of the basic oxidation processes, namely the interaction between elemental oxygen and rubbers.

The understanding of these chemical processes has been derived largely from the work on model systems, and, generally, on thin sheets of vulcanizate.

From an engineering point of view, the chemistry of oxidation has not yet answered the question of how long a bulky rubber component will last in service conditions, especially at elevated temperatures.

In conventional ageing tests, mechanical properties, for example stiffness and strength, are based on thin test-pieces. The properties are usually obtained after oven-ageing for a specific time at a specific temperature. The ageing behaviour of thin rubber test-pieces is not necessarily the same as that of thick blocks or indeed of the surface of thick blocks. This is evident from a comparison of the two test samples (one thin, one thick) illustrated in Figure 8.1, both having been subjected to the same ageing conditions. Elliott(69) has found that dumbbell test-pieces prepared from thick blocks of rubber and then aged sometimes have tensile strengths and elongations at break substantially lower than expected. This was found to be due to the method of preparing the dumbbells, which tends to create flaws which weaken the rubber. A novel technique was adopted by Knight and Lim(70) for their studies of the ageing of thick blocks of rubber vulcanizate. They used ten 2.5-mm thick sheets



Figure 8.1 Two pieces of rubber which have been aged for the same time: the thicker piece is still flexible, even at the surface, but the thinner one has become hard and brittle.

clamped together and were thus able to obtain tensile strength as a function of depth from the exposed surfaces. Unfortunately, this method cannot be applied to the study of rubber components after varying periods in service.

The difference in strength between the surface and the bulk rubber can be easily evaluated by using the puncture test. Moreover, this technique permits the determination of the change in strength of thick rubber components which are subjected to different periods of ageing and at different temperatures.

In 1974, an engineering company provided Tun Abdul Razak Laboratory with a rubber sample from a 96-year-old rubber bearing from a viaduct in Melbourne, Australia. This chapter investigates the ageing behaviour of thick rubber blocks whose formulation is based on that of the 96-year old rubber to enable prediction of long-term performance of rubber to be evaluated in conjunction with a study of the 96-year-old rubber.

8.2 Conditions of natural rubber pad after 96 years service

The rubber pads were about 2.5-cm thick and Figure 8.2 shows the locations of the pads between the steel structures and the supporting piers of the viaduct. Figure 8.3 shows a clean-cut section

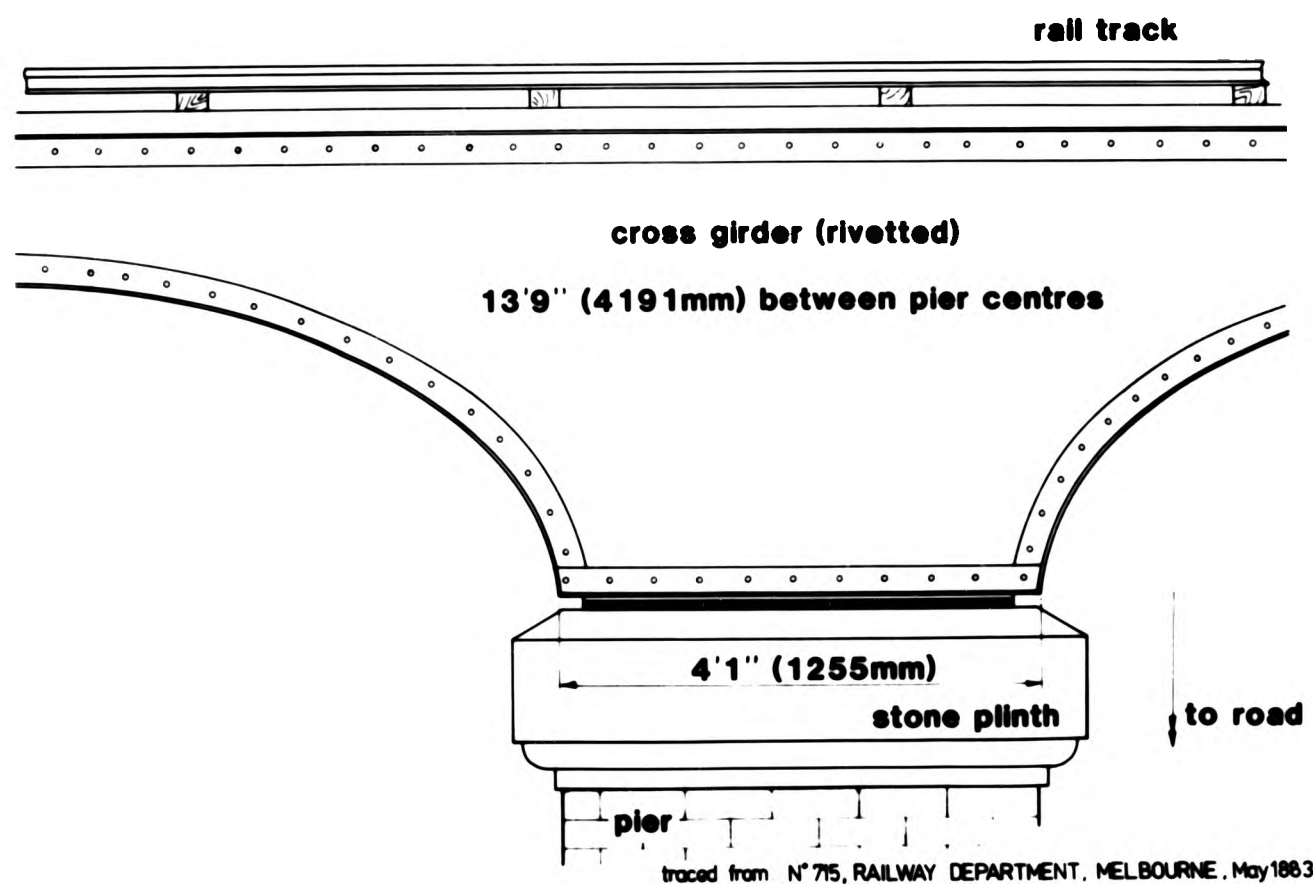


Figure 8.2 Drawing of Melbourne Railway Viaduct incorporating natural rubber pads in 1889.



Figure 8.3 Cut section through 96-year-old rubber pad showing that degradation was limited to an outer skin.

through the sample to illustrate the depth of any ageing of the rubber. The surface of the rubber is hard and shows evidence of oxidation. Below a depth of about 1.5 mm, however, the rubber is free from such degradation and was found still to have a hardness of only 63 IRHD. There was no evidence of significant deterioration of the rubber below this depth and in the centre of the pad. This provides a convincing illustration of the fact that the weathering of natural rubber in normal conditions is limited to the surface. This result further illustrates that so-called accelerated ageing tests exposing thin rubber sheets to elevated temperatures can give a misleadingly pessimistic view of the longevity of bulky engineering components.

8.3 Experimental method

The formulation of the 96-year-old rubber was determined using thermogravimetric analysis (TGA)(71) and thin layer chromatography(TLC)(71) techniques. The analyses suggest the following composition in parts by weight:

natural rubber	100
calcium carbonate	70
ferric oxide	10
sulphur	11

About 2.5 parts of other material, possibly dirt, was also present. As the amount of free sulphur was less than 0.1%, the rubber was fully cured. The analysis also showed no evidence of curing residues or synthetic antioxidants. This is not surprising, because curing system other than of sulphur plus metal oxide did not come into use until 1906, and synthetic antioxidants were not used until the 1940s.

A fresh natural rubber compound was prepared using the above formulation. 'Red Ochre' was used for ferric oxide and 5 parts of pine tar oil was added to the formulation to aid mixing. The rubber blocks were direct-compression- moulded for three hours at 140°C to dimensions of 23 x 23 x 2.54 cm. The rubber blocks were then cut into 2.5 cm test cubes.

The author was also provided with 10-year-old samples of similar rubber prepared according to the above formulation. These were originally prepared by the late Dr. Lindley.

Ageing was carried out for various times, in air-circulating ovens set at selected temperatures up to 200°C. One block was used for each combination of ageing time and temperature. After removal from the ovens, the blocks were allowed to cool at 23°C before being tested at room temperature. The blocks were cut open with a razor blade, and several

puncture tests were carried out on both the exterior surface and the cut surfaces of the bulk rubber. Puncture tests were carried out using a 0.5-mm diameter indenter with 5 μ m corner radius. Puncture tearing energies were subsequently obtained for each puncture test using the equation $T_c \cong F(1 - \lambda_c)/2\pi r_o$.

8.4 Variation of puncture energy with time of ageing

These tests were carried out on 2.5 cm cubes aged in air at 23, 40, 70, 100, 125, 150, 175 and 200°C. The variations of puncture energy of the surface and bulk with time of ageing are shown in Figures 8.4-8.11. The puncture energy scales are linear and the time of ageing scale is logarithmic. Figure 8.4 shows the results of air-ageing at 23°C. The 96-years point was obtained from the original rubber from the Melbourne viaduct rubber pad. The puncture energy of the surface and the bulk were similar within the first six months of ageing time. Then the puncture energy dropped sharply. In the case of the rubber at the surface, the puncture energy dropped sharply between six months and four years of ageing. With further ageing it showed little change, but with the limited data available there is an indication of a minimum at about 10 years with a subsequent small rise between 10 and 96 years.

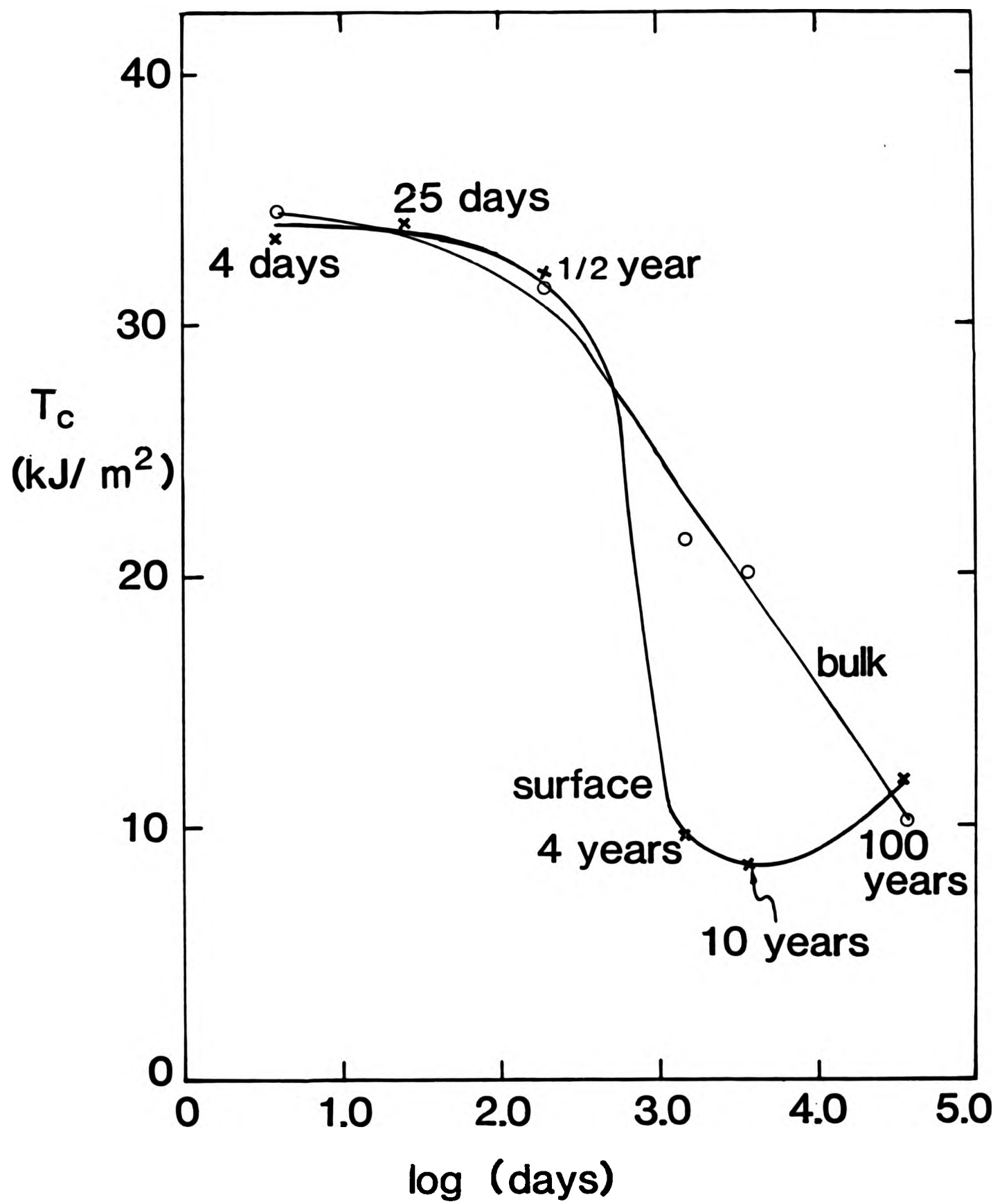


Figure 8.4 Variation of puncture energy of the surface and bulk of rubber with time of ageing in air at 23°C.

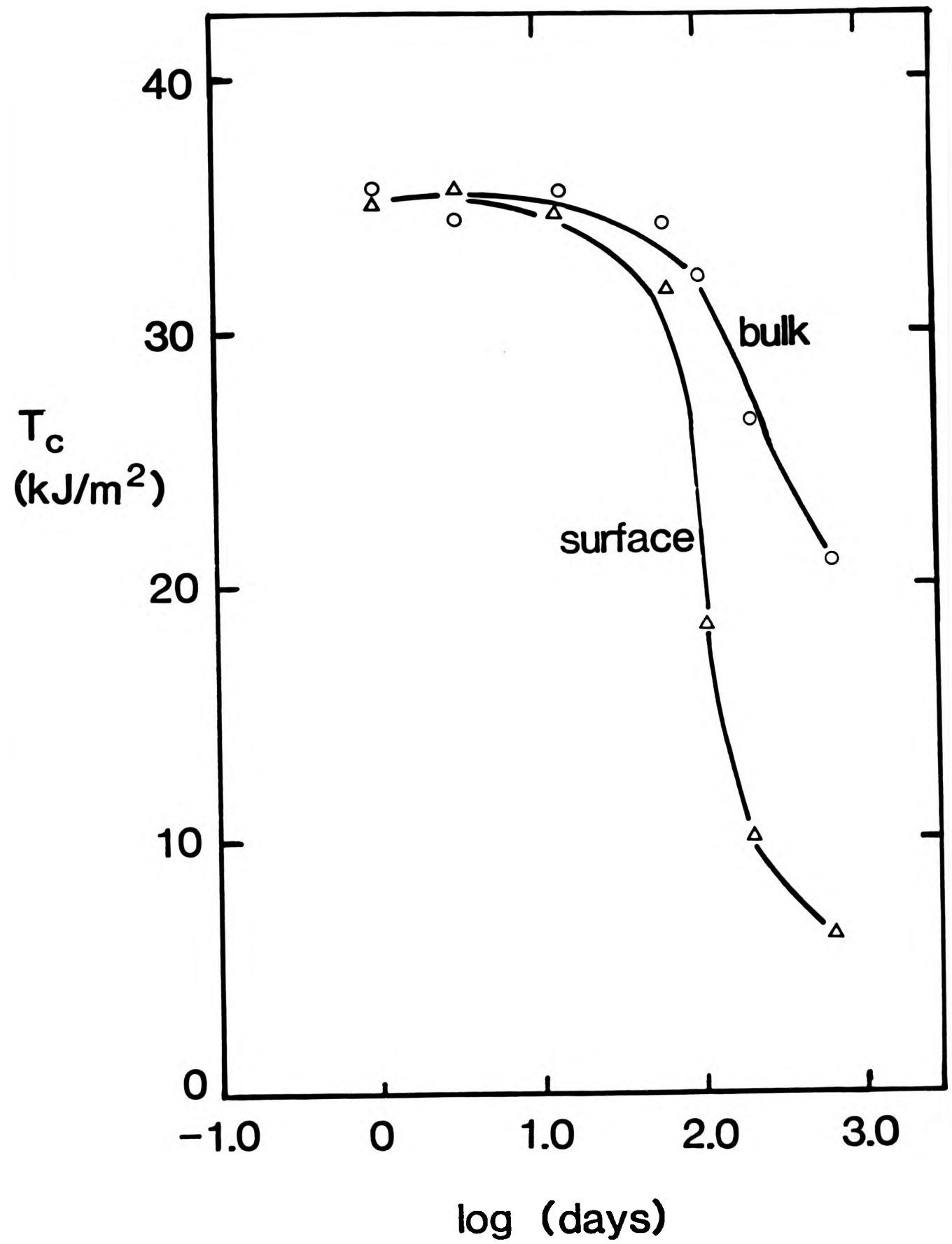


Figure 8.5 Variation of puncture energy with time of ageing at 40°C.

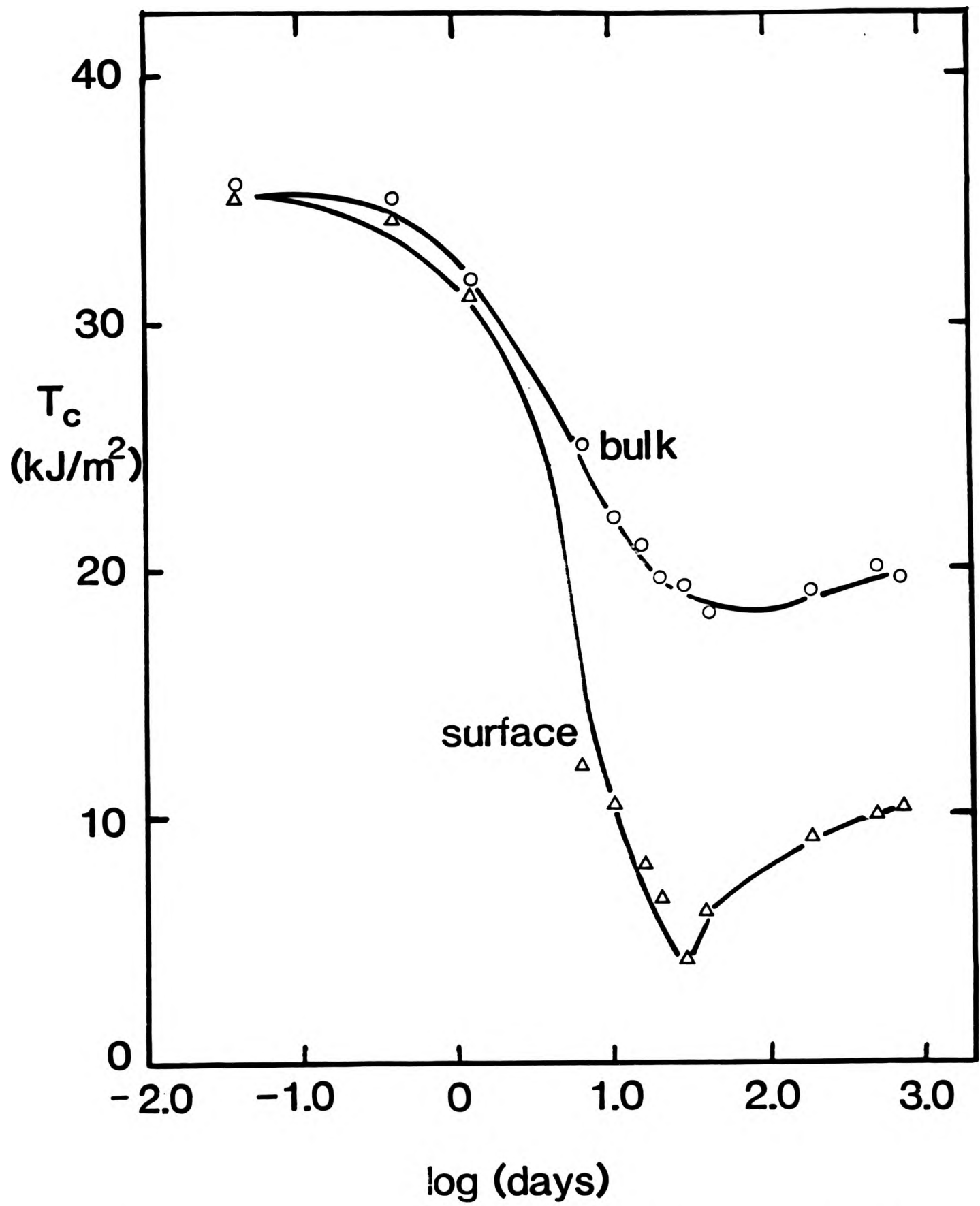


Figure 8.6 Variation of puncture energy with time of ageing at 70°C.

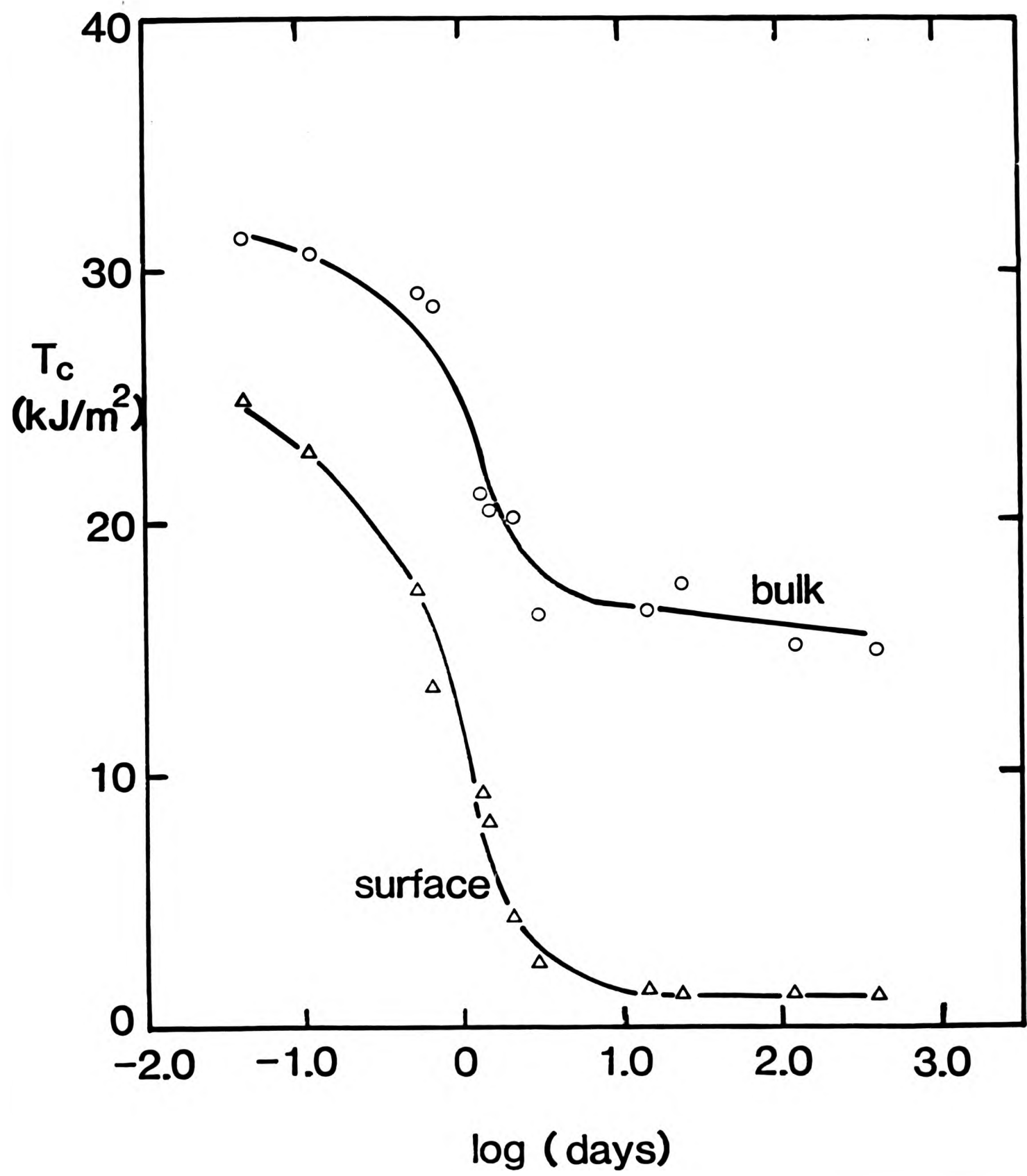


Figure 8.7 Variation of puncture energy with time of ageing at 100°C.

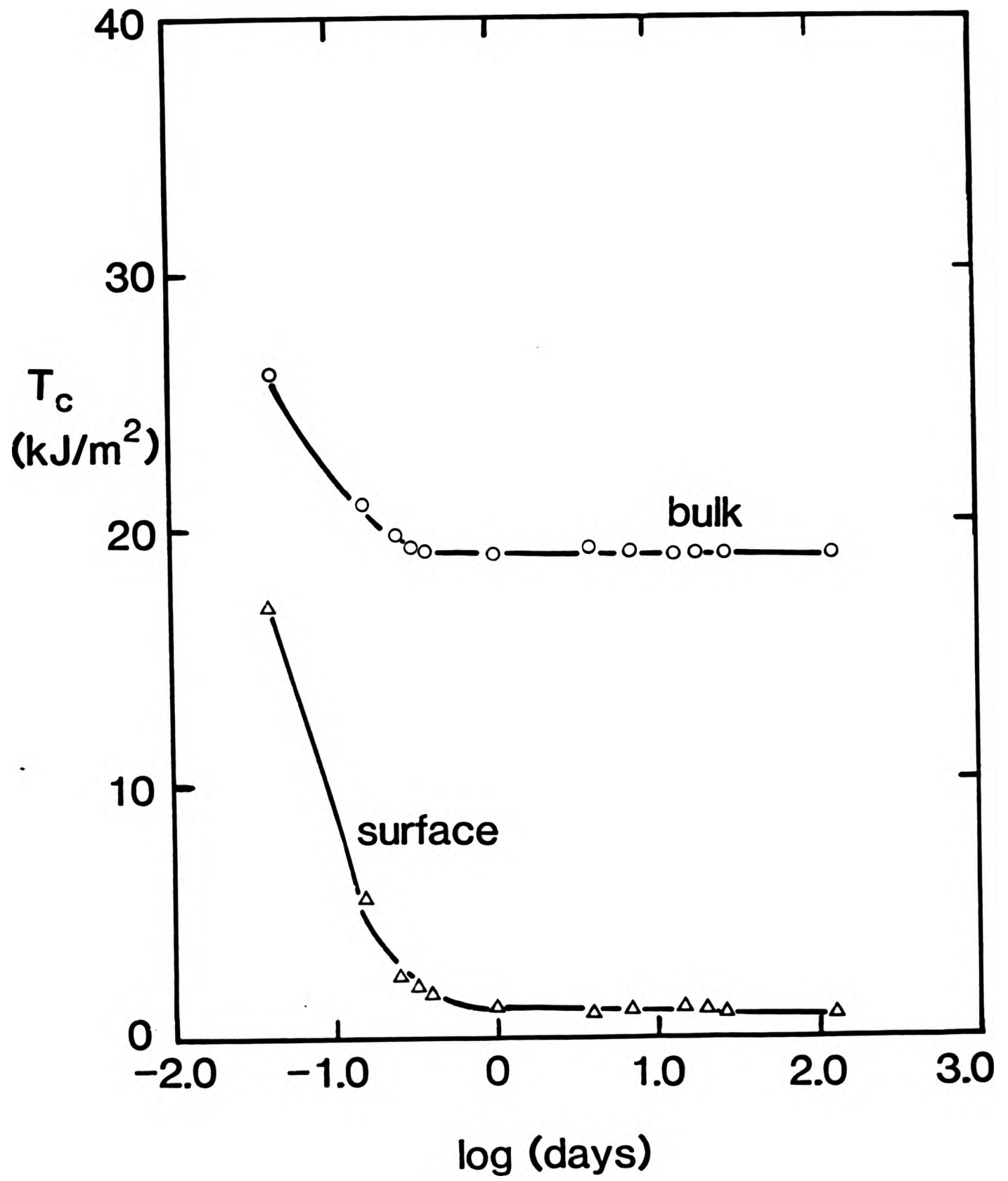


Figure 8.8 Variation of puncture energy with time of ageing at 125°C.

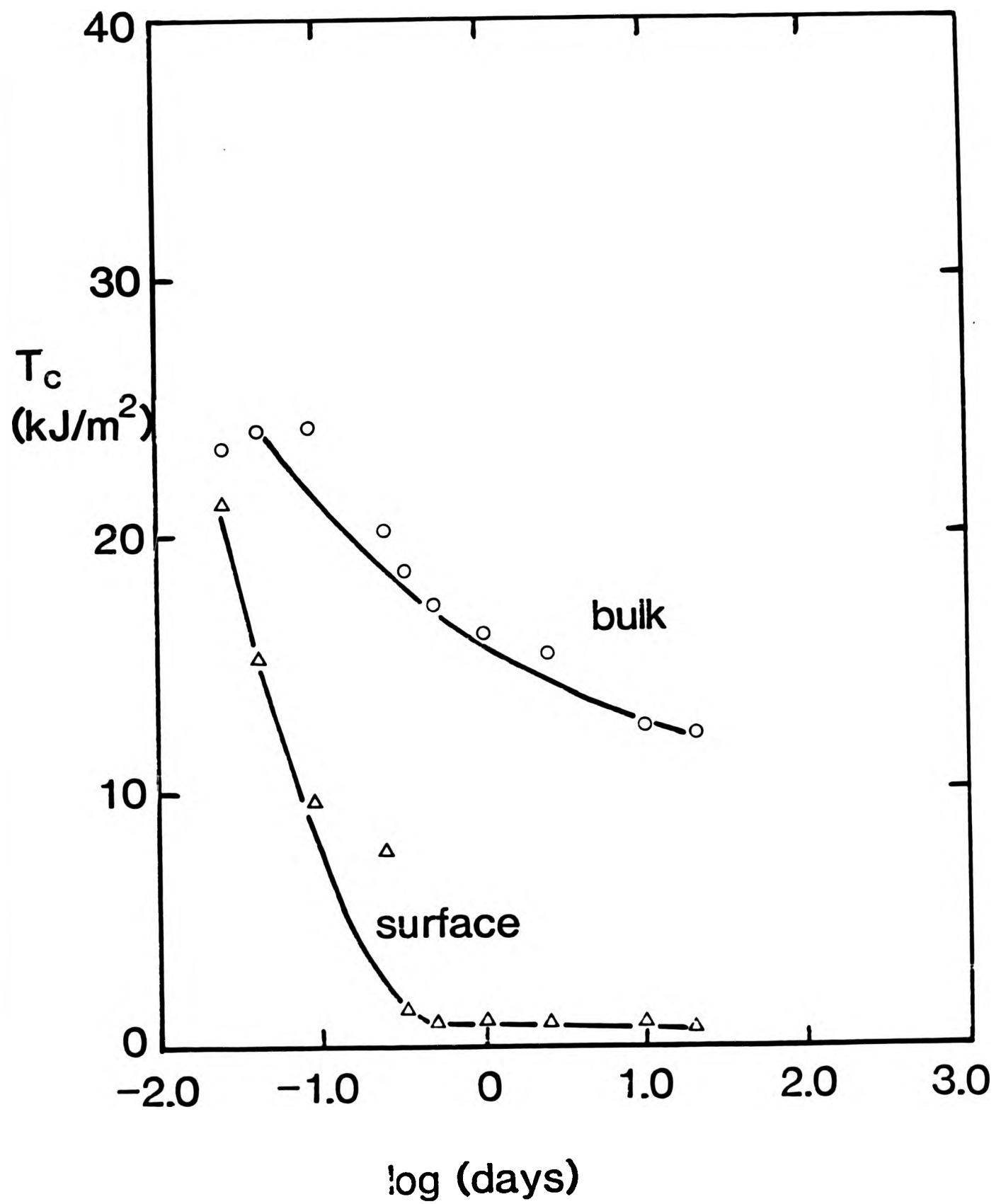


Figure 8.9 Variation of puncture energy with time of ageing in air ovens at 150°C.

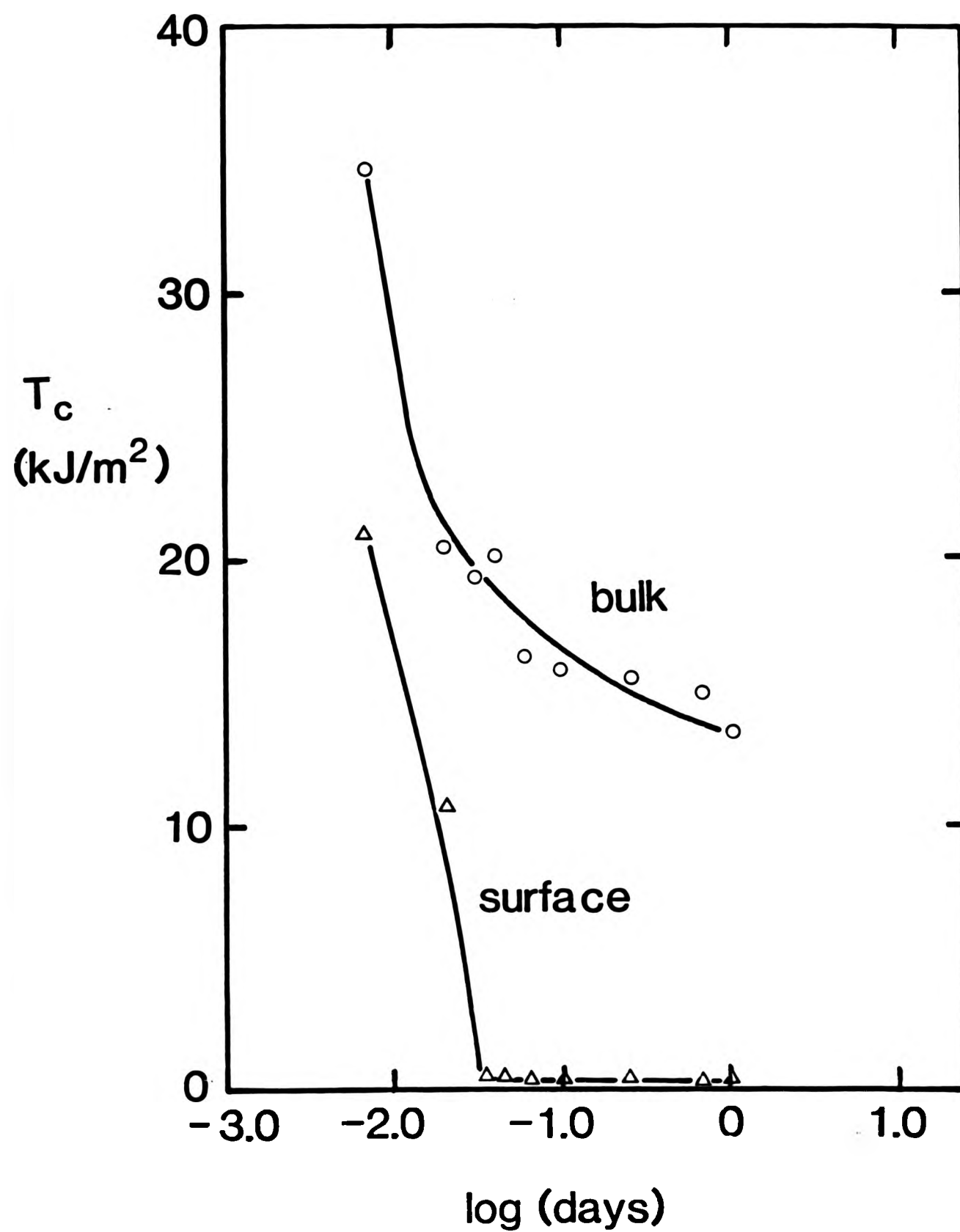


Figure 8.10 Variation of puncture energy with time of ageing in air oven at 175°C.

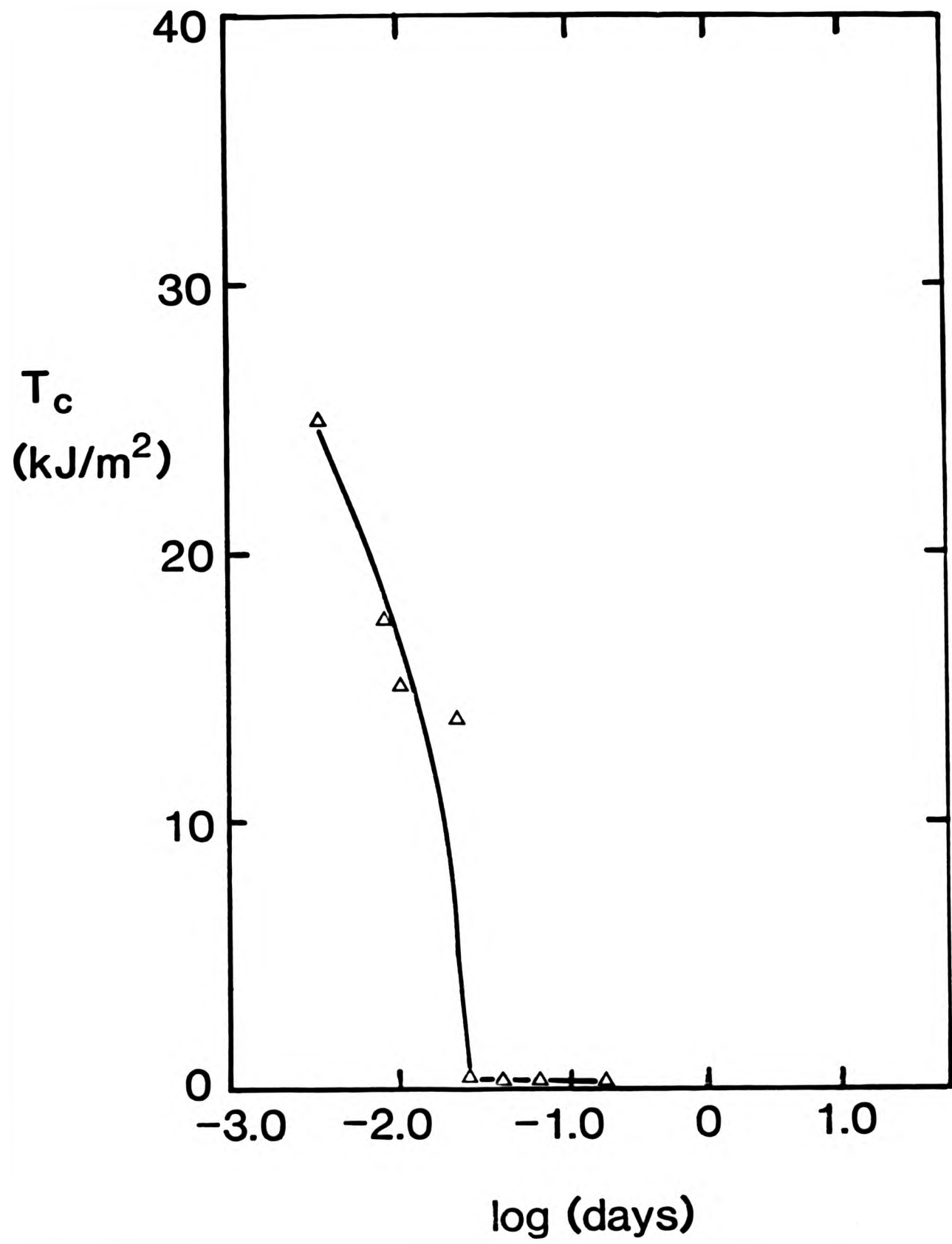


Figure 8.11 Variation of puncture energy with time of ageing in air oven at 200°C.

In addition, the hardness(80 IRHD) of the surface of the 96-year-old rubber is higher than the hardness of the surface of the 10-year old rubber(42 IRHD). In the case of the rubber in the bulk, the minimum puncture energy was not observed - the puncture energy was reduced to 10.0 kJ/m^2 after 96 years in service.

For the rubber aged at 40°C (see Figure 8.5) a minimum puncture energy was not observed for either the surface or the bulk. This is probably due to insufficient ageing time because a minimum puncture energy could be seen when the rubber was aged at 70°C (Figure 8.6). In this case, both the surface and the bulk puncture energies showed minima. Moreover, at the minimum puncture energy the surface of the rubber is soft, and with increasing ageing time, the surface becomes hard. The increase in puncture energy corresponds to the formation of a thin layer of hard skin as shown in Figure 8.12. This rubber was aged at 70°C for 181 days.

Figures 8.7 to 8.11 show the results of ageing at 100°C and higher. It can be seen that in all cases there was no minimum puncture energy for both the surface and the bulk of the rubber. The surface rubber puncture energy decreased with increasing ageing time, and at characteristic times t_a attained the lowest puncture energy value and remained at this value with increasing ageing times. The time t_a decreased with increasing temperature.



Figure 8.12 A hard skin on a rubber block aged at 70°C
for 181 days.

In addition, the lowest puncture energy attained decreased with increasing temperature. For example, at 100°C and 200°C, the lowest puncture energies were 1.25 and 0.25 kJ/m² respectively. The formation of a thin skin could be observed after ageing time t_a , but the skin was soft and sticky at 175 and 200°C.

The puncture energy in the bulk rubber aged at 100°C and 125°C was reduced to the lowest value and it appeared that the puncture energy did not subsequently vary with increasing ageing time. However, at 150°C and 175°C the puncture energy showed a gradual reduction with increasing ageing time and did not show a constant value. The puncture energy could not be obtained with rubber blocks aged at 200°C because in the bulk of the rubber there were small holes as shown in Figure 8.13 which interfered with the puncture test.

8.5 Uptake of oxygen

It has been shown that oxidative degradation in rubber is accompanied by an increase in oxygen content(72). Thus measurement of oxygen uptake provides a simple and quick way of evaluating the degree of degradation that has taken place in the rubber. Therefore it would be of interest to find out the variation of oxygen content in the surface



Figure 8.13 Holes in the rubber bulk aged at 200°C.

and in the bulk of the aged rubber blocks previously used for the determination of puncture energy. The instrument used was a Perkin-Elmer 240 Elemental Analyzer, which can give the value of the oxygen content to an accuracy of $\pm 0.3\%$ of the actual oxygen content. The method consisted of pyrolysing the sample in a stream of helium at 975°C , over carbon, when the resulting oxygen was converted to carbon monoxide. The carbon monoxide was then passed through copper oxide at 670°C , where the carbon monoxide was converted to carbon dioxide. The amount of carbon dioxide was then measured. The machine subsequently gave the oxygen content in weight % (w/w), i.e., as g of oxygen per 100 g of rubber vulcanizate.

Figure 8.14 shows the variation with time of ageing at 23°C of the oxygen content of the surface and the bulk rubber. The results also include the oxygen content of the 96-year-old rubber. It can be seen that the bulk rubber did not increase in oxygen content up to ten years of ageing. The oxygen content in the bulk increased by about 4 % after 96 years of ageing in air. However, the increase in the oxygen content was more pronounced in the surface. The total oxygen content increased by about 12 % after 96 years in air. Figure 8.15 shows the increase in the oxygen content in the bulk of rubbers aged at different temperatures and times. Except for

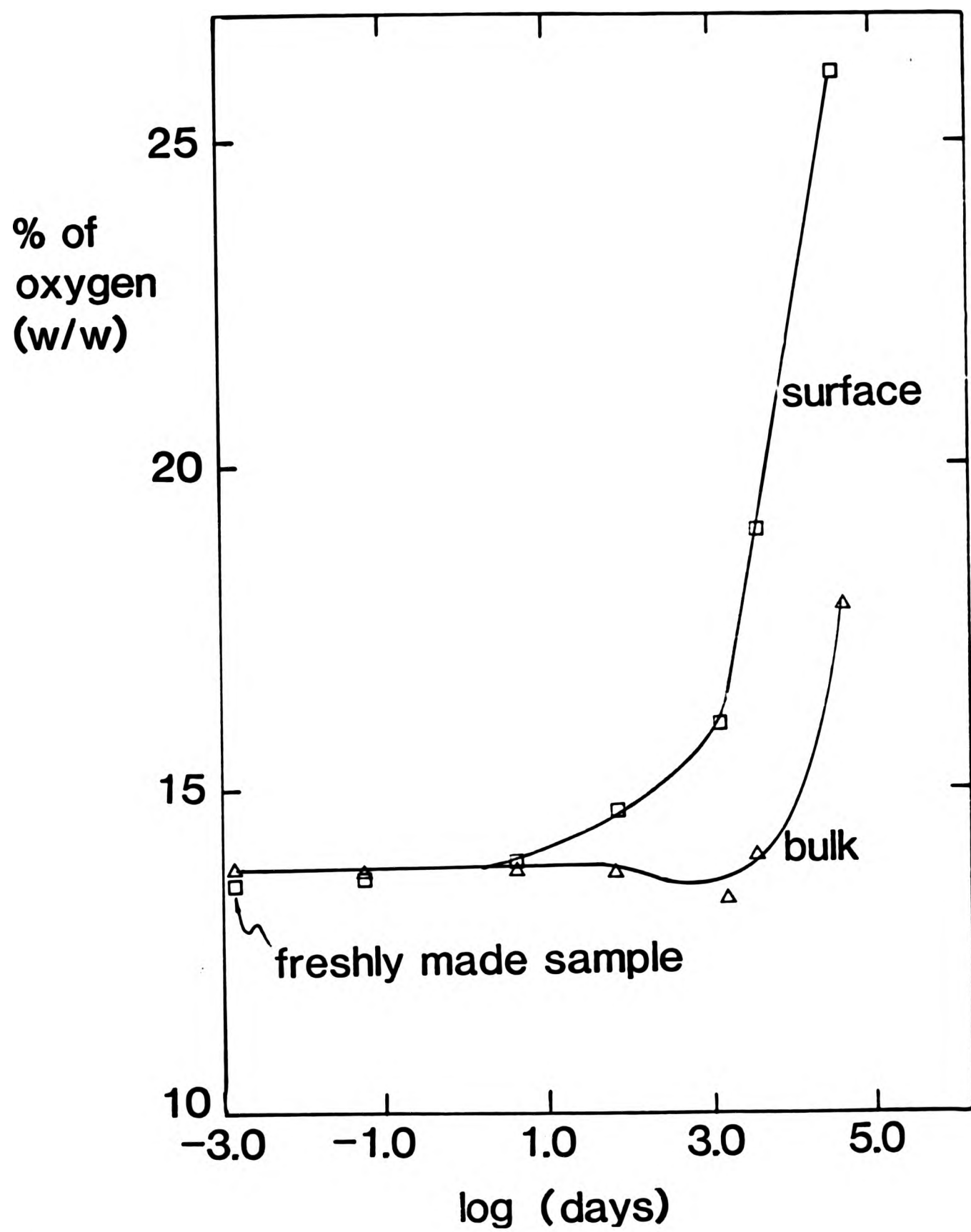


Figure 8.14 Variation of oxygen with ageing time at 23°C.

Surface(□), bulk(Δ).

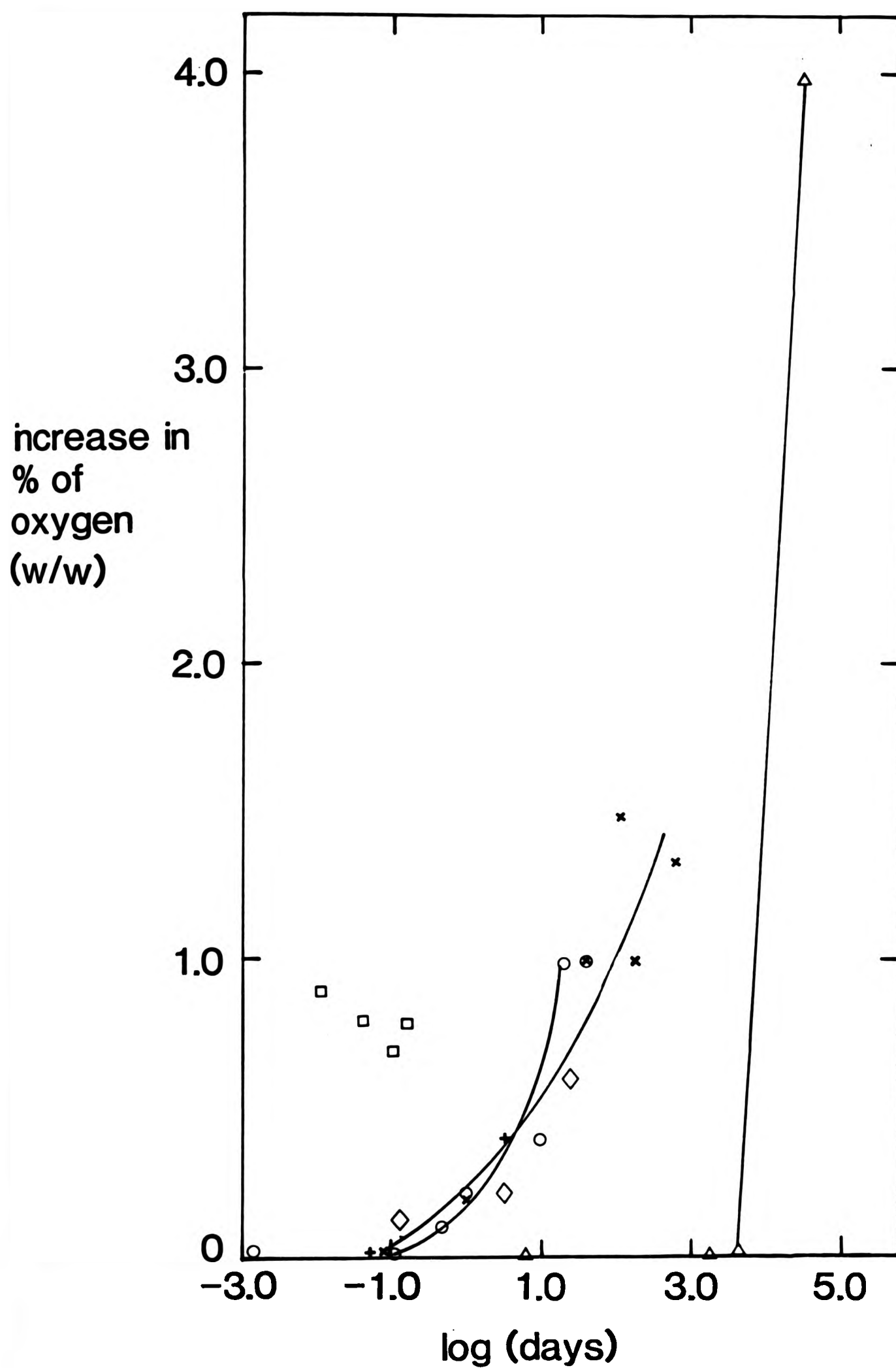


Figure 8.15 Increase in % of oxygen in the bulk of the rubber with ageing time: 23°C(Δ), 70°C(*), 125°C(o), 150°C(◇), 175°C(+), and 200°C(□).

the 4 % increase for the 96-year-old rubber, the increases in the oxygen content in all other cases were less than 2 %. The increase in the oxygen content is much higher in the surfaces of the rubbers, as shown in Figure 8.16. Most of the increase is around 10%. It can also be seen that the increase in the oxygen content is much quicker at higher temperatures than say at 70 or 23°C.

8.6 Discussion

In general terms, puncture energy decreases with ageing. At very long ageing time near ambient temperature (as represented by the Melbourne bridge sample) there is some indications of a slight rise in puncture energy of the surface. Further evidence for a puncture energy minimum is obtained for ageing at 70°C in both the bulk and the skin. Measurements at 40°C may not have been continued long enough to reveal the minimum. At 100°C and above, the minimum is not observed. For the surface, the puncture energy decreases progressively to a very low level and then remains approximately constant.

A characteristic time t_a can be defined for each ageing temperature which represents the time to reach either the minimum in the puncture energy curve or the time to attain the low level of puncture energy characteristic of long term ageing. At the

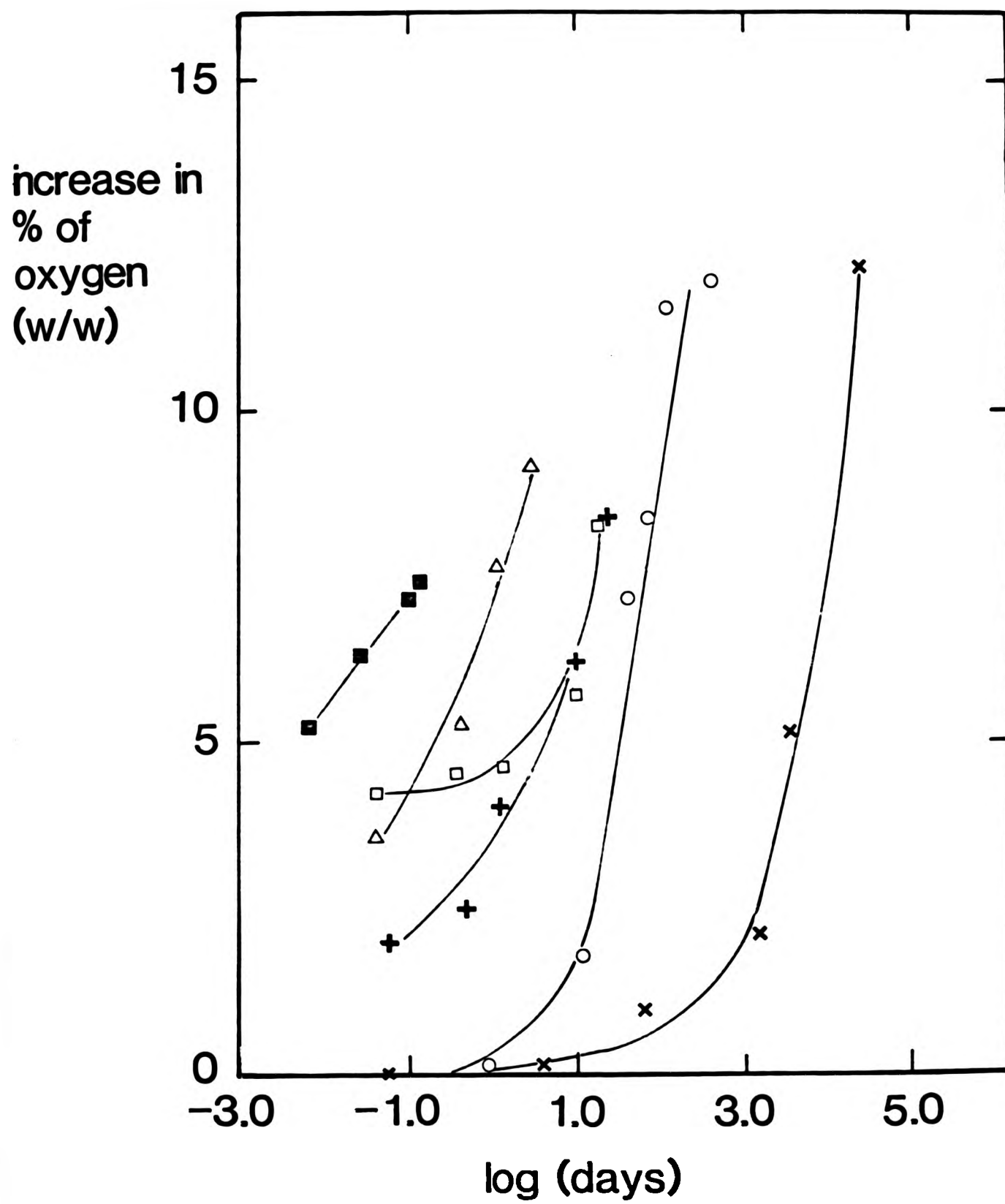


Figure 8.16 Increase in % of oxygen in the surface of the rubber with ageing time: 23°C(x), 70°C(o), 125°C(+), 150°C(□), 175°C(Δ) and 200°C(■).

higher temperatures (>70°C) this time has been taken as the time to the first puncture energy value which lies clearly with the group of nearly constant energies.

The time t_a , can be considered as a measure of the rate of the ageing process. A plot of t_a versus reciprocal absolute temperature (Figure 8.17) is approximately linear and an Arrhenius activation energy of 78.5 kJ/mole can be evaluated from its slope. This activation energy agrees well with a value of 80 kJ/mole reported by Lindley and Teo(55) for ageing of a modern accelerated efficient vulcanizate system. The network structure of the efficient vulcanizing system consists of mainly monosulphidic crosslinks(73), whereas the vulcanizate studied here is based on metal oxide/sulphur system and therefore would give different crosslinking network structure. The two vulcanizate vulcanizate structures have different long-term maturing characteristics. The similarity in the activation energies for the ageing of the two materials suggests that this ageing is primarily the effect of oxidation rather than maturing reactions.

The occurrence of oxidation is clearly shown by the change in the oxygen content of the samples. The change is more pronounced in the surface than in the bulk of the sample, and the pattern parallels the puncture energy data from surface and bulk

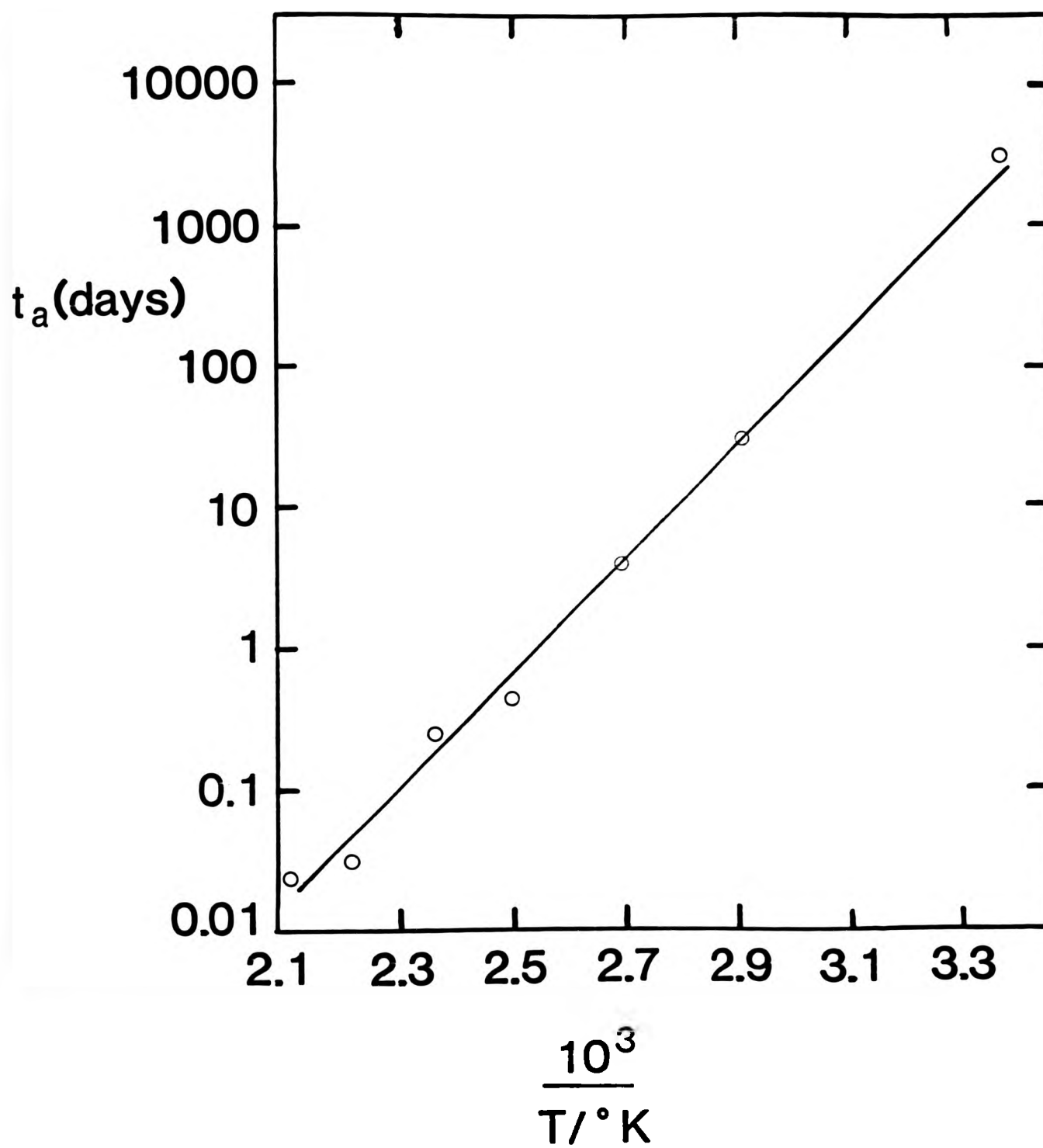


Figure 8.17 Arrhenius plot of the logarithm of the time t_a against reciprocal temperature.

measurements. The observations support the proposal made by Van Amerongen(74) and Stenberg et al(75,76,77) that the surface skin acts as a protective barrier for the bulk of the sample. An important feature of the present results is that the effects of this surface skin can be detected even at quite modest ageing temperatures.

Puncture energy therefore bears a general relationship to oxidative ageing for the specific case of the metal oxide/sulphur vulcanizate system studied here. The study has taken specific advantage of the availability of 10-year-old and 96-year-old samples which have been exposed to natural air ageing conditions and the results for these samples have been shown to be consistent with the shorter term, accelerated ageing results.

The increase in the puncture energy after the minimum is obviously advantageous to rubber components, but the reason for the increase is not obvious. Two competing processes during ageing, namely chain scission and crosslinking, influence the puncture energy of the rubber.

Initially the puncture energy is reduced due to oxidative chain scission as observed. With prolonged ageing, a stage will be reached where most of the rubber at the surface has reacted with oxygen and forms an oxidised skin thus preventing further oxygen penetration. In this situation it is probable that

the crosslinking becomes dominant, since the rubber used in this investigation has no accelerator ingredient to increase the rate of crosslinking and to increase the efficiency of utilization of sulphur in forming the crosslinks. Thus the initial degree of crosslinking formed after vulcanization is low(78) even though 11 part of sulphur per 100 part of rubber was used. Smith et al(79) showed that a slow crosslinking reaction takes place at long reaction times which gradually increase the number of crosslinks. However, the increase in the number of crosslinks will not be that high because of the inefficiency of the rubber vulcanizing system. It has been shown(80) that the strength of rubber passes through a maximum as the degree of crosslinking is increased. Therefore, the apparent increase in the puncture energy with increasing ageing time might have been caused by a small increase in the number of crosslinks. A large increase in the number of crosslinks would have reduced the puncture energy.

However the increase in the puncture energy after the initial drop was not observed when the rubbers were aged at 100°C or higher. This may be explained by the fact that at high temperatures the crosslinks are thermally unstable(81). At temperatures around 200°C, the main polyisoprene chains themselves become susceptible to decomposition(82). At the surface, where oxygen is

available, the situation is worse as the unstable crosslinks and the main chains can readily undergo oxidative ageing.

CHAPTER NINE
STUDY OF USED RUBBER COMPONENTS

9.1 Introduction

The puncture test has been shown to be very useful in investigating changes in the strength of thick rubber blocks subjected to high temperatures. It is here applied to the study of two used rubber components. The puncture test is particularly useful in these cases, because it can provide localised information on strength, and thus enable strength contours to be drawn up for a bulky piece of rubber.

The condition of a natural rubber bearing which has been in service for twenty years is first discussed. In contrast to the much older Melbourne rubber pad, this bearing presumably compounded to modern standards.

The second part of this chapter will discuss the condition of a tyre which has been immersed in sea water for forty years.

9.2 Twenty-year-old rubber bearing

9.2.1 Introduction

Natural rubber bridge bearings have now been in service in the United Kingdom for over 25 years. It is therefore important to be able to assess their present condition and to predict their remaining life. The bearings are installed between the bridge deck and the piers to allow thermal contraction and expansion of the deck to take place without damaging the piers. Such bearings normally consist of vulcanized rubber internally reinforced with steel plates. They can be designed to function over a wide range of of shear and compressive stresses.

9.2.2 Experimental method

A bearing was removed after about 20 years in service from a bridge carrying the M2 motorway in Kent. The location of the bearing was fairly typical and not subject to extreme mechanical or chemical conditions. The bearing was made when the bridge bearing specifications BS 1154:1952 was in force.

The average dimensions of the bearing as measured after removal from the bridge were about 40.8 x 28 x 18 cm; they are probably its original dimensions. Figure 9.1 shows the bearing supporting the bridge deck prior to removal.



Figure 9.1 Bearing under a bridge deck.

The upper surface of the bearing was rough and appears to have 'set' slightly leaving an imprint of the surface of the concrete beam which the bearing supported. The bottom surface was relatively smooth because it was in contact with a smooth mortar bedding. All of the outer surfaces exposed to the atmosphere were smooth and showed no evidence of ozone cracking even when examined with a 10X magnifying glass.

The bearing was cut into two sections as shown in Figure 9.2. Detailed puncture tests were carried out on the smaller section over two different surface areas, each of which had dimensions of about 12cm x 2cm. One region was from the inner rubber layer and the other from outer rubber cover which is exposed to the atmosphere. The regions were marked with a grid and puncture tests performed at 2mm intervals over the whole area.

Conventional test-pieces were cut from several locations in the smaller section in order to investigate any variation in physical properties as a result of ageing. Any such changes would be expected to be greater near the surface exposed to the atmosphere. The test-pieces were ground on both sides to a smooth finish. Those cut from the outer cover which incorporated a moulded surface exposed to the atmosphere had only their cut surfaces ground smooth. There were thus inevitable physical

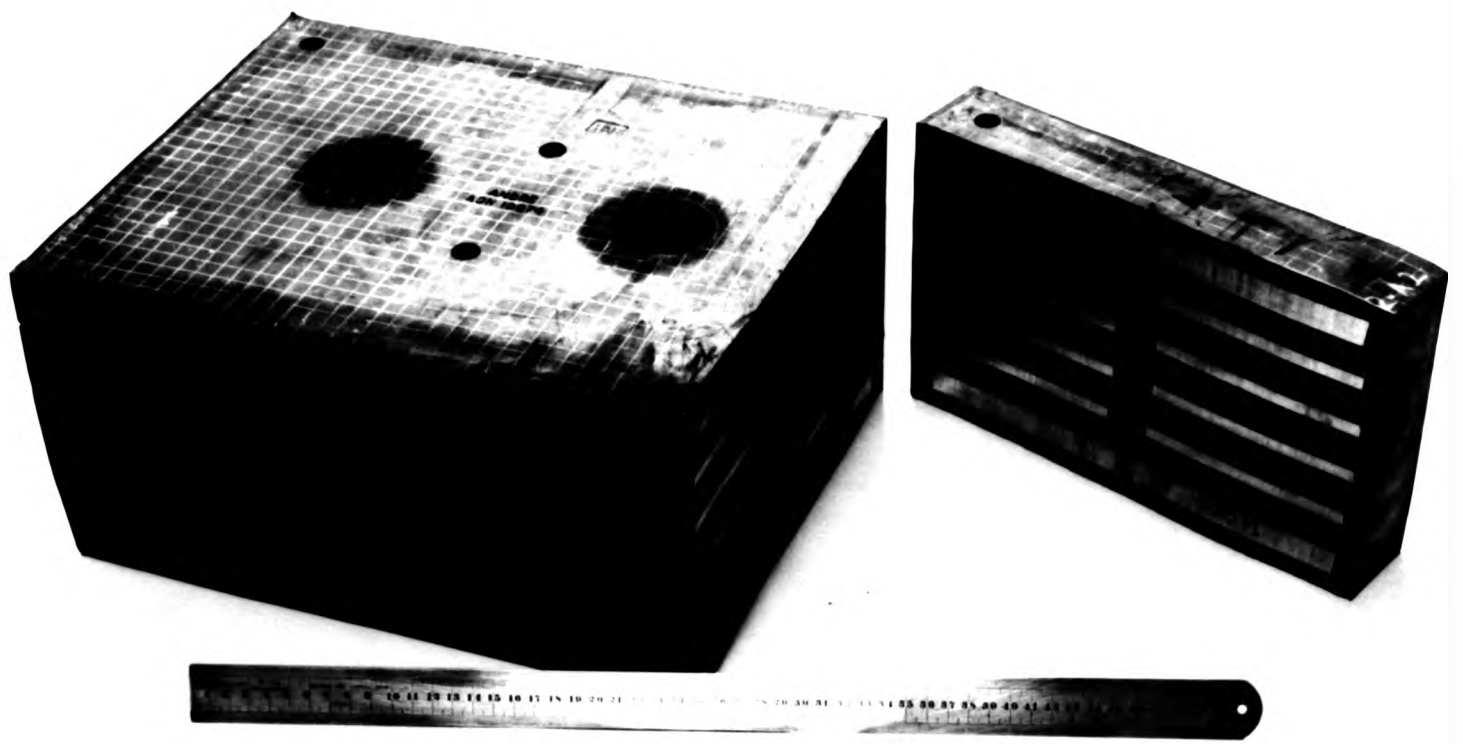


Figure 9.2 Two cut sections of the bearing.

differences between the method of preparing test-pieces from the outer exposed cover and from other locations. This difference is most likely to affect tensile strength(TS) and elongation at break(EB). Any fine scratches in the outer exposed surface would cause reduced values for TS and EB, so that the low values here cannot necessarily be attributed to oxidation of the rubber.

The tearing energy was obtained by the trouser tear test and carried out by the method described in Chapter Four. All other conventional tests reported in this Chapter were carried out by the staff of the Physical Testing Group of the Tun Abdul Razak Laboratory.

Oxygen content analysis was also carried out at different locations. The procedure for this analysis is described in Section 8.5 of Chapter Eight.

9.2.3 Contour strength

Figure 9.3 shows a puncture energy contour of the surface of the inner rubber layer. The puncture energy values indicate the relative strengths of the rubber at different positions. The contour shows that areas near and remote from the edge do not differ significantly in strength, suggesting that no serious degradation in the rubber had taken place even near to the outer exposed surface. The average

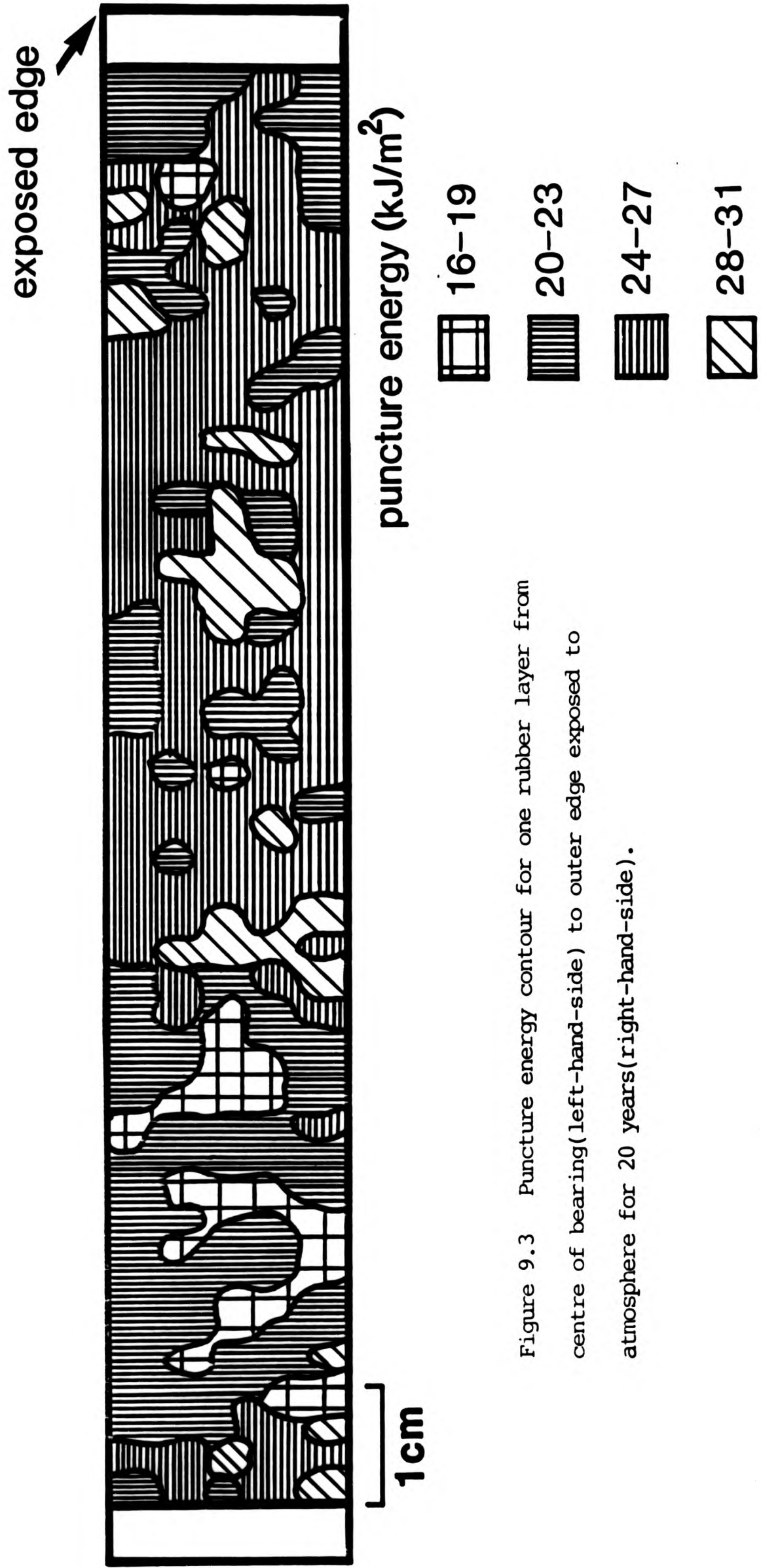


Figure 9.3 Puncture energy contour for one rubber layer from centre of bearing (left-hand-side) to outer edge exposed to atmosphere for 20 years (right-hand-side).

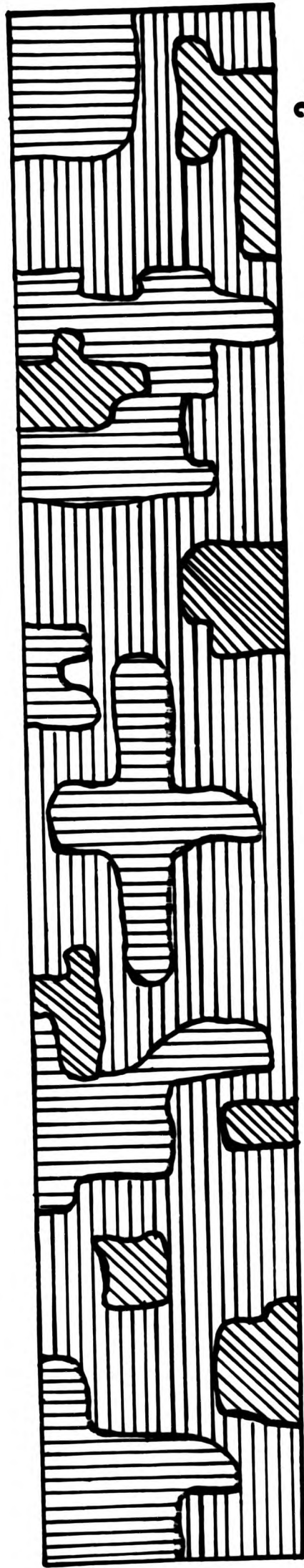
tearing energy of the inner layer as determined by trouser tear test was low, being approximately 15kJ/m^2 . This is probably because the trouser test-pieces had been weakened by the flaws induced during their preparation.

Figure 9.4 shows a puncture energy contour of the surface of the exposed outer rubber cover. The overall puncture energy was lower than the inner rubber layer. This was not unexpected, because the rubber surface was exposed to the atmosphere and some degree of degradation must have taken place. The low puncture energy values in some small regions may indicate that these regions might have been in contact with oils or corrosive agents during the twenty years in service. This highlights the merit of using puncture test which can provide highly localised strength information. The results from trouser tear tests were also low, being approximately 9kJ/m^2 .

The oxygen analysis showed that the exposed rubber surface had one to two percent higher oxygen content than the bulk rubber. This higher level may be attributed to atmospheric oxidation, and is consistent with moderate degradation.

9.2.4 Physical properties based on conventional tests

The physical properties of the inner rubber



puncture energy (kJ/m^2)

 13-16

 17-20

 21-24

1 cm

Figure 9.4 Puncture energy contour of a surface of the exposed outer rubber cover.

layers, and the exposed and unexposed rubber covers, are summarised in Table 9.1. These properties are compared with the bridge bearing specifications of BS 1154:1952 and the new, more stringent BS 5400:1983. Each value is the average of similar test-pieces from the same type of location.

There is a trend to slightly poorer tensile properties towards the outer cover. The lower TS and EB may not be significant because these test-pieces contain one exposed surface which was likely to contain scratches. The presence of the latter means that this result does not necessarily imply degradation in the rubber. There is no significant change in the tensile properties after seven days ageing at 70°C.

Rubber from the outer cover showed marginally poorer ozone resistance, with some small edge cracks after 2-3 days at a test concentration of 25 parts per hundred million (pphm), while rubber from the inner layers showed no cracks at all after four days at a concentration of 50pphm. However, there were no ozone cracks whatsoever on the outer surface of the bearing exposed to the atmosphere for twenty years. This perhaps suggest that the accelerated ageing test is unrealistically severe.

The physical property requirements in force when the original bearings were manufactured were those listed in BS 1154:1952 Z14 or Z15. The

Table 9.1 Comparison of test data with BS 1154: 1952
and BS 5400 : 1983

Test	BS 1154		BS 5400	Layers*		
	(Z14)	(Z15)		A	B	C
Hardness, IRHD	62-70	72-80	66-75	71	70	69
Tensile Strength, MPa	13.8(min)	10.4(min)	15.5(min)	17.2	15.1	11.6
Elongation at Break, %	350(min)	250(min)	300(min)	440	400	340
Compression Set 1 day at 70°C, %	30(max)	35(max)	30(max)	16.5	-	20
<u>Change after 7 days at 70°C:</u>						
Hardness, IRHD	-0,+4	-0,+4	10(max)	+2	-	+3
Tensile Strength, %	-10,+10	-10,+10	15(max)	-8%	+2%	+4%
Elongation, %	-15,+0	-15,+10	20(max)	-6%	+8%	+2%
<u>Compression Set after:</u>						
14 days at -10°C %	-	-	70(max)	+12%	-	+16%
7 days at -25°C %	-	-	70(max)	+13%	-	+15%
<u>Ozone resistance</u>						
4 days at 25pphm	-	-	no cracks	no cracks	some small cracks	some small cracks

*

A - Inner structural layers
B - Outer cover layers not exposed to atmosphere
C - Outer cover layers exposed to atmosphere

(Min) = minimum
(Max) = maximum

measured hardness values place the rubber between the requirements in Z14 and Z15. It can be seen that the inner rubber layers of the bearing still meet all of the requirements by a substantial margin. Rubber cut from the outer cover still meets all the requirements for harder rubbers, Z15, but just fails the tensile requirements for Z14. However this may be due to the method of test-piece preparation as explained above. It can also be seen that rubber from the inner layers also meets the new, more stringent BS 5400 specifications. Rubber from the outer cover would meet all of the new requirements except for TS, EB and ozone resistance.

9.2.5 Summary and conclusions

The bridge bearing appears to have been formulated to BS 1154 (1952), and was found still to meet the requirements of that specification. In general, any deterioration in the condition of the rubber, even at the outer exposed surfaces, was found to be small. The localised strength contour obtained by the puncture test showed no evidence of any serious degradation.

9.3 Condition of a tyre after 42 years immersion
in sea-water

9.3.1 Introduction

There have been several laboratory studies of the absorption of water by rubbers(83,84,85), but relatively few reports of the effect of long-term exposure at offshore sites. Sea-water trials of up to fourteen years have been reported(86,87) on plastics and rubbers used for cable covers. Exposure was in shallow water sites chosen for an abundance of marine growth (Florida and Carolina, USA). Some materials, especially silicone rubber, were reported to be damaged by marine borers (e.g., pholads) burrowing into the surface. However, nitrile rubber, styrene butadiene rubber and polychloroprene suffered only slight damage after seven years, while no damage at all was reported for natural rubber after that time.

The present study investigated the condition of a natural rubber tyre recovered from the deck of a sunken vessel resting in 24-30m of water off the NW coast of Scotland.

9.3.2 Experimental method

Figure 9.5 shows a general view of the tyre during recovery. The tyre was taken to the Tun Abdul

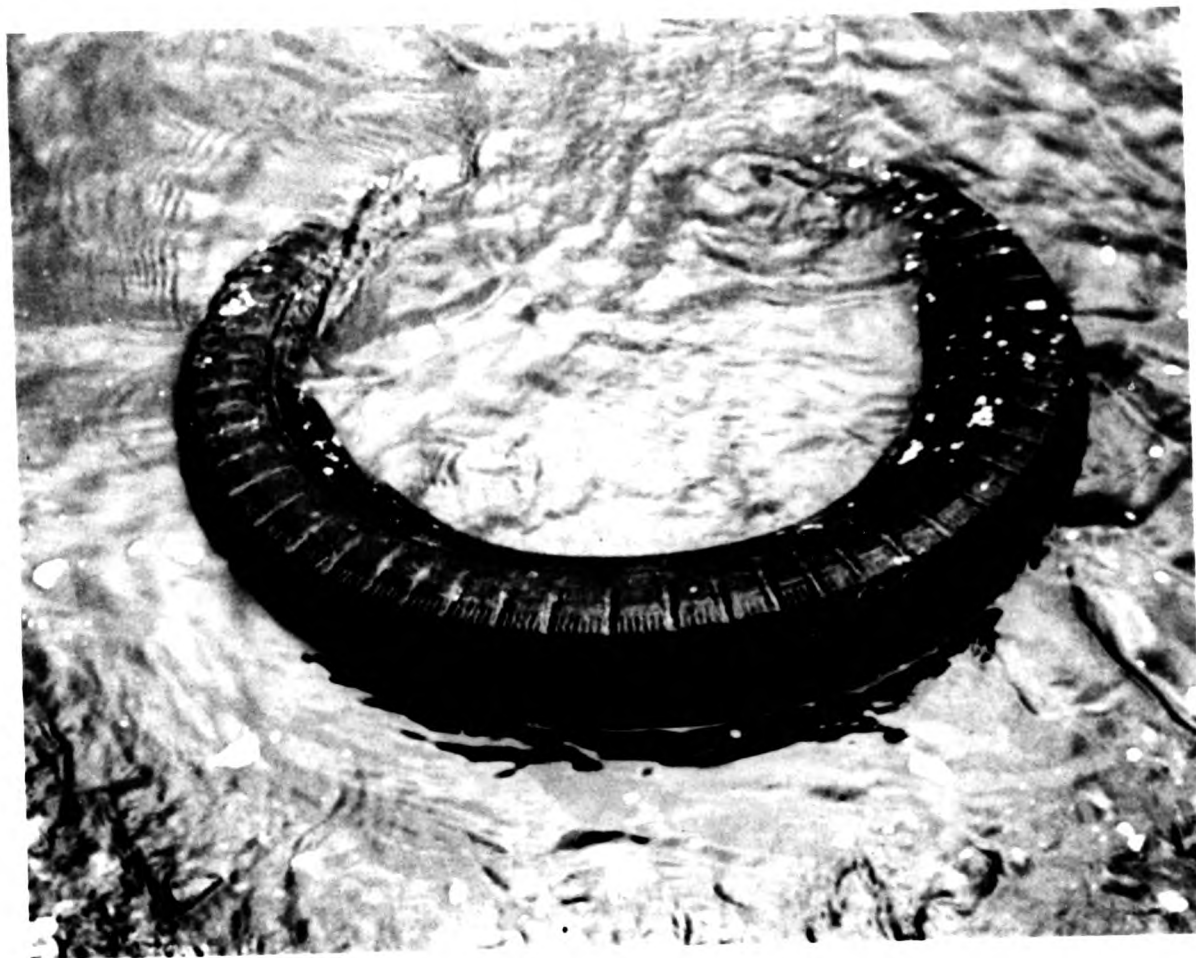


Figure 9.5 General view of the tyre during recovery after 42 years immersion in sea-water.

Razak laboratory and dried at room temperature. It was found(88) that a tyre sample reached an equilibrium 'final' dry weight after about 135 days. Then the tyre was cut into sections from which 2mm layers were prepared and ground smooth. Standard test-pieces were prepared from these layers. In addition, puncture tests were carried out on one of the sections using 0.5-mm diameter indenter with 5 μ m corner radius.

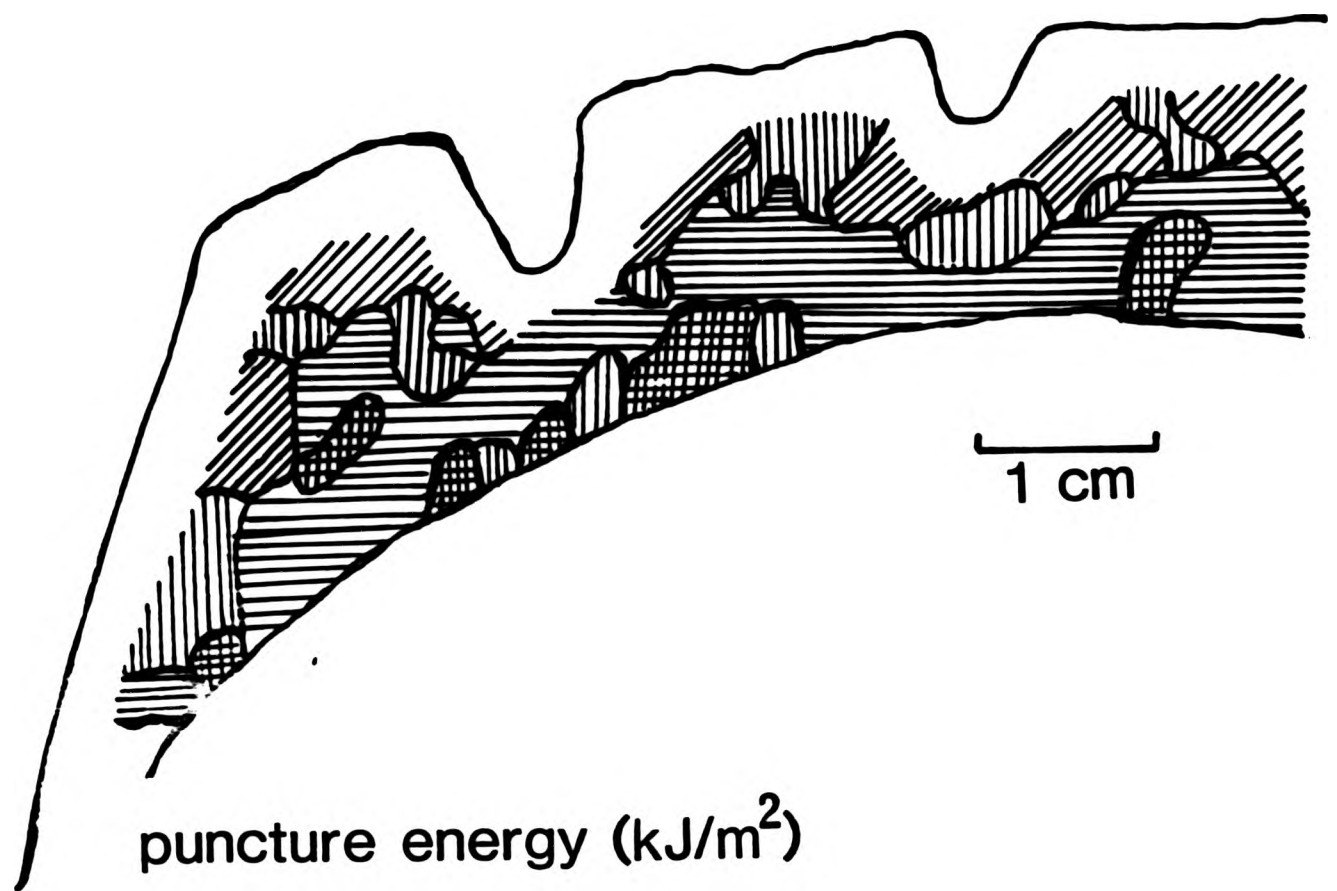
Chemical analyses were performed by the Analytical Department of the Tun Abdul Razak Laboratory in order to determine the main ingredients of the tyre and permit preparation of new rubber samples using the likely formulation of the tyre. The methods(71) used were thermogravimetric analysis and thin layer chromatography. These showed the approximate composition to be as given in Table 9.2. Oxygen analyses were also carried out at different locations using the method described in Section 8.5.

9.3.3 Contour strength

Figure 9.6 shows the puncture energy contour of the surface of a section of the tyre. The results show the puncture energy over the tread region to be higher than in the region near the carcass. The difference is just large enough to be significant, and may indicate some ageing towards the outer

Table 9.2 Composition of 42 years old tyre

<u>Ingredient</u>	<u>part by weight</u>
Natural rubber	100
Carbon black filler	40
Sulphur	2.5
Zinc oxide	5.5
Stearic acid	2.0
Mercaptobenzothiazole	0.75



-  34-38
-  29-33
-  24-28
-  19-23

Figure 9.6 Contour map of puncture energy across a section through the tyre.

surface. Alternatively, the difference could have been caused by different processing methods having been used for the tread and for the carcass of the tyre. Modern tyres use different rubber compounds for these regions, so comparisons cannot easily be made with a new tyre.

Measurements on the surface of the tread gave an average puncture energy of about 42kJ/m^2 , higher than the values shown in the contour map. This may indicate the formation of a hard skin on the surface, similar to that which had formed on the surface of the 96-year-old rubber bearing discussed in Chapter Eight. However, oxygen analyses at the surface and below the tread surface indicate no significant differences in oxygen content throughout the tyre, an observation which suggests that no major oxidation has taken place on the surface. The cause of the apparent high puncture energy on the tread surface could have been due to deposits of other materials adhering to the tread surface. This possibility was investigated using a scanning electron microscope.

9.3.4 Scanning electron microscopy

A section through the tyre tread was examined by scanning electron microscopy. The tread surface appeared to be highly particulate in character (see Figure 9.7a). Examination of the section revealed a



Figure 9.7 (a) Scanning electron micrograph of outer tread surface with particulate 'crust'.

layer of aggregated particulate material with a maximum thickness of 50 μm , (Figure 9.7(b)). Electron probe analysis of both the tread surface and the bulk rubber beneath the surface showed normal levels of sulphur in each case, but an increased amount of aluminium in the tread surface. In addition, the tread sample showed a strong presence of iron which was not detected in the bulk rubber. A scan for iron is shown superimposed on Figure 9.7b. The full element scan for samples from each region are shown in Figure 9.8. There may also have been a slightly reduced level of zinc in the tread surface sample. Figure 9.7c shows a section through the sample with a superimposed plot of sulphur content as measured by the intensity of the appropriate K_{α} X-ray peak. There is clearly no significant difference between the surface layer and bulk rubber. The corresponding photograph with superimposed iron content (Figure 9.7b) clearly shows a strong presence of iron only in the surface layer.

The likely explanation for the surface layer is that a sediment of iron oxide was formed over the years from corrosion products of the vessel structure. This formed a fine layer which interacted slightly with the rubber surface to form a very thin skin of ca. 0.05mm thickness. It is difficult to say from this evidence whether this fine surface layer was purely the result of accretions of

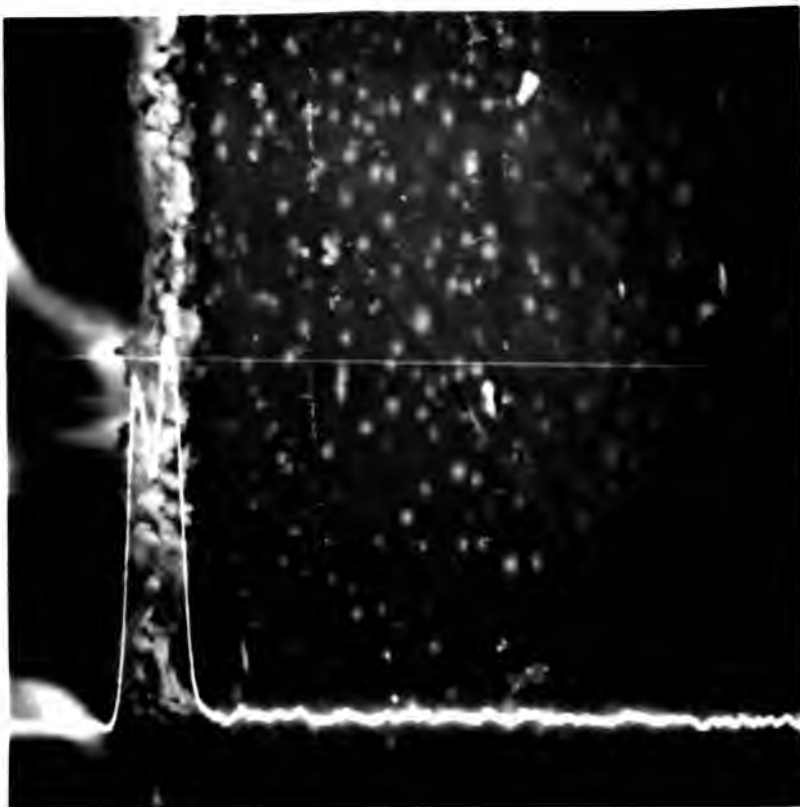


Figure 9.7 (b) Scanning electron micrograph showing a profile of section through the tread segment with outer layer of particulate material of maximum thickness $50\ \mu\text{m}$. The superimposed line scan for Fe shows the outer layer to be different composition from the underlying rubber.

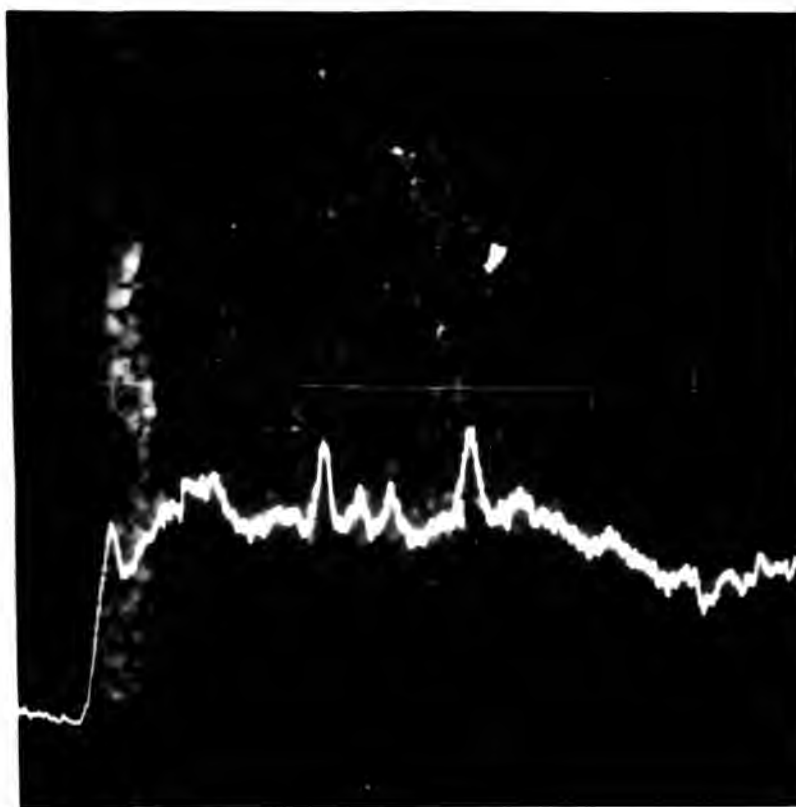


Figure 9.7 (c) Similar micrograph to (b) with line scan for Sulphur.

intensity
(uncorrected)

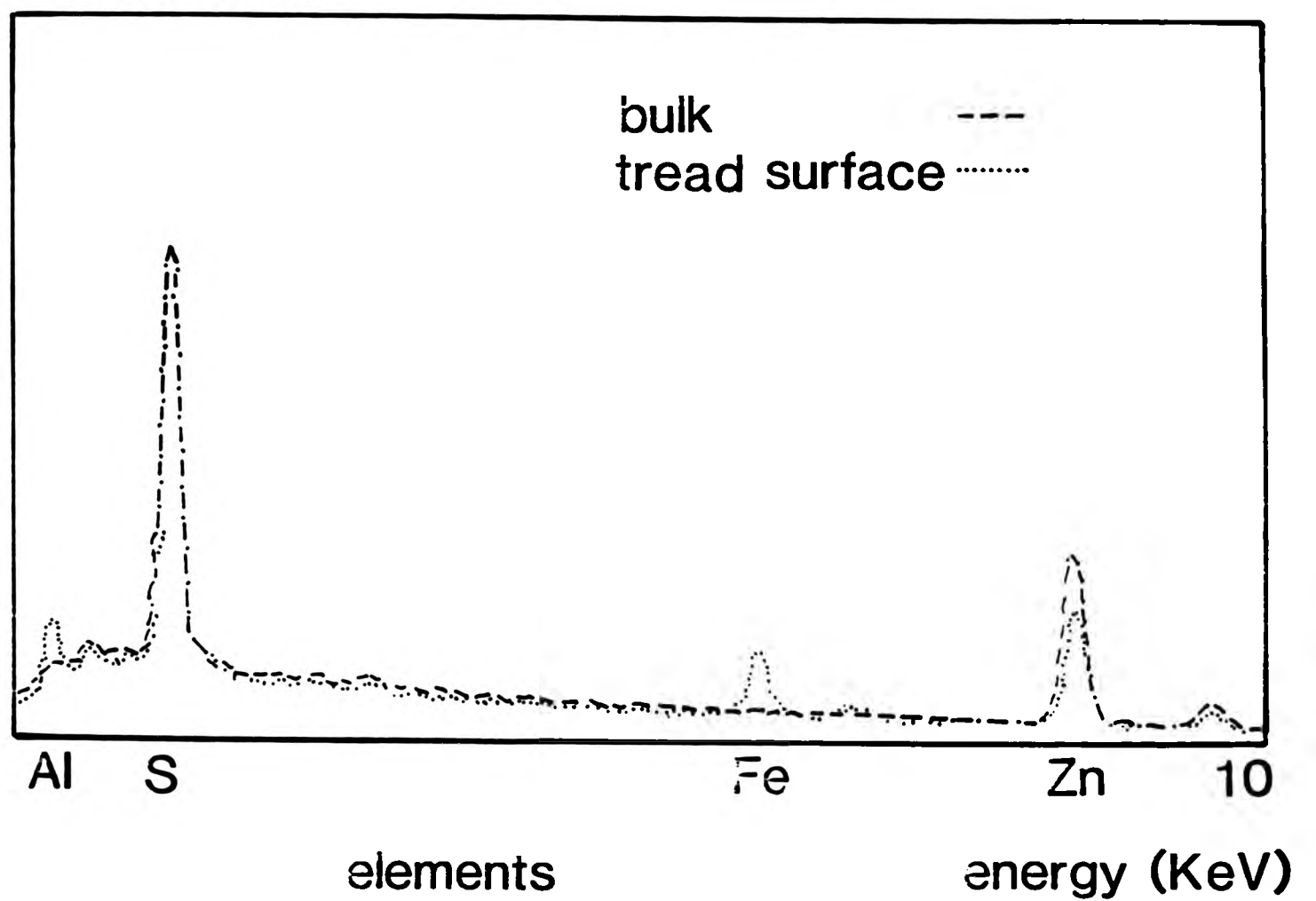


Figure 9.8 Element scans for tread surface (including surface 'crust') and bulk rubber (no 'crust') under tread, obtained using a Hitachi S 500 Scanning Electron Microscope with a Link energy dispersive spectrometer.

extraneous matter, or whether some chemical degradation of the rubber surface had occurred.

9.3.5 Physical properties of rubber samples

The physical properties of the tyre and the results obtained from rubber made to a formulation similar to that which was believed to have been used for the tyre (Table 9.2), are summarized in Table 9.3. The formulation of the rubber inevitably involved some speculation, and was undoubtedly not exactly the same. However, it does provide a general indication of the sort of physical properties that are expected when the rubber was new.

The results showed the rubber to be in good condition. There was little difference in physical condition between the rubber taken from the tyre after immersion for forty-two years in sea water and new rubber made to a similar formulation.

9.3.6 Conclusions

The puncture energy contour and the standard test results show that after 42 years immersion in sea water the condition of the tyre was as good as rubber moulded to a similar formulation.

Table 9.3 Physical properties of the tyre after 42 years sea-water immersion

Test	Tyre	New rubber sheet of similar formulation
Tensile Strength	29.0 MPa	30.0 Mpa
Tensile modulus at 300% stress	13.5 Mpa	11.0 Mpa
Elongation at break	512%	600%
Trouser tearing energy	40.0 kJ/m ²	36.0 kJ/m ²
Hardness	71 IRHD	61 IRHD

CHAPTER TEN

CONCLUSIONS AND SUGGESTIONS FOR FURTHER WORK

Work has been carried out to identify the important features in the puncture process for rubber in order to assist the fracture mechanics analysis of the puncture test. The most helpful observation was the formation of a ring crack as the initial stage of the puncture process. The ring crack was treated as a starter crack which eventually, at a certain force, grew catastrophically. An equation has been derived for the puncture energy. The values of puncture energy so obtained were found to agree well both with the catastrophic tearing energy obtained from the trouser tear tests and with the value derived from the direct determination based on the force/deflection curve and the total area of the crack. The agreement was found to hold only for the indenter with a sharp corner radius. Further analysis is required to modify the equation in order to take account of the corner radius.

In deriving the puncture energy equation, the energy stored in the rubber both surrounding the indenter and beneath it was considered. The energy beneath the indenter was determined using a model experiment based on the biaxial stretching of rubber sheets by inflation. It was found that the energy

stored in this region was very small. An equation was derived to predict the stress exerted on the wall of the puncture hole. Using this equation, the energy stored in the rubber surrounding the indenter was found to be insignificant. Thus an adequate expression for the puncture energy is simply $F(1 - \lambda_c)/2\pi r_0$, where F is the force at which puncture takes place.

The advantage of the puncture test as a method of assessing the strength properties of rubber components has been shown. The test was used to study the strength of thick rubber blocks which had been exposed to long-term ageing and to high temperatures. A 96-year-old rubber pad from a Melbourne bridge was found to be in good condition and still functioning. Such longevity is believed to be due to the formation of a hard surface skin, which is impervious to oxygen penetration and thus protects the rubber underneath. The data obtained at high temperature were extrapolated to a 23°C by means of an Arrhenius plot; the results obtained agreed well with the data from the 96-year-old rubber. The prediction of long-term ageing at ambient temperature from short-term, high temperature experiments may not be applicable to other vulcanizates.

It has also been shown that the puncture energy contour did not indicate any serious degradation in the rubber of a bearing after twenty years in service.

A portable puncture test could be developed so that on-site evaluation of rubber bearings can be made without removal of the bearings. In this situation, the components being tested will be under strain and the analysis will require modifications to take account of this.

REFERENCES

1. Kelly, A., 'Strong Solids', ch. 1, Clarendon Press, 1966.
2. Andrews, E.H., 'Fracture in polymers', ch. 4, Oliver & Boyd, 112, 1968.
3. Griffith, A.A., Phil. Trans., A221, 163, 1920.
4. Inglis, C.E. Trans. Inst. Naval Archit. (London), 55, 219, 1913.
5. Rivlin, R.S. and Thomas, A.G., J. Polym. Sci., 10, 291, 1953.
6. Greensmith, H.W., J. Appl. Polym. Sci., 7, 993, 1963.
7. Lindley, P.B., J. Strain Analysis, 7, 132, 1972.
8. Thomas, A.G., Schweizer Arch. angew. Wiss. Tech, 34, 182, 1968.
9. Thomas, A.G., J. Polym. Sci., 18, 177, 1955.
10. Lindley, P.B. and Thomas, A.G., Proc. Int. Rubber Conf., 4th, London, 428, 1962.
11. Lake, G.J. and Lindley, P.B., Rubber J. 146, 10, 24, 1964.
12. Lake, G.J. and Lindley, P.B., J. Appl. Polym. Sci., 9, 1233, 1965.
13. Breidenbach, R.F. and Lake, G.J., Rubb. Chem. Technol., 52, 96, 1979.
14. Breidenbach, R.F. and Lake, G.J., Phil. Trans. R. Soc.

- Lon. A299, 189, 1981.
15. Gent, A.N., Fielding-Russel, G.S., Livingstone, D.I. and Nicholson, D.W., J. Mat. Sci., 16, 949, 1981.
 16. Clapson, B.E. and Lake, G.J., Rubb. J., 152, 36, 1970.
 17. Lindley, P.B. and Stevenson, A., Rubb. Chem. Tech., 55, 337, 1981.
 18. Stevenson, A., Rubb. Chem. Tech., 59, 208, 1986.
 19. Kinloch, A.J. and Young, R.J., "Fracture behaviour of polymers", Applied Science Publishers, London, ch. 3, 1983.
 20. Williams, J.G., "Fracture mechanics of polymers", Ellis Horwood Limited, Chichester, ch. 5, 1984.
 21. Hertz, H.R., J. Reine Angew. Math. 92, 156, 1881; Hertz's Miscellaneous Papers, Chapters 5 and 6, MacMillan Press, London, 1882.
 22. Frank, F.C. and Lawn, B.R., Proc. Roy. Soc. Lond. A299, 291, 1967.
 23. Lawn, B.R., J. Appl. Phys. 39, 4828, 1968.
 24. Langitan, F.B. and Lawn, B.R., J. Appl. Phys. 40, 4009, 1969.
 25. Lawn, B.R., Wilshaw, T.R. and Hartley, N.E.W., Int. J. Frac., 10, 1, 1974.
 26. Huber, M.T., Ann. Physik, 14, 153, 1904.
 27. Mikosza, A.G. and Lawn, B.R., J. Appl. Phys., 42, 5540, 1971.
 28. Wilshaw, T.R., J. Phys. D: Appl. Phys., 4, 1567, 1971.

29. Shubnikov, A.V. and Zinserling, K., Z. Krist., 83, 243, 1932.
30. Hartley, N.E.W. and Wilshaw, T.R., J. Mat. Sci., 8, 265, 1973.
31. Heavens, J.W., Ph.D. Thesis, University of Bristol, 1972.
32. Howess, V.R. and Tolansky, S., Proc. Roy. Soc. Lon., A230, 287, 1955.
33. Howess, V.R., "Physical Properties of Diamond", edited by R. Berman, Ch. 6, Clarendon, Oxford, 1965.
34. Lawn, B.R. and Komatsu, Phil. Mag., 14, 689, 1966.
35. Johnson, O.W., J. Appl. Phys., 37, 2521, 1966.
36. Boussinesq, J., "Application des Potentiels a l'Etude de l'Equilibre et du Mouvement des Solides Elastiques", Gauthier-Villars, Paris, 1885. Discussed in S.P. Timoshenko and J.N. Goodier, "Theory of Elasticity", McGraw-Hill, New York, pp. 398, 1970.
37. Lawn, B.R. and Swain, M.V., J. Mat. Sci., 10, 113, 1975.
38. Marshall, D.B. and Lawn, B.R., J. Mat. Sci., 14, 2001, 1979.
39. Arora, A., Marshall, D.B., Lawn, B.R. and Marshall, D.B., J. non-Cryst. Solids, 31, 415, 1979.
40. Lawn, B.R., Evans, A.G. and Marshall, D.B., J. Am. Ceram. Soc., 63, 574, 1980.
41. Scott, J.R., Trans. Inst. Rubber Ind., 11, 224, 1935.
42. Scott, J.R., J. Rubber Res., 12, 117, 1943.

43. Timoshenko, S.P. and Goodier, J.N., "Theory of Elasticity", McGraw-Hill, New York, pp. 398, 1970.
44. Gent, A.N., Trans. I.R.I., 34, 46, 1958.
45. Stiehler, R.D., Decker, G.E. and Bullman, G.W., Rubb. Chem. Tech., 52, 255, 1979.
46. Vickers, H.H. and Robinson, S.B., Proc. Int. Rubb. Conf. Washington D.C., 128, 1959.
47. Livingstone, D.I., Yeh, G.S., Rohall, P. and Gehman, S.D., J. Appl. Polym. Sci., 5, 442, 1961.
48. Yeh, G.S. and Livingstone, D.I., Rubb. Chem. Tech., 34, 937, 1961.
49. Schallamach, A., "The chemistry and physics of rubber-like substances", ch. 13, ed. Bateman, L., Maclaren and Son, 1963.
50. Livingstone, D.I. and Hildenbrand, L.E., Rubb. Chem. Tech., 37, 14, 1964.
51. Dozortsev, M.S. and Nechiporenko, A.G., Soviet Rubb. Tech. 26, 41, 1967.
52. Lukomskaya, A.I and Dozortsev, M.S., Soviet Rubb. Tech. 30, 22, 1971.
53. Mikhailov, V.G., Panchuk, F.A. and Putankin, K.S., Int. Polym. Sci. Tech., 2, (8), 53, 1975.
54. Kusano, T., Murakami, K. and Yamakawa, T., Nippon Gomu, No. 12, 763, 1980.
55. Lindley, P.B. and Teo, S.C., Plast. Rubb:Mat. Appl., 2, 82, 1977.
56. Ab-Malek, K., M.Phil. Thesis, CNNA, 1982.
57. Dobie, W.J., Materials Research & Standards, 9, 24, 1969.

58. Warkenthin, T.A., *Rubb. Age*, 60, 197, 1946.
59. Dunn, J.R., Gelinas, L.P. and Klingender, R.C., "Factors influencing the chipping resistance of polybutadiene vulcanizates", paper presented at A.C.S., Divn. of Rubb. Chem., Spring meeting, 1968.
60. Lake, G.J. and Yeoh, O.H., *Proc. Int. Conf. on Deformation Yield and Fracture of Polymers*, Cambridge, July 1982.
61. Lake, G.J. and Yeoh, O.H., *Int. J. Fracture*, 14, 509, 1978.
62. Ab-Malek, K. and Stevenson, A., *J. Mater. Sci.*, 19, 585, 1984.
63. Brown, R.P., "Physical Testing of Rubbers", ch. 4, Applied Science Publishers Ltd., 1979
64. Treloar, L.R.G., "The physics of rubber elasticity", ch. 5, Clarendon Press, Oxford, 1975.
65. Treloar, L.R.G., "The physics of rubber elasticity", ch. 10, Clarendon Press, Oxford, 1975.
66. Timoshenko, S.P. and Goodier, J.N., "Theory of elasticity", McGraw-Hill, New York, ch. 4, 1970.
67. Greensmith, H.W., MRPRA unpublished work.
68. McDonel, E.T. and Shelton, J.R., *J. Chem. Eng. Data*, 4, 360, 1959.
69. Elliott, D.J., Private communication.
70. Knight, G.T. and Lim, H.S., *Int. Rubb. Conf.*, Kuala Lumpur, 5, 57, 1975.
71. Tidd, B.K., *Plast. and Rubb.: Mat. Appl.*, 2, 100, 1977.

72. Wake, W.C., Tidd, B.K. and Loadman, M.J.R., "Analysis of rubber and rubber-like polymers", ch. 6, Applied Science Publishers, 1983.
73. Elliott, D.J. and Tidd, B.K., Progress of Rubber Technology, 34, 83, London, IRI (1974).
74. Van Amerongen, G.J., Rubb. Chem. Technol., 37, 1065, 1964.
75. Stenberg, B., Shur, Y.I. and Jansson, J.F., J. Appl. Polm. Sci.; App. Polym. Symp. 35, 511, 1979.
76. Stenberg, B. and Dickman, O., Plast. and Rubb. Processing and Applications, 4, 337, 1984.
77. Stenberg, B. and Bjork, F., Polymer Testing, 5, 245, 1985.
78. Glazer, J. and Cotton, F.H., "The applied science of rubber", ch. 12, ed. Naunton, W.J.S., Arnould, London, 1961.
79. Smith, D.A, Russell, R. and Welding, G.N., Proceeding of the Fourth Rubber Technology Conference, London, 1962.
80. Thomas, A.G., Mullins, L. and Greensmith, H.W., "The chemistry and physics of rubber-like substances", ch. 10, ed. Bateman, L., Maclaren, London, 1963.
81. Morrison, N.J. and Porter, M., Plast. and Rubb. Processing and Applications, 3, 295, 1983.
82. Barnard, D., 75 years of rubber research international conference held in Colombo, September 1984.
83. Barrie, J.A., Machin, D. and Nunn, A., Polymer, 16, 811, 1975.

84. Southern, E. and Thomas, A.G., ACS Symp. Series, 127, 375, 1980.
85. Cassidy, P.E. and Aminabhari, T.M., Rubb. Chem. Technol. Rev., 56, 594, 1983.
86. Snoke, L.R., Bell System J., 36, 1095, 1957.
87. Connolly, R.A., J. Mater., 5, 339, 1970.
88. Ab-Malek, K and Stevenson, A., J. Mat. Sci., 21, 147, 1986.

THE BRITISH LIBRARY DOCUMENT SUPPLY CENTRE

ON THE PUNCTURE STRENGTH OF RUBBER.

TITLE

.....

.....

K. AB-MALEK. PH.D.

AUTHOR

.....

Attention is drawn to the fact that the copyright of this thesis rests with its author.

This copy of the thesis has been supplied on condition that anyone who consults it is understood to recognise that its copyright rests with its author and that no information derived from it may be published without the author's prior written consent.



**THE BRITISH LIBRARY
DOCUMENT SUPPLY CENTRE**

Boston Spa, Wetherby
West Yorkshire
United Kingdom

REDUCTION X **12**

D76202